FUNCTIONALIZATION OF ALKANES AND OTHER HYDROCARBONS BY HIGH-OXIDATION STATE IRIDIUM. CATALYST DESIGN AND MECHANISTIC STUDY

By

YANG GAO

A dissertation submitted to the

School of Graduate Studies

Rutgers, The State University of New Jersey

In partial fulfillment of the requirements

For the degree of

Doctor of Philosophy

Graduate Program in Chemistry and Chemical Biology

Written under the direction of

Alan S. Goldman

And approved by

_____

_____

_____

_____

New Brunswick, New Jersey

May, 2018

ABSTRACT OF THE DISSERTATION

FUNCTIONALIZATION OF ALKANES AND OTHER HYDROCARBONS BY HIGH-OXIDATION STATE IRIDIUM. CATALYST DESIGN AND MECHANISTIC STUDY

By

YANG GAO

Dissertation Director:

Alan S. Goldman

The selective dehydrogenation of alkane and alkyl groups has a great impact on the synthesis of fuels and both commodity and fine chemicals. In this thesis, the work described is aimed at developing and understanding alkane functionalization using high-oxidation state Ir complexes. Simple Lewis acid such as Na^+, Li^+ or BAr_3 were discovered to catalyze two of the most relevant and fundamental organometallic reactions with an Ir(III) species, (Phebox)Ir(OAc)(H) (Phebox = 2,6-bis(4,4-dimethyloxazolinyl)-3,5-dimethylphenyl): olefin insertion and C–H addition (and their respective microscopic reverse reactions). The results of DFT calculations indicate that the Lewis acid primarily promotes the opening of a vacant coordination site via interaction with acetate ligand.

An acceptorless *n*-alkane dehydrogenation system was developed co-catalyzed by (Phebox)Ir(OAc)(H) and $NaBAr^F_4$. Attempts to catalyze transfer dehydrogenation with (Phebox)Ir(OAc)(H)/Na^+ afforded unexpected results. Alkane solutions of

(Phebox)Ir(OAc)(H)/Na^+ with 1-alkene added as hydrogen acceptor, in contrast with PCP-type catalysts, selectively effected transfer dehydrogenation of the olefins, olefin disproportionation to give mostly dienes. When ethylene was added as a hydrogen acceptor, we obtained high yields of dienes and polyenes, derived from ethylene oligomerization and dehydrogenation. These results indicate that Na^+ catalyzed both insertion of olefins into the Ir-alkyl bond of (Phebox)Ir(OAc)(Alkyl), as well as C–H activation by the same species. (Phebox)Ir(OAc)(H)/Na^+ system was also discovered to catalyze the norbornene isomerization to form nortricyclane.

An Ir(I) complex, (Phebox)Ir(η^2-C_2H_4)$_2$, was synthesized and discovered to catalyze the ethylene dehydrogenative coupling reaction via an iridacyclopentane intermediate. DFT calculation suggest that the iridacyclopentane intermediate undergoes a very unusual β-hydride elimination to give 1,3-butadiene.

Acknowledgement

First, I would like to thank you, Prof. Alan Goldman for your guidance and encouragement over the last 5 years. I greatly appreciate the opportunities and help that you have given me. I would also like to thank all of the Goldman group members that I have had the chance to work with. Thank you for the company in the lab and all suggestions on the problems I faced.

I would particularly like to thank Dr. Kathleen Field, Dr. Akshai Kumar and Dr. Meng Zhou for getting me started in the group and for your help and support. Thank you Dr. Thomas Emge for the great help on crystal structure determination. To Prof. Karsten Krogh-Jespersen and Dr. Changjian Guan I owe a huge thank you for your contribution to the computation part of this thesis.

I owe my family and friends a huge thank you for all of your support and encouragement throughout this process. Thank you my parents for all love and self-sacrifice on my behalf and always supporting my decisions. And of course, thank you my fiancée, Yuwei Tian. You make my life rich and colorful and I can't express how grateful I am to you for being extremely loving and supportive. I am very appreciative that we were able to do this together and can't wait to start the new chapter of our lives.

Dedication

For my family

Table of Contents

List of Figures

List of Schemes

List of Tables

Introduction

Alkenes, probably the most important class of feedstocks in the chemical industry, are readily transformed into an array of value-added fine chemicals, commodity and fuels. The dehydrogenation of alkanes, the most abundant and inexpensive hydrocarbons, is a simple and attractive route to produce alkenes. Transition-metal-based catalysts have shown considerable promise in this context, affording high turnover numbers and the very desirable selectivity for functionalization of the terminal position. To date such catalysts have generally involved electron-rich highly unsaturated (14-electron) metal centers in low oxidation states.[1-3]

In 1979, Crabtree and coworkers[4] reported the first example of stoichiometric alkane dehydrogenation, using $[IrH_2(acetone)_2L_2][BF_4]$, **1**, (L = PPh_3). Saturated cycloalkanes were observed to react with **1** in the presence of *t*-butylethylene (TBE) as the hydrogen acceptor to yield cycloalkenes (Scheme 1.1). The first systems for catalytic homogeneous dehydrogenation of alkanes were discovered independently by the Felkin[5-7] and Crabtree groups[8,9]. Crabtree et al. reported that Ir(III) species, $IrH_2(\eta^2\text{-}O_2CCF_3)(PR_3)_2$ (**2**, R = *p*-FC_6H_4; **3**, R = cyclohexyl(Cy)), can catalyze the dehydrogenation of cyclooctane in the presence of TBE as acceptor, 30 TONs achieved at 150 °C with **2**. Photolysis-driven dehydrogenation of cyclic and linear alkanes could be carried out at 25 °C, in the absence of H_2 acceptor (Scheme 1.2). For example, 7 TONs were achieved when using cyclooctane as substrate and **3** as catalyst.

Scheme 1.1. Stoichiometric Cycloalkane Dehydrogenation by $[IrH_2(S)_2L_2][BF_4]$

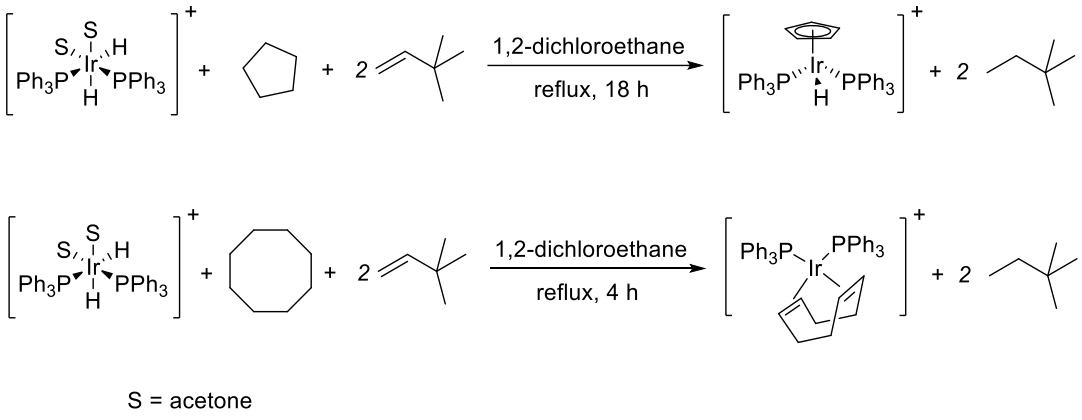

Scheme 1.2. Thermal and Photochemical Dehydrogenation of Cyclooctane by Ir

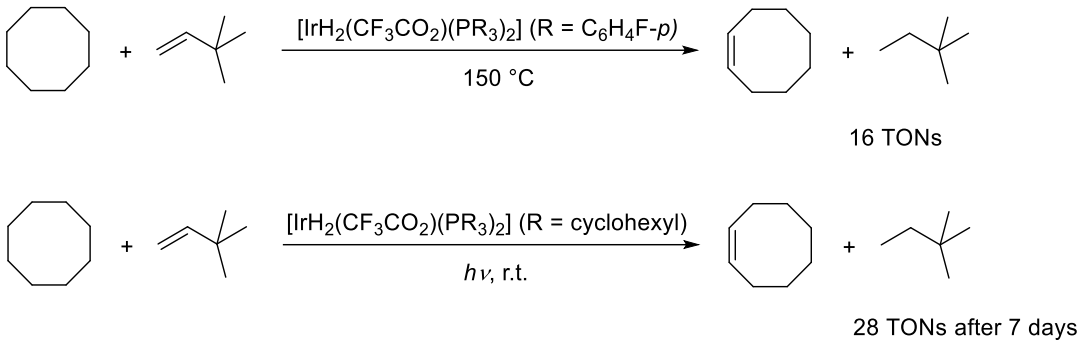

Jensen, Kaska and coworkers[10] discovered that a PCP pincer-ligated iridium complex, (^{t}Bu4PCP)IrH_2 (**4**), was extremely effective for alkane transfer dehydrogenation. In the case of **4** catalyzed COA/TBE system, 82 TONs/h was achieved at 150 °C, remarkably, increased to 12 TONs/min at 200 °C, with no catalyst decomposition observed over one week. Catalysis was found to be inhibited by nitrogen with formation of stable dinitrogen complexes[11,12] and by excess TBE. Employing the high thermal stability of **4**, Kaska, Jensen and Goldman investigated the dehydrogenation of alkanes in the absence of acceptor, an extremely endothermic reaction that would require high temperature.

Acceptorless dehydrogenation of cyclodecane was achieved with either **4**, or the sterically less-crowded, (^{iPr4}PCP)IrH_2, **5**, which is more effective than *t*-Bu derivative **4**. 1000 TONs were obtained at 200 °C with **5**[13].

Acceptorless dehydrogenation of linear alkanes to value-added α-alkenes is quite attractive economically. However, there are several drawbacks using current method. The reaction slows down with time, probably due to either (or both) thermodynamically favorable back reaction when product builds up or formation of Ir(I) olefin complexes, which inhibit the catalysis. Moreover, although α-alkenes have been proven to be the kinetic product of acceptorless alkane dehydrogenation, isomerization of α-alkenes always happens and leads to the formation of the more stable internal alkenes. The mechanism for α-alkene isomerization was initially proposed as the classic "hydride addition mechanism". For example, an initial 2-1 insertion of α-alkene into Ir-H bond gave an Iridium alkyl complex which can yield an internal alkene via 3,2-β-hydride elimination (**Figure 1.1**). However, recent experimental and computational studies[14] suggest that isomerization occurs through a π-allyl hydride intermediate generated from a (PCP)Ir(olefin) complex (**Figure 1.1**).

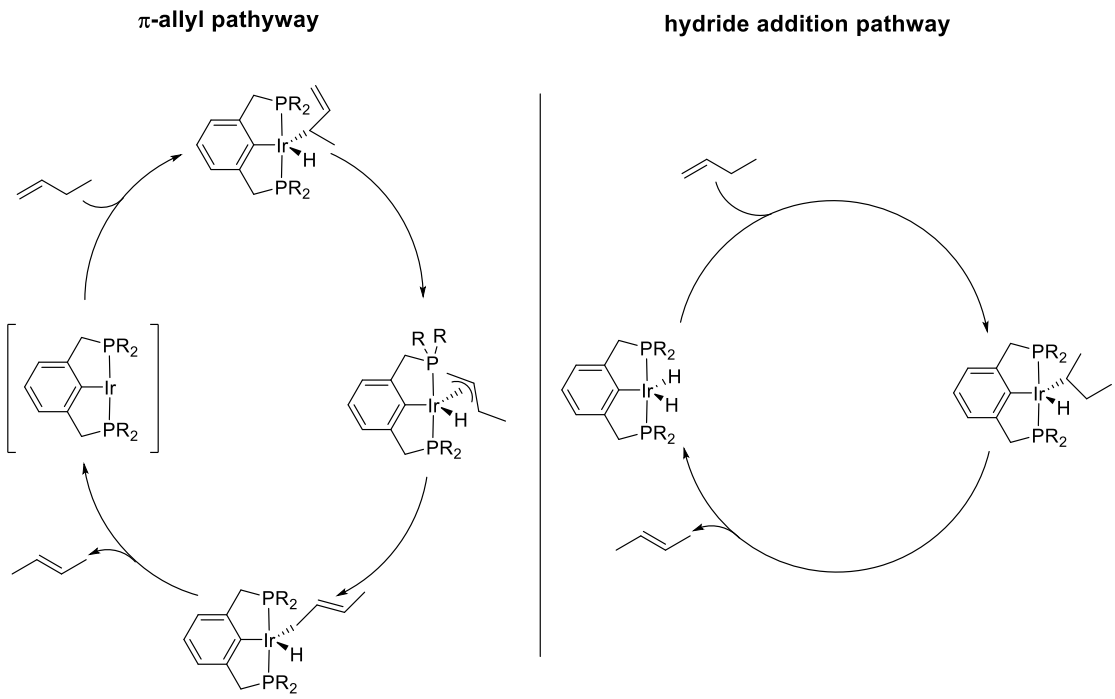

Figure 1.1. α-Alkene isomerization: possible mechanistic cycles.

Figure 1.2 depicts catalytic cycle[15] proposed for (PCP)Ir catalyzed n-alkane/alkene transfer dehydrogenation, illustrated with butane/TBE. Beginning with the 16-electron species (PCP)IrH_2, insertion of TBE into Ir-H bond generates the iridium alkyl hydride complex. Reductive elimination leads to formation of 2,2-dimethylbutane and active 14-electron Ir(I) species, which undergoes the oxidative addition of butane to butyl hydride complex, followed by β-hydride elimination to produce 1-butene as the primary product and regenerate (PCP)IrH_2.

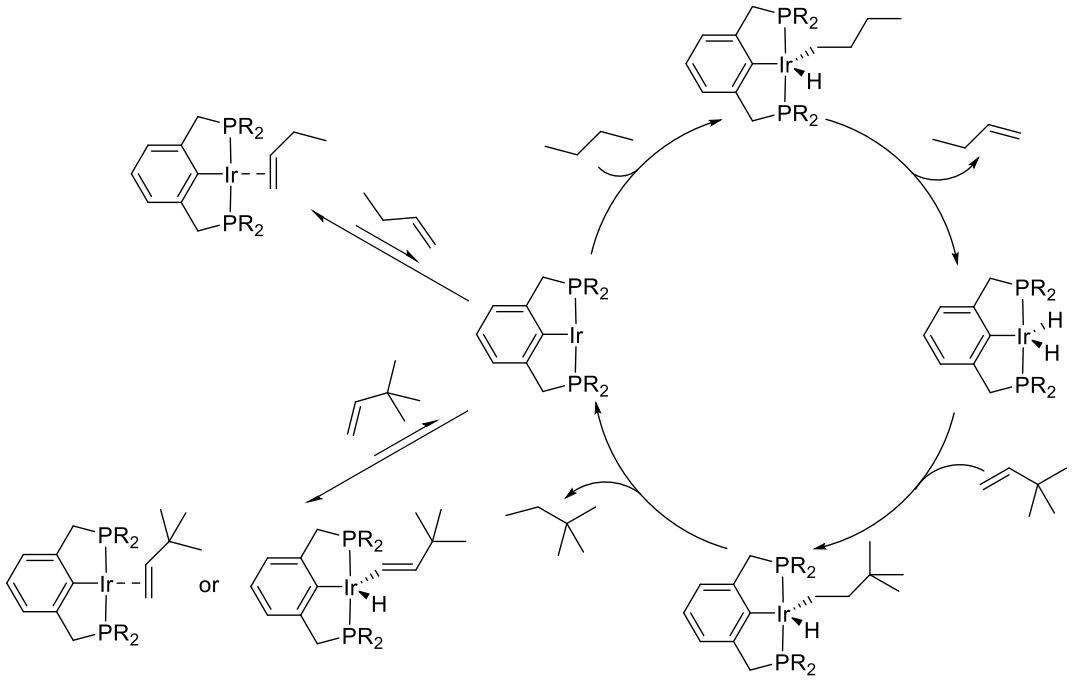

Figure 1.2. Pincer-iridium-catalyzed *n*-butane/TBE transfer dehydrogenation mechanistic cycle.

Sterically crowded catalysts such as **4**, favor the corresponding dihydride complex as the resting state in the absence or under low concentration of strongly bonding alkenes. When high concentration of olefin is present, the resting state can be Ir-olefin complexes. As shown in the **Figure 1.2**, complexes with bulky ligand are found to form an iridium(III) hydride vinyl complex with TBE, while sterically less hindered complexes tend to form Ir(I)-TBE π-complex. The α-alkene product produced in the catalysis binds more strongly than TBE. In general, high acceptor concentration and use of less sterically hindered acceptors such as ethylene and propylene would be expected to retard the activity of the catalyst whose resting state is an olefin complex.

Goldman's group has recently reported the transfer dehydrogenation of light alkane using ethylene or propylene as the acceptor at 200-240 °C catalyzed by ($^{i\text{Pr}}$PCP)Ir(C_2H_4).[16]

Surprisingly, the solid (catalyst)/gas-phase (reactants) systems afforded high rates with much greater yields of α-alkenes than that obtained from solution-phase experiments. The amount of iridium(III) dihydride species under solid/gas-phase condition is extremely small, considering the relatively high concentration of less hindered and active hydrogen acceptor (**Figure 1.3**). Therefore, the rate of α-alkenes isomerization is slower than the alkane dehydrogenation rate, giving high yield of α-alkenes.

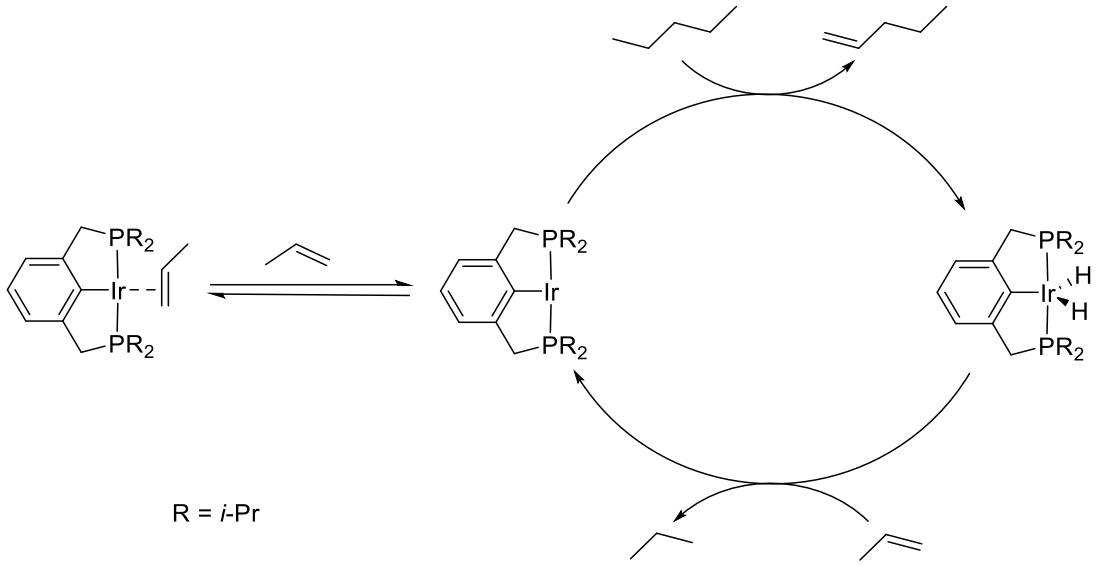

Figure 1.3. Catalytic cycle for pentane/propylene transfer dehydrogenation.

In 2012, Nishiyama[17] reported that *n*-octane reacts with (^{dm}Phebox)Ir(OAc)$_2$(H$_2$O), **6**, in the presence of 1 eq K_2CO_3 at 160 °C to give (^{dm}Phebox)Ir(OAc)(*n*-octyl), **7** (Scheme 1.3). Shortly thereafter, Goldberg and Goldman[18] reported that at 200 °C, in the absence of K_2CO_3, reaction between *n*-octane and **6** produces a new Ir(III) species, (^{dm}Phebox)Ir(OAc)(H), **8**, and octenes. Independent experiment of **7** under the same reaction condition confirmed its intermediacy in this reaction. 1-octene was observed as the major octane product at early reaction times (3 h, 30% conversion), however, the

product mixture was mostly internal octenes when the reaction was finished in 120 h. Notably, the alkane dehydrogenation by **6** can be performed under N_2 and even promoted by the presence of water. In addition, addition of excess amount of olefin did not affect the reaction rate. A detailed computational study on alkane C-H bond activation by **6** was undertaken by Cundari's group[19], suggesting a concerted metalation-deprotonation mechanism as shown in Scheme 1.4.

Scheme 1.3. Activation of *n*-Octane by 3

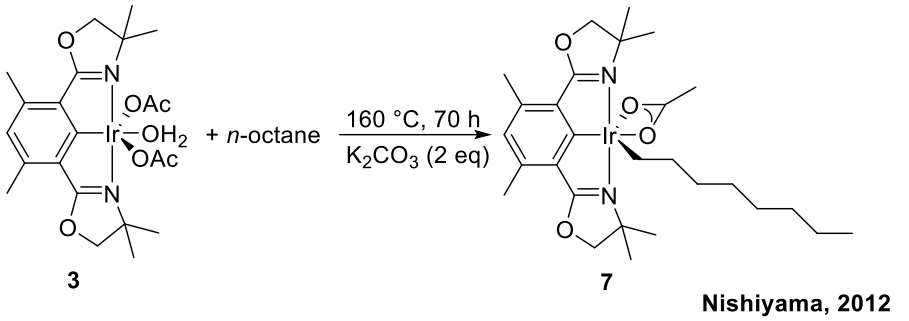

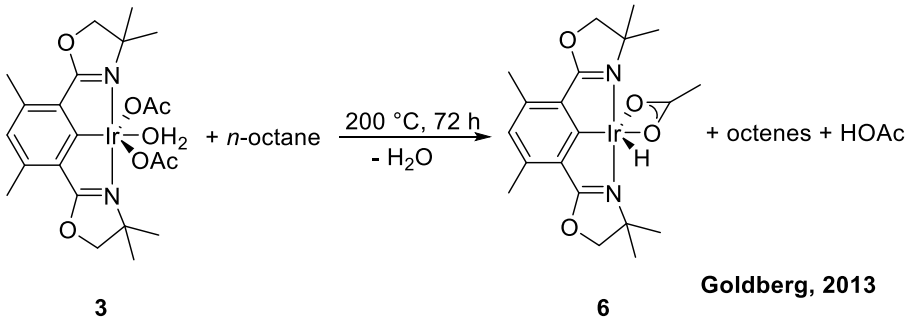

Scheme 1.4. Proposed Mechanism for 3 Mediated n-Octane Dehydrogenation

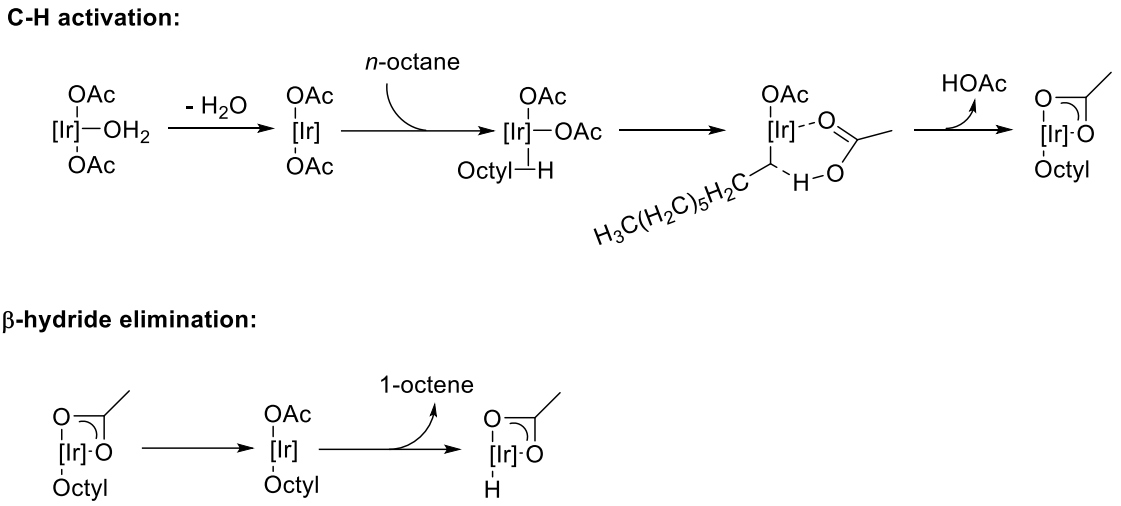

Shortly after, Goldberg showed that (^{dm}Phebox)Ir(OAc)(H), **8**, the product from **6** mediated alkane dehydrogenation, can react with O_2 and 1 equiv of acetic acid to regenerate **6** quantitatively under room temperature.[20] Although they have not run the catalytic system successfully; this discovery, together with reaction in Scheme 1.6, suggest that O_2 may be used as an oxidant in alkane dehydrogenation catalysis. The potential catalytic cycle is shown in Figure 1.4. The high temperature (200 °C) required for alkane dehydrogenation may raise the issue of incompatibility between iridium species and O_2.

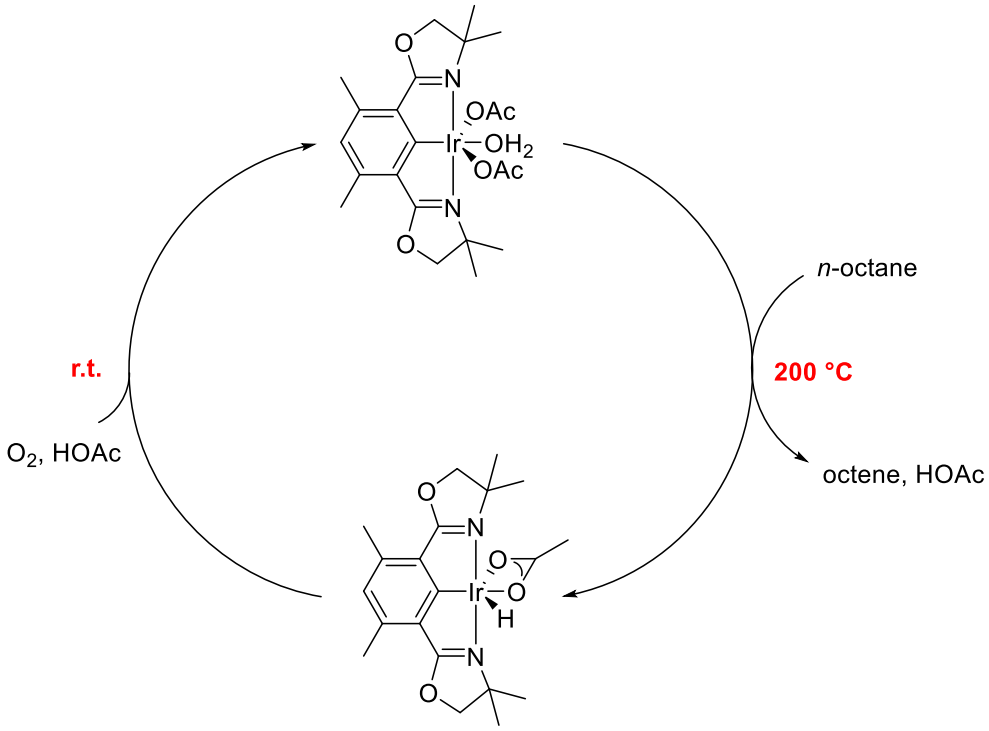

Figure 1.4. Proposed Ir(III) catalyzed cycle of *n*-octane oxidative dehydrogenation.

Our work focuses on the optimization of this (Phebox)Ir(III) mediated alkane dehydrogenation reaction. Both Goldberg and Cundari's studies have indicated that β-H elimination of Ir-Alkyl species (Scheme 1.4) is the rate-determining step in the dehydrogenation process. We discovered that this step can be accelerated, by orders of magnitude with simple Lewis acids such as Na^+, Li^+ and $B(C_6F_5)_3$. β-H elimination of **7** was observed even at -15 °C in the presence of 5% $NaBAr^F_4$ (BAr^F_4 = tetrakis[(3,5-trifluoromethyl)-phenyl]borate) (eq 1.1), as compared with a very slow reaction at 160 °C in the absence of Na^+. DFT calculations reveal that the role of the Lewis acid is to stabilized the de-chelated (η^1) acetate of (Phebox)Ir(OAc)R (R = alkyl or H).

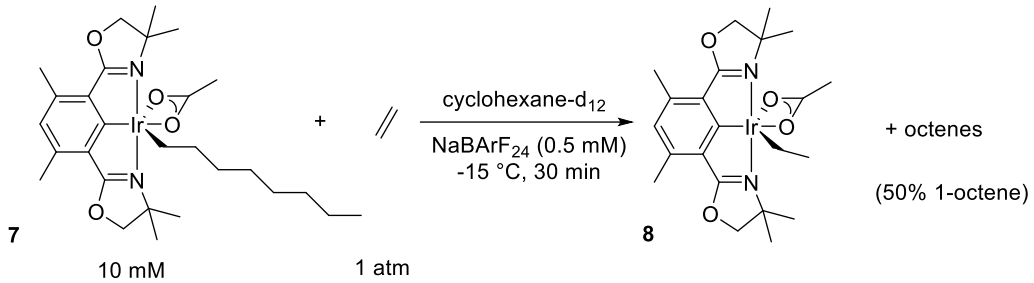

(1.1)

Moreover, Na^+ was also found to accelerate the rate of hydrogenolysis of (Phebox)Ir(OAc)(alkyl) (ca. 200 fold), the reverse of C-H activation by **8**. The sum of C-H activation by **8**, and the β-H elimination of (Phebox)Ir(OAc)(Alkyl), comprises an acceptorless alkane dehydrogenation cycle (Figure 1.5); this has been tested and indeed acceptorless alkane dehydrogenation was found to be accelerated by the addition of $NaBAr^F_4$, using *n*-dodecane as substrate. Notably, this Ir(III)-catalyzed alkane dehydrogenation system is not inhibited by N_2 or H_2O.

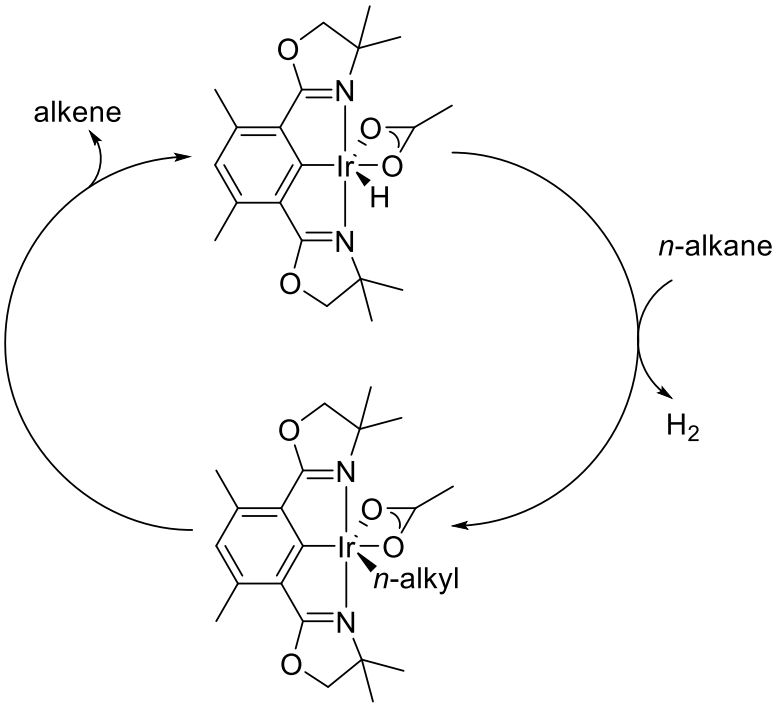

Figure 1.5. Acceptorless *n*-alkane dehydrogenation cycle.

After establishing the acceptorless alkane dehydrogenation system co-catalyzed by **8** and $NaBAr^F_4$, transfer dehydrogenation of alkane with olefin as acceptor was tried but failed using the same catalyst system. Alkene disproportionation was observed as the major reaction with olefin polymerization as the side reaction. For example, when **8** and $NaBAr^F_4$ in octane/1-hexene (1:1) was heated at 150 °C, 2,4-hexadiene isomers were formed as the major dehydrogenation products with formation of hexane (eq 1.2), indicating that dehydrogenation of alkene is more favorable than that of alkane in this co-catalyst system. Notably, no dehydrogenation products were obtained, in the absence of $NaBAr^F_4$, under the otherwise same reaction condition.

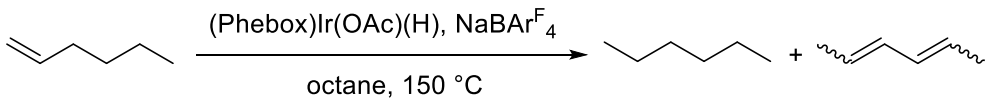

(1.2)

We discovered that this co-catalyst system can be applied to the isomerization of norbornene, shown in eq 1.3. In the absence of $NaBAr^F_4$, no reaction was observed. Using acetic acid, in the presence or the absence of $NaBAr^F_4$ without the iridium complex, also leads to no reaction, ruling out the possibility of acid catalysis.

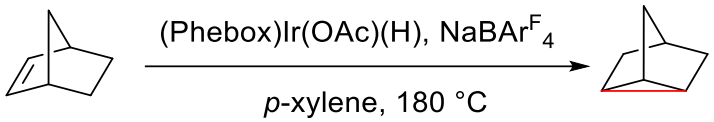

(1.3)

We have also developed an ethylene dehydrogenation-oligomerization system co-catalyzed by **8** and $NaBAr^F_4$, where ethylene plays two roles, the monomer to form oligomers, and the H_2 acceptor for dehydrogenation of resulting oligomers, as shown in eq 1.4. C_{10} and C_{12} polyenes were found to be the major products through the reaction (40 mM after 2 h and 134 mM after 24 h). Under the same reaction condition, but in the absence of $NaBAr^F_4$ only trace amounts of products, mainly butenes and hexenes, were obtained.

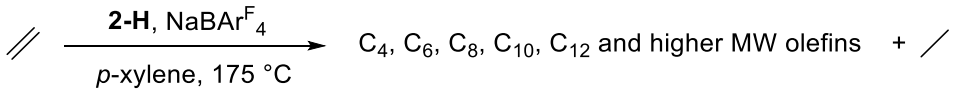

(1.4)

When 1,3-butadiene was used to react with ethylene, oligomerization and dehydrogenation reactions were both observed, as shown in eq 1.5. C_6 olefins were first formed, with 96% selectivity for linear olefins; these were then converted to C_8 olefins, with the branched olefins as the dominant species. The shift of selectivity from linear C_6 products to branched C_8 products may be caused by steric effect and is under study via DFT calculations.

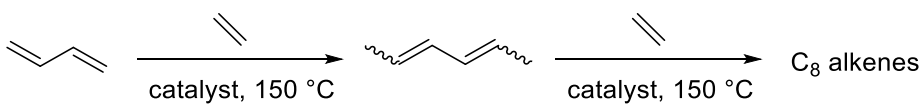

(1.5)

Synthesis of 1,3-butadiene from ethylene dehydrogenative coupling was achieved with (Phebox)Ir(C_2H_4)$_2$ as the catalyst. Kinetic studies suggest that butenes, the major side products, are not the intermediates and therefore, the pathways proceeding through dimerization and following butene dehydrogenation are ruled out. The key intermediate, and a major resting state is trapped under CO atmosphere and characterized as an iridacyclopentane by both NMR spectroscopy and X-ray crystallography. (Figure 1.6) DFT calculation suggests that the iridacyclopentane intermediate undergoes a surprisingly facile β-H elimination, enabled by a partial dechelation (κ^3- κ^2) of the supporting Phebox ligand.

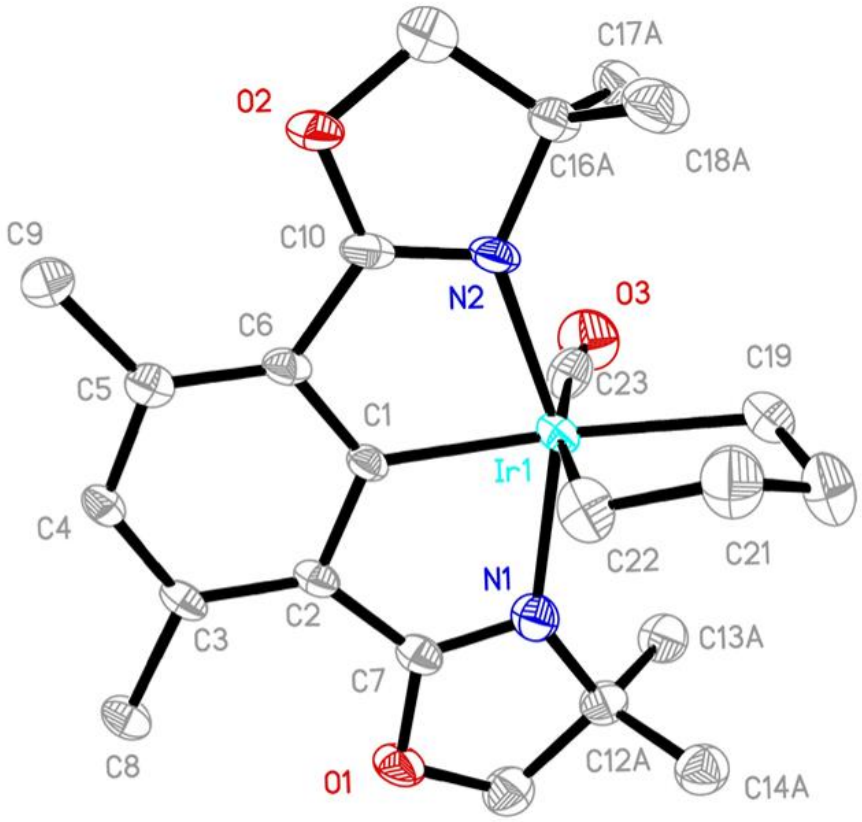

Figure 1.6. ORTEP diagram of iridacyclopentane complex, thermal ellipsoids at 50% probability, H atoms omitted for clarity.

Reference

(1) Kumar, A.; Goldman, A. S. In *The Privileged Pincer-Metal Platform: Coordination Chemistry & Applications*; van Koten, G., Gossage, R. A., Eds.; Springer International Publishing: Cham, 2016, p 307.

(2) Choi, J.; MacArthur, A. H. R.; Brookhart, M.; Goldman, A. S. *Chem. Rev.* **2011**, *111*, 1761.

(3) Dobereiner, G. E.; Crabtree, R. H. *Chem. Rev.* **2010**, *110*, 681.

(4) Crabtree, R. H.; Mihelcic, J. M.; Quirk, J. M. *J. Am. Chem. Soc.* **1979**, *101*, 7738.

(5) Baudry, D.; Ephritikhine, M.; Felkin, H.; Holmes-Smith, R. *J. Chem. Soc., Chem. Comm.* **1983**, 788.

(6) Felkin, H.; Fillebeen-Khan, T.; Gault, Y.; Holmes-Smith, R.; Zakrzewski, J. *Tetrahedron Lett.* **1984**, *25*, 1279.

(7) Felkin, H.; Fillebeen-Khan, T.; Holmes-Smith, R.; Lin, Y. *Tetrahedron Lett.* **1985**, *26*, 1999.

(8) Burk, M. J.; Crabtree, R. H.; Parnell, C. P.; Uriarte, R. J. *Organometallics* **1984**, *3*, 816.

(9) Burk, M. J.; Crabtree, R. H.; McGrath, D. V. *J. Chem. Soc., Chem. Commun.* **1985**, 1829.

(10) Gupta, M.; Hagen, C.; Flesher, R. J.; Kaska, W. C.; Jensen, C. M. *Chem. Commun.* **1996**, 2083.

(11) Lee, D. W.; Kaska, W. C.; Jensen, C. M. *Organometallics* **1998**, *17*, 1.

(12) Ghosh, R.; Kanzelberger, M.; Emge, T. J.; Hall, G. S.; Goldman, A. S. *Organometallics* **2006**, *25*, 5668.

(13) Xu, W.; Rosini, G. P.; Gupta, M.; Jensen, C. M.; Kaska, W. C.; Krogh-Jespersen, K.; Goldman, A. S. *Chem. Commun.* **1997**, 2273.

(14) Biswas, S.; Huang, Z.; Choliy, Y.; Wang, D. Y.; Brookhart, M.; Krogh-Jespersen, K.; Goldman, A. S. *J. Am. Chem. Soc.* **2012**, *134*, 13276.

(15) Renkema, K. B.; Kissin, Y. V.; Goldman, A. S. *J. Am. Chem. Soc.* **2003**, *125*, 7770.

(16) Kumar, A.; Zhou, T.; Emge, T. J.; Mironov, O.; Saxton, R. J.; Krogh-Jespersen, K.; Goldman, A. S. *J. Am. Chem. Soc.* **2015**, *137*, 9894.

(17) Ito, J.-i.; Kaneda, T.; Nishiyama, H. *Organometallics* **2012**, *31*, 4442.

(18) Allen, K. E.; Heinekey, D. M.; Goldman, A. S.; Goldberg, K. I. *Organometallics* **2013**, *32*, 1579.

(19) Pahls, D. R.; Allen, K. E.; Goldberg, K. I.; Cundari, T. R. *Organometallics* **2014**, *33*, 6413.

(20) Allen, K. E.; Heinekey, D. M.; Goldman, A. S.; Goldberg, K. I. *Organometallics* **2014**, *33*, 1337.

Chapter 2. Exploration of Lewis Acid Effect on Reactivity of Iridium Acetate Complexes

Majority of this chapter is reproduced with permission from

β-Hydride Elimination and C–H Activation by an Iridium Acetate Complex, Catalyzed by Lewis Acids. Alkane Dehydrogenation Cocatalyzed by Lewis Acids and [2,6-Bis(4,4-dimethyloxazolinyl)-3,5-dimethylphenyl]iridium

Yang Gao, Changjian Guan, Meng Zhou, Akshai Kumar, Thomas J. Emge, Ashley M. Wright, Karen I. Goldberg, Karsten Krogh-Jespersen, and Alan S. Goldman

J. Am. *Chem. Soc.*, **2017**, 139, 6338−6350

Introduction

The selective catalytic dehydrogenation of alkanes and alkyl groups has great potential with respect to the synthesis of fuels and both commodity and fine chemicals. Transition-metal-based catalysts have shown considerable promise in this context, affording high turnover numbers and the very desirable selectivity for dehydrogenation of the terminal position. To date such catalysts have generally involved electron-rich highly unsaturated (14-electron) metal centers in low oxidation states.[1-3]

In 2012, Nishiyama reported that (Phebox)Ir(OAc)$_2$(OH$_2$) (**1**; Phebox = 2,6- bis(4,4-dimethyloxazolinyl)-3,5-dimethylphenyl) activates the terminal C-H bond of *n*-octane to form (Phebox)Ir(OAc)(*n*-octyl) (**2-Oc**) at 160 °C in the presence of potassium carbonate.[4] The Goldberg lab reported that if **1** is heated in *n*-octane to 200 °C (without added base), (Phebox)Ir(OAc)(H) (**2-H**) and free octenes are obtained (eq 2.1). This reaction, shown in eq 2.1, is the stoichiometric (heterolytic) dehydrogenation of *n*-octane by an Ir-OAc unit.[5] The higher temperature of 200 °C, relative to the C-H activation at 160°C, was apparently necessary to induce β-H elimination of **2-Oc.**

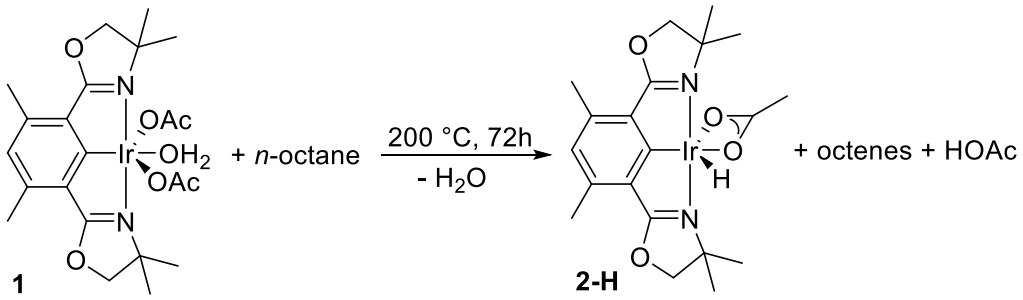

(2.1)

Notably, the reaction shown in eq 2.1 was not inhibited by the presence of N_2 or water,[5] in contrast with the well-known catalytic dehydrogenation of *n*-alkanes by ^{R4}PCP (^{R4}PCP = 2,6-(R_2PCH_2)$_2$$C_6H_3$)) pincer-iridium complexes[2,6] (the rate of eq 2.1 was even slightly

promoted by the presence of water). Nishiyama proposed that alkane activation by **1** proceeded via a concerted metallation-deprotonation (CMD) mechanism;[4,7-11] this proposal was later supported by DFT calculations by Cundari and co-workers.[12] We considered that the difference between the alkane reactions of (^{R4}PCP)Ir and (Phebox)Ir, with respect to inhibition by N_2 or water, might be explained in terms of the intermediacy of Ir(I) intermediates in the case of (^{R4}PCP)Ir and the lack thereof in the case of (Phebox)Ir.

Subsequently, the Goldberg lab reported that **2-H** reacts with O_2 in the presence of acetic acid to regenerate **1**.[13] In combination with eq 2.1 this reaction would constitute a catalytic cycle for the dehydrogenation of *n*-octane using O_2 as a hydrogen acceptor, as illustrated in Scheme 2.1. On a practical level this represents a very attractive alternative to the use of olefinic hydrogen acceptors commonly employed with pincer Ir catalysts. Fundamentally, it further underscores a contrast with (^{R4}PCP)Ir catalysts which are highly sensitive to oxygen;[14] more generally, it highlights the potential advantages of catalytic cycles for Ir-catalyzed dehydrogenation that do not proceed via low-oxidation-state (Ir(I)) species.

Scheme 2.1. Hypothetical Cycle for Dehydrogenation of *n*-Octane by O_2, Catalyzed by (Phebox)Ir(acetate) Complexes, Based on Individually Observed Stoichiometric Reactions

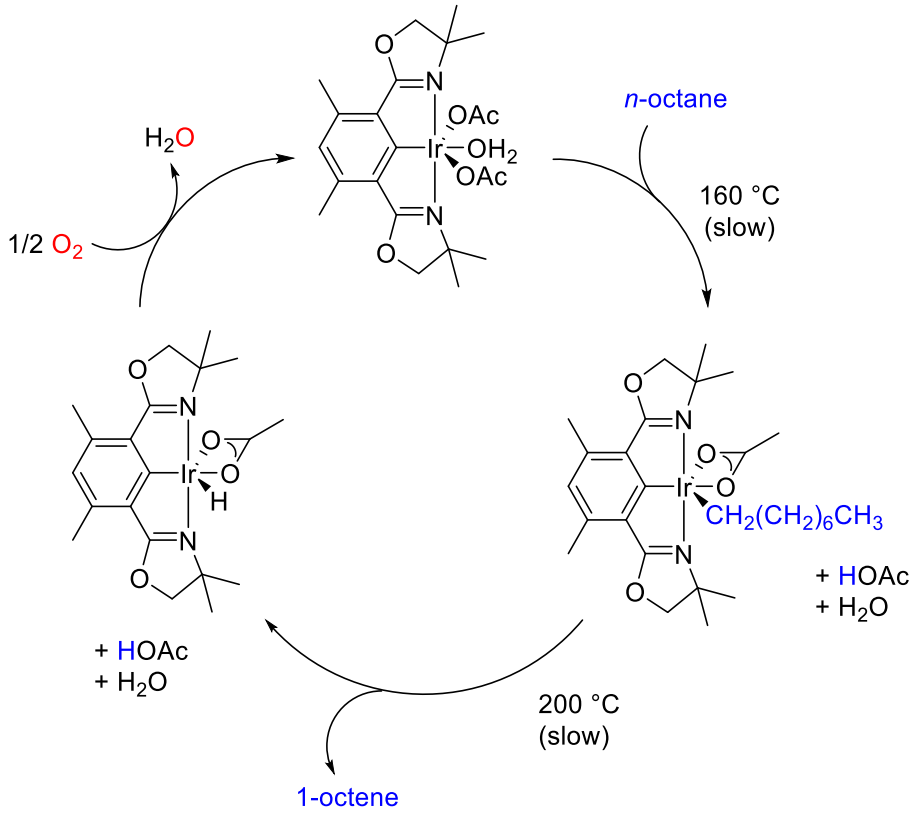

Unfortunately, although the reaction of **2-H** with O_2 proceeded cleanly at room temperature, at the high temperature (200 °C) required for the reaction shown in eq 2.1 (which comprises two of the steps of the catalytic cycle shown in Scheme 2.1), decomposition occurred in the presence of O_2. Thus it was not possible to achieve the catalytic oxidation of alkanes to alkenes by O_2 as indicated in Scheme 2.1.

A catalytic cycle for alkane dehydrogenation based on only high-oxidation state species offers several tantalizing possibilities. The use of O_2 as acceptor, and the tolerance for N_2, H_2O and other possible impurities is indicated above; this proposal is supported by reports

by Roddick of pincer-ligated Ru- and Os-based alkane dehydrogenation catalysts that are much less sensitive to N_2, H_2O, and even O_2 than (PCP)Ir catalysts.[15] In addition, such catalysts might circumvent other issues that plague cycles based on low oxidation state species (including but not limited to Ir(I)), such as catalyst inhibition by the olefin product. Many potential tandem systems can be envisioned that are based on dehydrogenation and a secondary olefin functionalization, but the corresponding reagents (or co-catalysts) would likely not be tolerated by (PCP)Ir or other low oxidation state intermediates. High-oxidation-state catalysts might also be less susceptible to inhibition by functional groups,[16-19] allowing dehydrogenation of potential substrates more complex than alkanes.

With the above points in mind we have begun to explore routes to promoting the kinetics of dehydrogenation (e.g. eq 2.1) by (Phebox)Ir species. Here we report that Lewis acids are found to increase by orders of magnitude the rate of the step shown in Scheme 2.1 with the highest barrier, β-H elimination by **2-alkyl**. In addition, C-H activation by **2-H** is promoted by Lewis acids. We report that **2-H** catalyzes acceptorless dehydrogenation and that the rate of this reaction is substantially increased by the presence of Na^+.

Results and Discussion

In view of the success of (^{R4}PCP)Ir complexes in C-H activation and alkane dehydrogenation,[2,6,20] the starting point of our study was an effort to address the possibility that (Phebox)Ir complexes might undergo reactions with alkanes via the 14-electron (Phebox)Ir(I) unit itself, in analogy with the isoelectronic (^{R4}PCP)Ir unit. To this end we attempted to generate a (Phebox)Ir(I) precursor, (Phebox)Ir(C_2H_4), in analogy with several examples of (^{R4}PCP)Ir(C_2H_4) as a catalyst precursor.[20,21] A solution (10 mM) of **2-H** in benzene-d_6 under 1 atm of ethylene showed no reaction after 24 h at room temperature (r.t.)

or 80 °C, while 5% **2-Et** and 4% **2-Ph** were formed after 25 h at 90 °C. Upon addition of 2.5 equiv NaO^{t}Bu, after 24 h at r.t., one major product was obtained which was determined by NMR spectroscopy and X-ray crystallography to be (Phebox)Ir(η^2-C_2H_4)$_2$ (**3**)[22] (eq 2.2, Figure 2.1).[23]

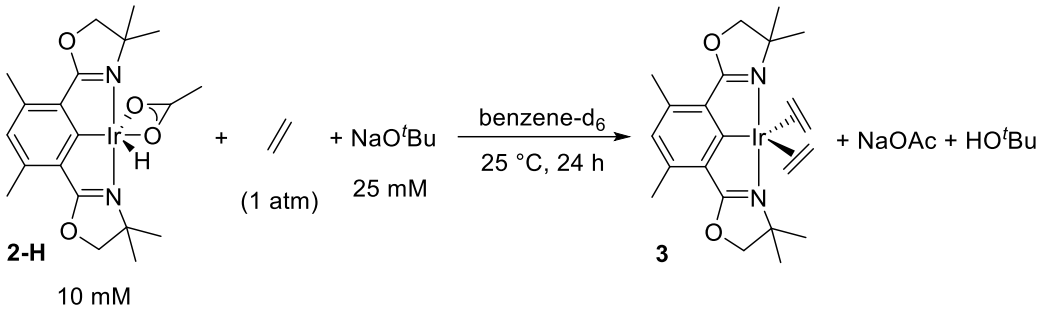

(2.2)

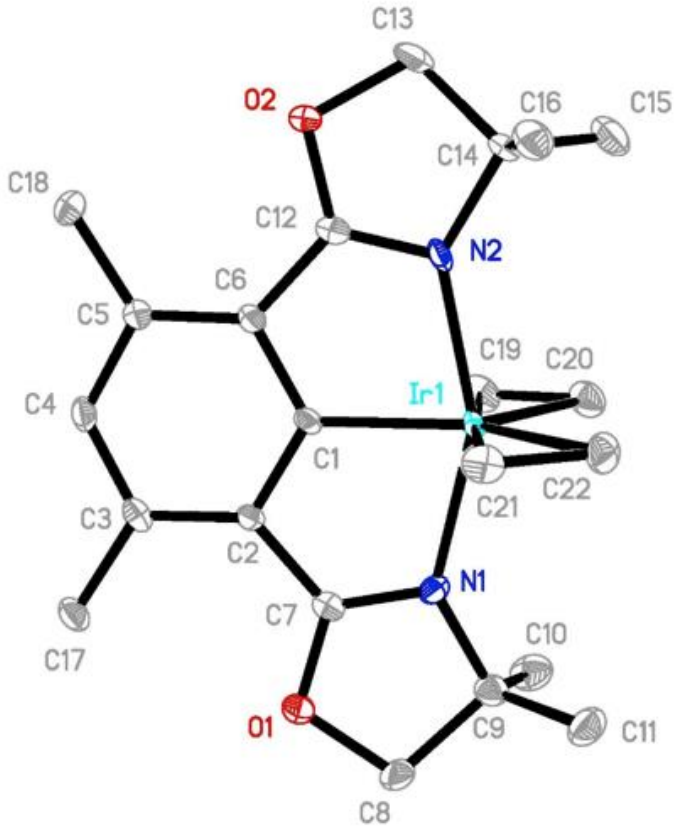

Figure 2.1. Crystal structure of complex **3**, ORTEP diagram shown at 50% probability level. Hydrogen atoms omitted for clarity. Selected bond lengths (Å) and angles (deg): Ir(1)−C(1), 1.995(9); Ir(1)−N(2), 2.074(8); Ir(1)−N(1), 2.096(8); Ir(1)−C(19), 2.129(9); Ir(1)−C(21), 2.136(10); Ir(1)−C(22), 2.161(10); Ir(1)−C(20), 2.165(10); C(19)−C(20), 1.425(15); C(21)−C(22), 1.444(14); C(1)−Ir(1)−N(2), 77.9(3); C(1)−Ir(1)−N(1), 77.7(3); C(1)−Ir(1)−C(19), 90.4(4); C(1)−Ir(1)−C(21), 94.7(4)

Complex **3** showed some activity as a catalyst for alkane transfer-dehydrogenation, but less than that of (^{R4}PCP)Ir complexes. For example, an *n*-octane solution of **3** (2 mM) and the hydrogen acceptor tert-butylethylene (TBE, 0.4 M), at 170 °C, gave 24 mM and 57 mM octenes (and equal amounts of 2,2-dimethylbutane) after 1 h and 24 h, respectively. (^{R4}PCP)Ir catalysts have been reported to give much faster rates at lower temperatures; for example, using (^{iPr4}PCP)IrH_4 (1 mM) as catalyst precursor, 106 mM and 265 mM octenes

are obtained at 150 °C after 15 min and 60 min, respectively under otherwise similar conditions.[24] Likewise, a refluxing (216 °C) *n*-dodecane solution of **3** (2 mM), under conditions typically used to effect acceptorless dehydrogenation,[25] gave dodecene in concentrations of 11 mM and 26 mM, after 1 h and 24 h respectively, which is significantly less than that obtained with (^{R4}PCP)Ir complexes.[25]

Lewis-acid catalyzed Ir-H addition to olefins. Quite surprisingly, the addition of only 0.22 equiv NaO^{t}Bu (instead of 2.5 equiv) to a solution of **2-H** otherwise identical to that described above, under ethylene (1 atm), led to the complete disappearance of **2-H** after 1 h at 25 °C, and the formation of a new complex (Phebox)Ir(OAc)(CH_2CH_3) (**2-Et**) as the main product (eq 2.3). Complex **3** was also formed, but only in 14% yield.

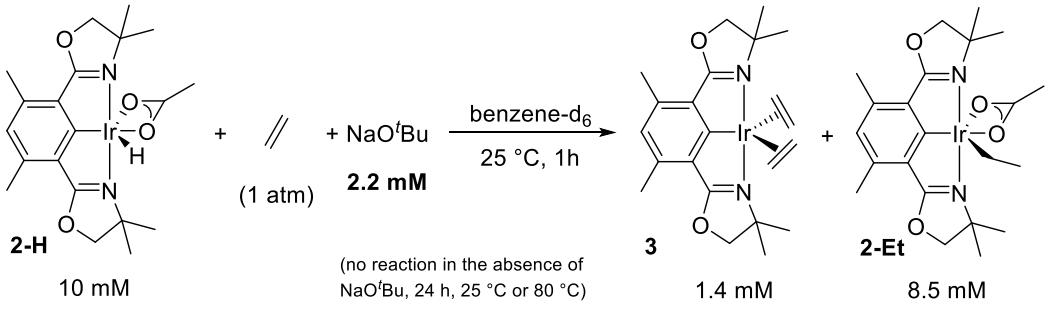

(2.3)

Subsequent addition of acetic acid (10 mM) to the solution resulted in the complete conversion of **3** to **2-Et**. The ^{1}H NMR spectrum (benzene-d_6) of **2-Et** revealed a triplet (3H, 0.97 ppm, $J_{H\text{-}H}$ = 7.5 Hz) and a quartet (2H, 0.64 ppm, $J_{H\text{-}H}$ = 7.4 Hz) attributable to the ethyl group. The ^{13}C NMR spectrum showed a signal at δ -11.4 ppm, assigned to the Ir-bound methylene group. These parameters are similar to those of **2-Oc** as reported by Nishiyama.[4] The molecular structure of **2-Et** was confirmed by X-ray diffraction.[23]

The formation of **3** (1.4 mM) in reaction 3 is easily attributed to the elimination of acetic acid promoted by the strong base NaO^{t}Bu (2.2 mM added). Complex **2-Et** (8.5 mM) by contrast, is not an acid-base reaction product; **2-Et** is the net product of ethylene insertion into the Ir-H bond of **2-H**. The role of NaO^{t}Bu in the formation of **2-Et** is thus apparently catalytic, but the mechanism of the catalysis, a priori, was not obvious. Considering the possibility that the Na^+ cation (rather than the *t*-BuO^- anion) may play the key role, we exposed a benzene-d_6 solution of **2-H** (10 mM) and $NaBAr^F_4$ (0.2 mM; BAr^F_4 = tetrakis[(3,5-trifluoromethyl)phenyl]borate) to 1 atm ethylene. Within 5 min, **2-H** had undergone conversion to **2-Et** as the only product in 99% yield (eq 2.4).

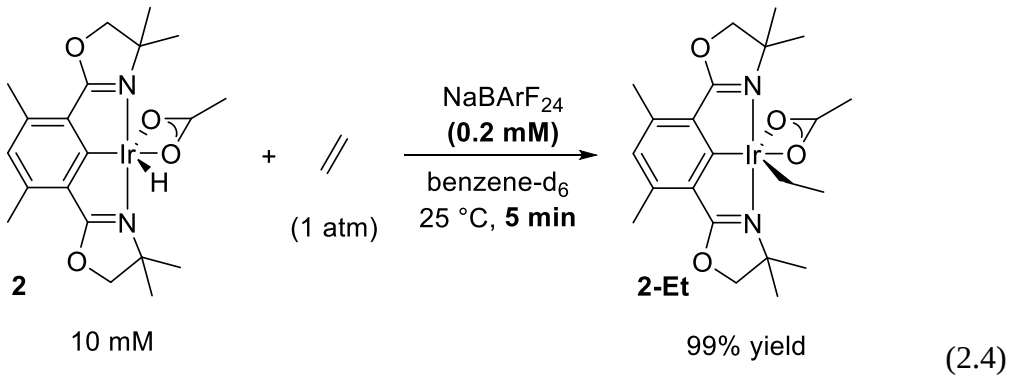

(2.4)

Notably, $NaBAr^F_4$ is apparently not soluble enough in pure benzene-d_6 to afford an observable ^{1}H NMR spectrum.[26] In the presence of **2-H**, however, the $BAr^F_4{}^-$ protons are easily observed (as singlets at δ 8.4 (8H) and δ 7.7 ppm (4H)), indicating an interaction between $NaBAr^F_4$ and **2-H** that is sufficiently favorable to solubilize the $NaBAr^F_4$. Accordingly, the ^{1}H NMR spectrum of **2-H** changed slightly upon addition of $NaBAr^F_4$; all signals in the **2-H** ^{1}H NMR spectrum were broadened and the hydride signal shifted slightly, from δ -33.8 ppm to -34.0 ppm. Confirming the role of the sodium cation in the catalysis of eq 2.4, when the Na^+-coordinating crown ether[27] 15-crown-5 (12 mM,

1,4,7,10,13-pentaoxacyclopentadecane) was added to an identical solution prior to addition of ethylene, the rate of ethylene insertion was negligible; less than 3% conversion was observed after 2 days at room temperature.

$NaBAr^F_4$ was also found to catalyze insertion of other *n*-alkenes into the Ir-H bond of **2-H** (Scheme 2.2). When 1 atm propene was added to a solution of **2-H** (10 mM) and $NaBAr^F_4$ (0.2 mM), complete conversion to (Phebox)Ir(OAc)(*n*-propyl) (**2-Pr**) occurred. In the ^1H NMR spectrum, two multiplets (2H, 1.82-1.54 ppm; 2H, 0.68-0.44 ppm) and one triplet (3H, 1.04 ppm, $J_{H—H}$ = 7.3 Hz) were observed, attributable to the *n*-propyl group. Reactions of 1-pentene (50 mM) or 1-octene (100 mM) proceeded similarly, both reaching completion within 1 h with the formation of (Phebox)Ir(OAc)($CH_2(CH_2)_nCH_3$) (n = 3, 6). Excess *n*-alkene was converted to internal olefins during the course of this reaction. Conversely, within 1 h the reaction of *trans*-2-pentene with **2-H** gave the *n*-pentyl complex **2-Pe**, i.e. the same product as obtained from the reaction with 1-pentene.

Scheme 2.2. Reaction of 2-H with *n*-Alkenes

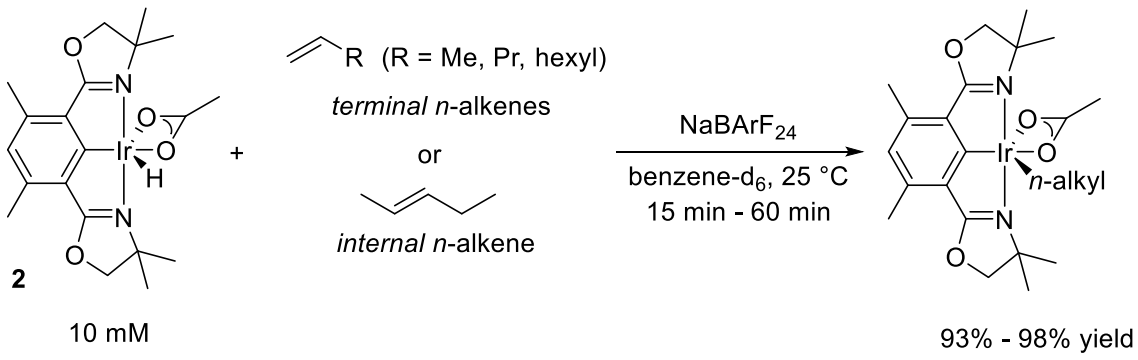

The catalytic activity of $NaBAr^F_4$, its greater activity relative to that of NaO^tBu, and the inhibition of catalysis by added crown ether, all indicate that the Na^+ cation is acting as a Lewis acid. Accordingly, various Lewis acids were screened for catalytic activity for the

reaction of **2-H** with ethylene. As indicated in Scheme 2.3, $NaBF_4$, $NaBPh_4$ and NaOAc were investigated. No ethylene insertion was observed even after 24 h at r.t. but none of these salts were detected in the reaction solution by ^1H NMR or ^{19}F NMR spectroscopy, indicating that they are insoluble in benzene. The lithium salt $[Li(OEt_2)_3][B(C_6F_5)_4]$, however, catalyzed an immediate insertion at room temperature. In addition to these simple metal cations, boranes were investigated. BPh_3 and $B(C_6F_5)_3$ were both found to greatly promote ethylene insertion, albeit less dramatically than either $NaBAr^F{}_4$ or $[Li(OEt_2)_3][B(C_6F_5)_4]$. As noted above, in the absence of a Lewis Acid, no insertion was observed even at 80 °C (even though the equilibrium lies fully to the right, as demonstrated by catalyzing the reaction with $NaBAr^F{}_4$ at that temperature).

Scheme 2.3. Catalysts Screened for Ethylene Insertion

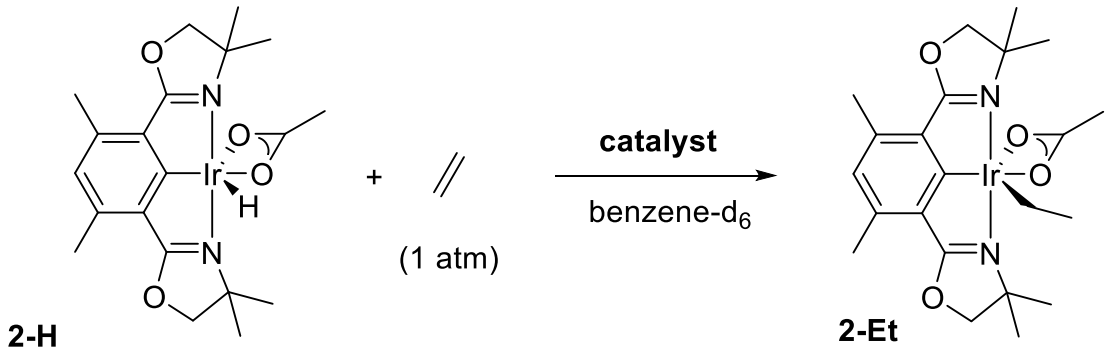

catalyst	
no additive	no reaction (80 °C, 1 day)
NaBArF(0.2 mM)	99% yield (25 °C, 5 min)
NaOAc, $NaBF_4$, $NaBPh_4$	no reaction (25 °C, 1 day)
$[Li(OEt_2)_3][B(C_6F_5)_4]$ (2 mM)	98% yield (25 °C, 5 min)
BPh_3 (5 mM)	99% yield (50 °C, 48 h)
$B(C_6F_5)_3$ (2 mM)	99% yield (25 °C, 2 h)

The kinetics of the $NaBAr^F{}_4$-catalyzed insertions of ethylene and propene into the Ir-H bond of **2-H** were investigated. Reactions of ethylene (10 °C) and propylene (10 °C and 25 °C) proceeded with kinetics that were zero order in **2-H** (Figure 2.2). Superficially at least, this is easily attributed to the catalyst ($NaBAr^F{}_4$) being saturated with substrate (**2-H**); note that **2-H** is present in excess. Since the $NaBAr^F{}_4$ is not soluble in pure benzene, but dissolves in the presence of **2-H**, it would indeed be expected that all $NaBAr^F{}_4$ in solution is initially bound to **2-H**. However, $NaBAr^F{}_4$ also binds to the product **2-Et**, so we would expect, assuming a fixed amount of $NaBAr^F{}_4$ in solution, that a decreasing fraction of it would be bound to **2-H** as the reaction proceeds, and the rate would decrease accordingly over the course of the reaction. Given the difficulties in quantifying the amount of $NaBAr^F{}_4$ in solution, however, we chose not to pursue the detailed kinetics of this system

further; instead we turned to kinetic investigations with a Lewis acid that is simpler to characterize in solution, $[B(C_6F_5)_3]$.

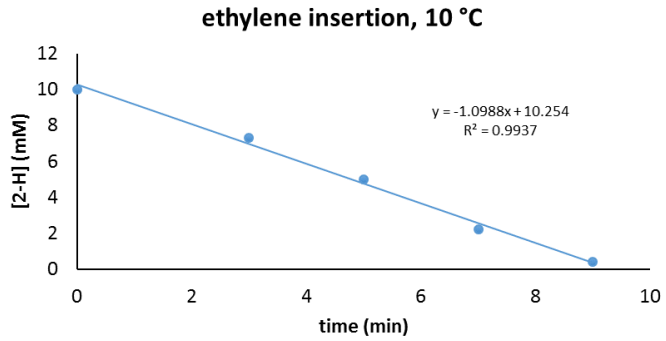

(a)

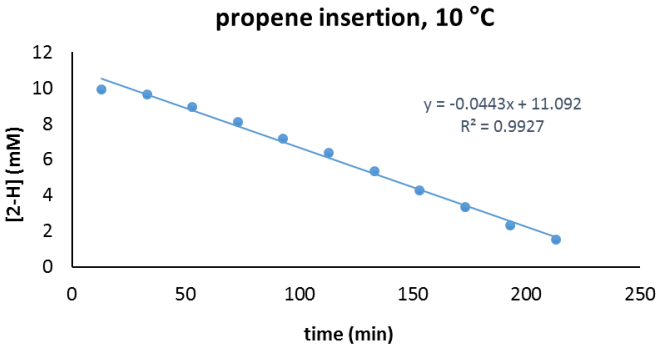

(b)

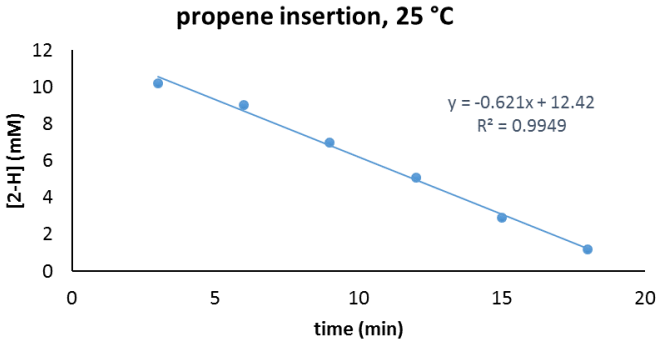

(c)

Figure 2.2. Insertion of olefin into the Ir-H bond of **2-H** catalyzed by $NaBAr^F{}_4$; plots of [**2-H**] vs. time. (a) Ethylene, 1 atm, 10 °C. (b) propene, 1 atm, 10 °C. (c) propene, 1 atm, 25 °C.

The initial rate of reaction of **2-H** with ethylene, catalyzed by $B(C_6F_5)_3$ (1 mM), was 0.107(4) mM/min, independent of $[\mathbf{2\text{-}H}]_o$ for initial concentrations 5 mM, 10 mM and 15 mM (Figure 2.3). Over time the reaction rates decreased, with departure from the initial rate being pronounced at ca. 50% completion. This is consistent with the $B(C_6F_5)_3$ catalyst binding competitively with the reaction product, **2-Et**, as its concentration accumulates. The initial reaction rate showed a linear dependence on the concentration of $B(C_6F_5)_3$ (Figure 2.4). The initial reaction rate also varied linearly with ethylene pressure (Figure 2.5).

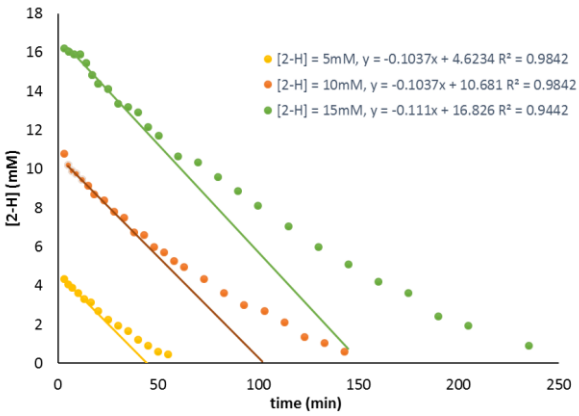

Figure 2.3. Insertion of ethylene (1 atm) into the Ir-H bond of **2-H** catalyzed by $B(C_6F_5)_3$ (1 mM), varying $[\mathbf{2\text{-}H}]_o$; plots of [**2-H**] vs. time.

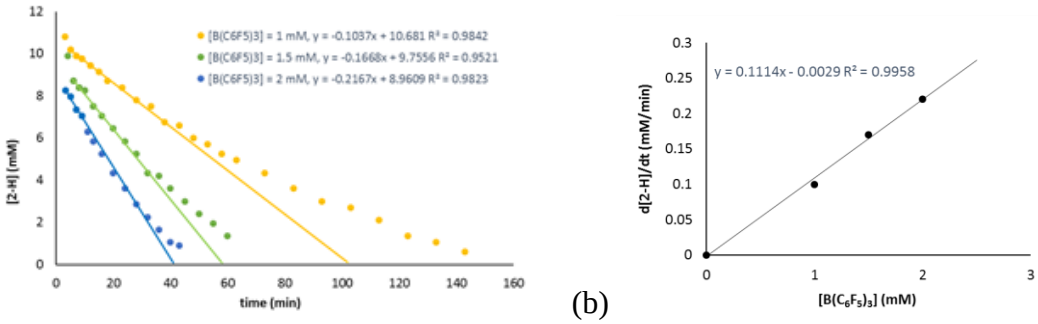

(a) (b)

Figure 2.4. Insertion of ethylene (1 atm) into the Ir-H bond of **2-H** catalyzed by

$B(C_6F_5)_3$, varying $[B(C_6F_5)_3]$. (a) plots of [**2-H**] vs. time. (b) plot of initial rates vs. $[B(C_6F_5)_3]$.

(a)

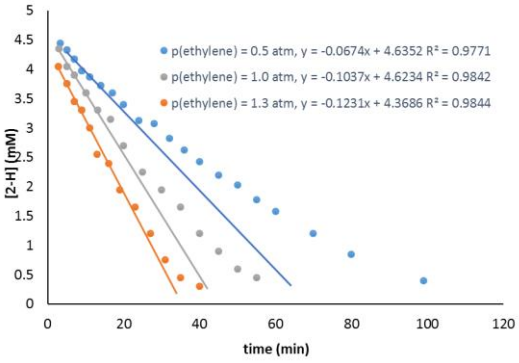

(b)

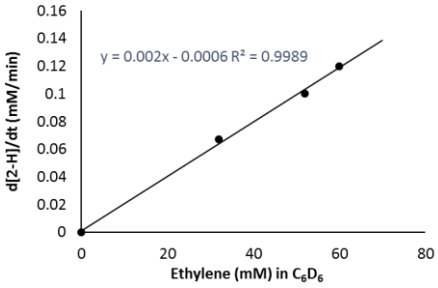

Figure 2.5. Insertion of ethylene into the Ir-H bond of **2-H** catalyzed by $B(C_6F_5)_3$ (1 mM); varying P_{C2H4}. (a) plots of [**2-H**] vs. time. (b) plot of initial rates vs. $[C_2H_4]$.

The kinetic data shown in Figures 2.3-2.5 are explained simply in terms of saturation of the Lewis acid catalyst in substrate **2-H**, as indicated in Scheme 2.4.

Scheme 2.4

$$\textbf{2-H} + \text{LA} \underset{}{\overset{K_1}{\rightleftharpoons}} \textbf{2-H}\bullet\text{LA} \quad (\text{LA} = \text{Lewis acid})$$

$$\textbf{2-H}\bullet\text{LA} + C_2H_4 \xrightarrow{k_1} \textbf{2-Et} + \text{LA}$$

$$-d[\textbf{2-H}]/dt = k_1[\textbf{2-H}\bullet\text{LA}]\bullet[C_2H_4]$$

$$[\textbf{2-H}\bullet\text{LA}] = K_1[\textbf{2-H}]\,[\text{LA}]$$

$$[\text{LA}] = [\text{LA}]_o - [\textbf{2-H}\bullet\text{LA}]$$

$$[\textbf{2-H}\bullet\text{LA}] = K_1[\textbf{2-H}]\,[\text{LA}]_o / \{1 + K_1[\textbf{2-H}]\}$$

Thus, in the limit where $K_1[\textbf{2-H}] >> 1$

$$[\textbf{2-H}\bullet\text{LA}] = [\text{LA}]_o$$

$$-d[\textbf{2-H}]/dt = k_1[\text{LA}]_o\bullet[C_2H_4]$$

Lewis-acid-catalyzed β-hydride elimination. For the dehydrogenation of *n*-octane by (Phebox)Ir(OAc)$_2$(H$_2$O) to afford **2-H** plus octenes (eq 2.1), β-hydride elimination of the intermediate **2-Oc** was found to be the rate-determining step,[5] only proceeding at a significant rate at ca. 200 °C. Remarkably, upon addition of $NaBAr^F{}_4$ to a cyclohexane-d_{12} solution of **2-Oc** (10 mM), the β-hydride elimination proceeded readily at 55 °C, to give 30% conversion after 30 min. The rate of formation of **2-H** was considerably slower after that, with 33% conversion observed after 1 h, but still continued slowly. The kinetics are complicated by an equilibrium between **2-H** and **2-Oc** plus 1-octene, combined with the isomerization of the 1-octene to give equilibrium concentrations of *cis* and *trans* 2-, 3-, and 4-octene (the internal octenes were the major species present, as determined by ^{1}H NMR).

Simulation and fitting of the kinetics data, combined with the known thermodynamics of 1-octene and internal octenes, yields an equilibrium constant for eq 2.5 (for 1-octene) of 1.4×10^{-5} M at 55 °C (see **Experimental** part). The data are consistent with β-hydride elimination being fast relative to octene double-bond isomerization, but the combination of reactions introduces too many degrees of freedom into the fitting process to allow us to determine any individual rate constants. In the case of the $NaBAr^F{}_4$-catalyzed β-hydride elimination of **2-Pe** at 70 °C ($[\mathbf{2\text{-}Pe}]_o$ = 8.6 mM) the reaction apparently reached equilibrium ([**2-H**] = 2.9 mM; 34% conversion) after 40 min, with 2-pentenes observed in the ^{1}H NMR spectrum as the major organic products.

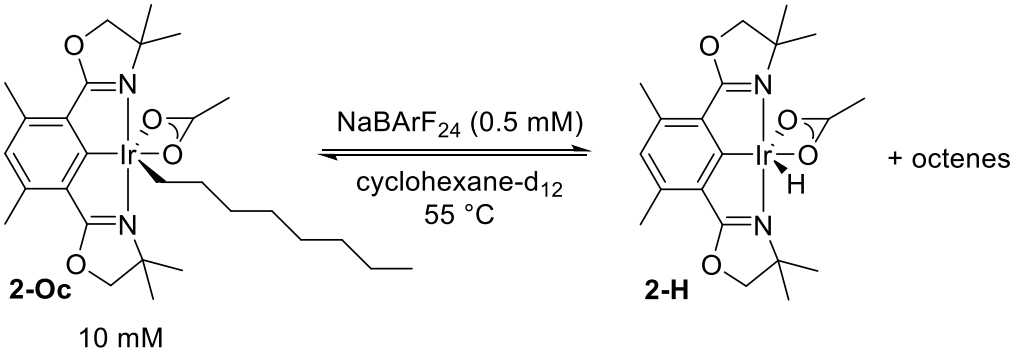

(2.5)

To simplify the analysis by preventing the back reaction of eq 2.5 (octene insertion into the Ir-H bond of **2-H**) we conducted the reaction of **2-Oc** (10 mM in *n*-octane) in the presence of ethylene. Ethylene is expected to undergo insertion into the Ir-H bond of **2-H** more rapidly, and more exothermically, than 1-octene at the low concentrations which would be produced by the β-H elimination reaction of **2-Oc** (and even more so relative to the isomerized, internal, octenes). In the absence of $NaBAr^F{}_4$, under 1 atm C_2H_4 at 125 °C, only 9% conversion of **2-Oc** to **2-Et** was observed after 13 h (eq 2.6). (Interestingly there was also 13% conversion to **2-vinyl**.) This corresponds to a pseudo-first-order rate constant

of ca. 1.9 x 10^{-6} s^{-1} at this temperature, and $\Delta G^{\ddagger}$ = 33.9 kcal/mol. In marked contrast, when a solution was prepared with $NaBAr^{F}_{4}$ (0.38 mM in toluene-d_8), addition of 1 atm C_2H_4 resulted in quantitative conversion of **2-Oc** to **2-Et** within 45 minutes at -15 °C (Figure 2.6).

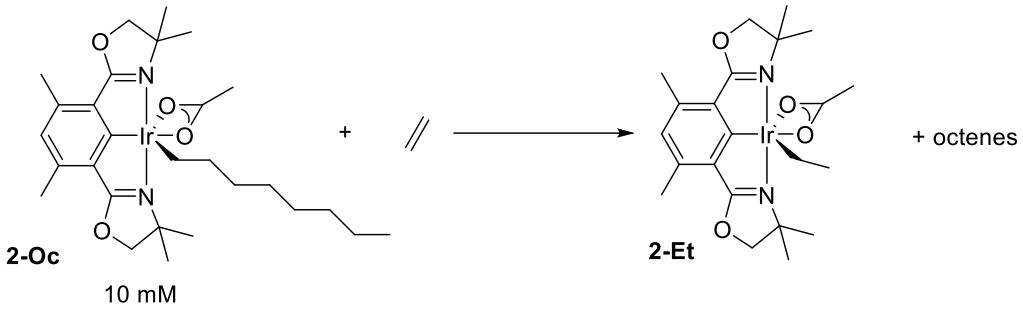

(2.6)

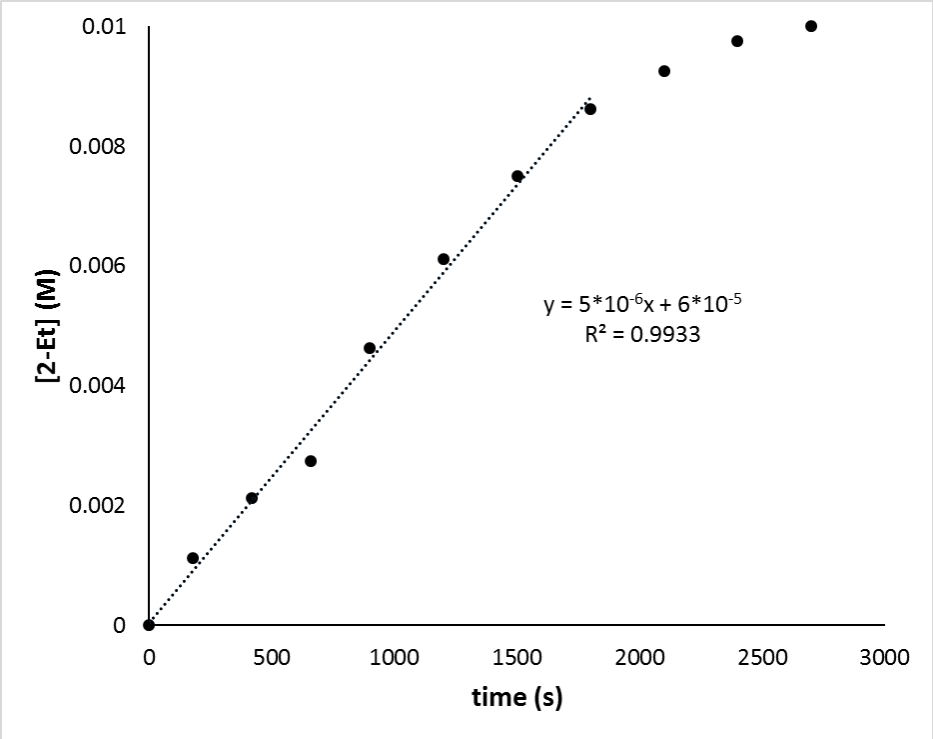

Figure 2.6. Plot of [**2-Et**] vs. time (eq 2.6). Reaction conditions: 1 atm C_2H_4, 10 mM **2-Oct**, 0.38 mM $NaBAr^F{}_4$ in toluene-d_8, -15 °C.

Olefin Insertion/β-Hydride Elimination: DFT Calculations. Since **2-H** is an 18e complex, it may be expected that opening a coordination site would be required to allow the insertion of ethylene into the Ir-H bond or, at the very least, that the availability of a vacant site would facilitate such an insertion. With that in mind, we considered that the catalytic effect of Lewis acids on the insertion/β-H elimination reaction might be attributable to dechelation of an acetate ligand via coordination at oxygen. To further explore this possibility, a series of electronic structure (DFT) calculations were carried out on the full metal pincer-ligand systems using the M06-L functional[28] the SDD effective core potential on Ir,[29] and valence basis sets of triple-zeta plus polarization quality (see Supporting Information for full computational details).[29-33] For the uncatalyzed reaction, Figure 2.7(a), the coordination of an ethylene molecule to **2-H**, trans to the Phebox

coordinating carbon (along with dechelation of the acetate ligand) is computed to be endergonic by 12.2 kcal/mol. We were unable to locate a proper TS on the potential energy surface for ethylene insertion into the Ir-H bond for this intermediate. When ethylene coordinates cis to the Phebox coordinating carbon, the calculations verify that in the ethylene insertion transition state, **TS-2-H/Et**, the acetate ligand is indeed coordinated in a κ^1 fashion (Ir-O distances are 2.19 Å and 3.46 Å; Figure 2.7(a)). However, the calculations predict that the barrier to ethylene insertion, unassisted by Lewis acid, is only 21.0 kcal/mol (Figure 2.7), well below that indicated by experiment (ca. 32 kcal/mol; see above).[34] The origin of this discrepancy is not clear but the calculated barrier to the actual insertion step, subsequent to ethylene coordination, is only $\Delta G^{\ddagger}$ = 3.5 kcal/mol, and is probably understated by the calculations.

Coordination of Na^+ to **2-H** is calculated to lower the barrier to ethylene insertion into the Ir-H bond to 13.1 kcal/mol (Figure 2.7(b)), a decrease of 7.9 kcal/mol, corresponding to a predicted increase in rate by a factor of ca. 10^5 relative to the uncatalyzed reaction. The Ir-O distances (2.19 Å and 3.47 Å) and the geometry of the Ir-H-ethene unit in the Na^+-coordinated TS are essentially the same as in the TS for the Na^+-free TS; the difference in the overall free energy barrier is chiefly due to the difference in energy of the respective ethylene adduct intermediates relative to the respective κ^2-acetate precursors **2-H** and **2-H•Na$^+$** (6.8 kcal/mol). In accord with our hypothesis, the Na^+ cation in the TS is tightly coordinated to the O atom not bound to Ir, with $d_{Na\text{-}O}$ = 2.085 Å (cf. 2.18 Å for the Na-O bond lengths in gas-phase κ^2-CH_3CO_2Na[35]). These data strongly support the proposition that the origin of the catalytic effect of the Na^+ ion is straightforward, specifically, binding

to the acetate terminal oxygen and thereby favoring the κ^1 versus κ^2 binding that is required by the insertion (or β-H elimination) transition state.[36]

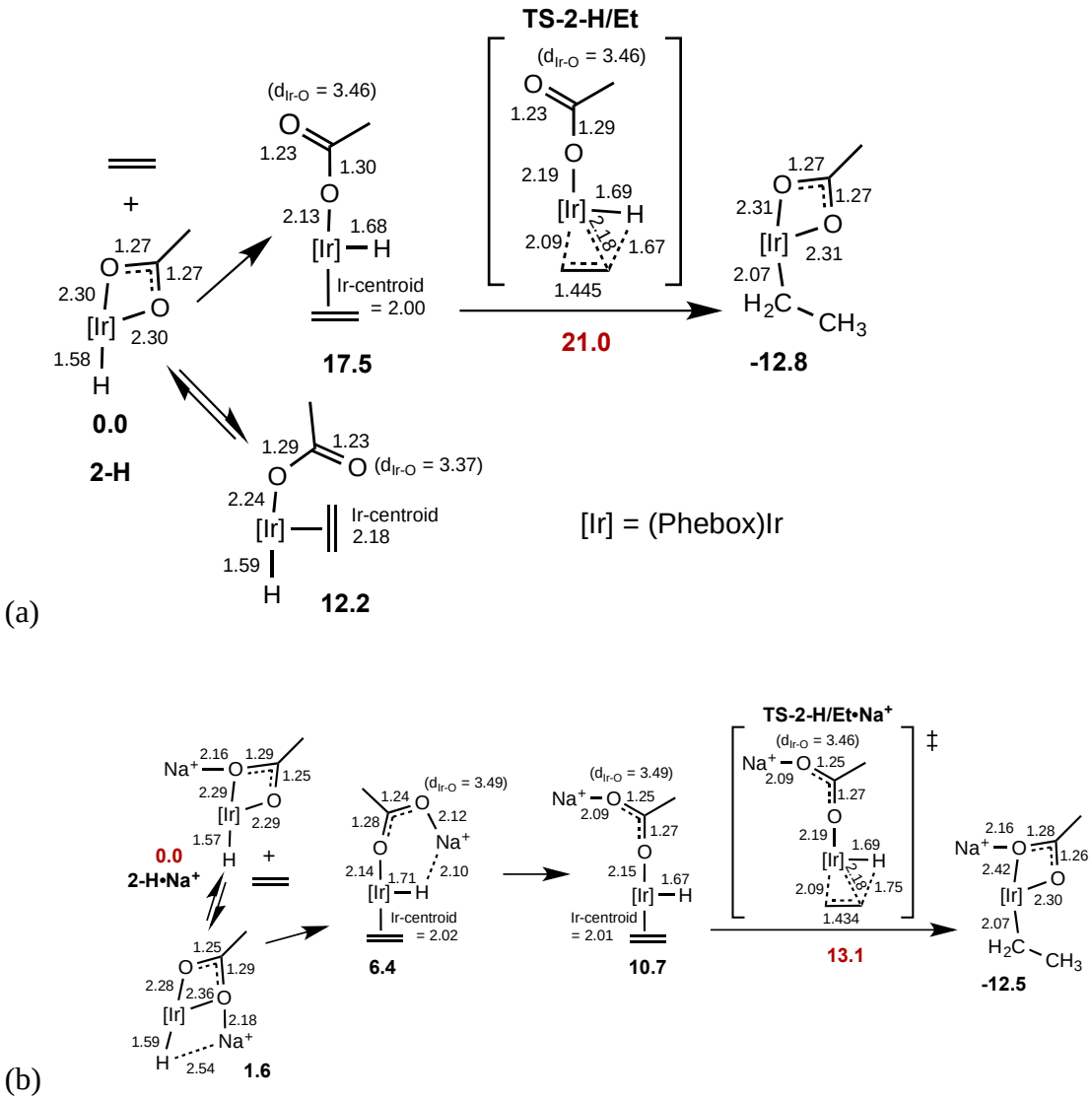

Figure 2.7. Free energies (kcal/mol) and selected bond lengths (Å) of intermediates and transition state for ethylene insertion into the Ir-H bond of **2-H**. (a) Unassisted by Lewis acid. (b) Promoted by Na^+.

C-H Addition or Elimination Promoted by Lewis Acids. The ability of a Lewis acid to open a coordination site in **2-H** or **2-R** to promote olefin insertion or β-H elimination, respectively, raised the question as to whether Lewis acids could catalyze other reactions

that might require a vacant coordination site. C-H bond activation was of particular interest in the context of this class of complexes and this work. To explore this possibility, we initially studied the (energetically downhill) microscopic reverse, a C-H bond elimination, specifically the hydrogenolysis of an Ir-C bond (eq 2.7).

2-R + H_2 ⇌ **2-H** + R-H (2.7)

In accord with the above hypothesis, the rate of reaction between **2-alkyl** and H_2 was substantially increased by the presence of $NaBAr^F{}_4$. In the absence of $NaBAr^F{}_4$, **2-Et** did not react to any significant extent under an atmosphere of H_2 at room temperature. At 50 °C, hydrogenolysis to afford **2-H** and ethane occurred, but in only 3% yield after 24 h. In contrast, in the presence of $NaBAr^F{}_4$ (1.2 mM), the reaction proceeded at 25 °C to give 75% yield of **2-H**, and ethane as revealed by a characteristic signal at δ 0.80 ppm in the ^{1}H NMR spectrum. No ethylene was observed in solution.

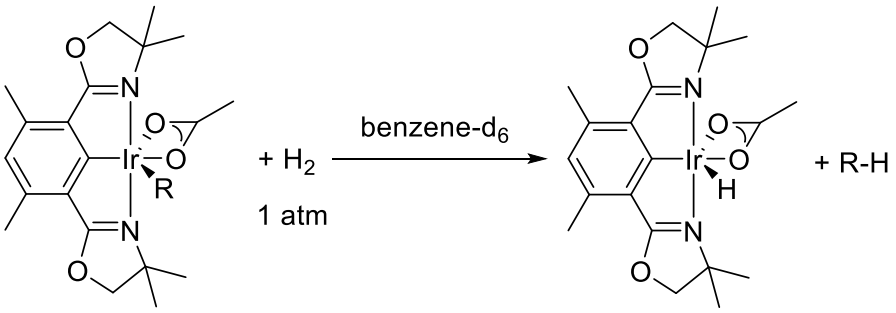

10 mM	R = Et	50 °C, 24 h	3% yield
	R = Et	$NaBArF_{24}$, 25 °C, 24 h	75% yield
	R = Pr	$NaBArF_{24}$, 25 °C, 12 h	75% yield

(2.8)

Analysis of the $NaBAr^F{}_4$-catalyzed reaction of **2-Et** or **2-Pr** with H_2 is complicated by the fact that $NaBAr^F{}_4$ also catalyzes the β-H elimination reaction of these species. Since the β-H elimination is reversible with the equilibrium lying far to the alkyl side (*vide supra*) we

presumed that it was not involved in the net hydrogenolysis. Nevertheless we wished to investigate a species that would preclude this complicating factor in the study of hydrogenolysis (and, in the future, potentially other reactions as well). Toward this end we synthesized **2-Me**, which was characterized by ^{13}C and ^{1}H NMR spectroscopy and single-crystal X-ray diffractometry. As with **2-Et** and **2-Pr**, no reaction of **2-Me** with H_2 was observed in the absence of $NaBAr^F_4$ at 25 °C, whereas in the presence of $NaBAr^F_4$ the complex was converted to **2-H** (75% yield) and methane (δ 0.16 ppm in the ^{1}H NMR spectrum) within 24 h (Figure 2.8).

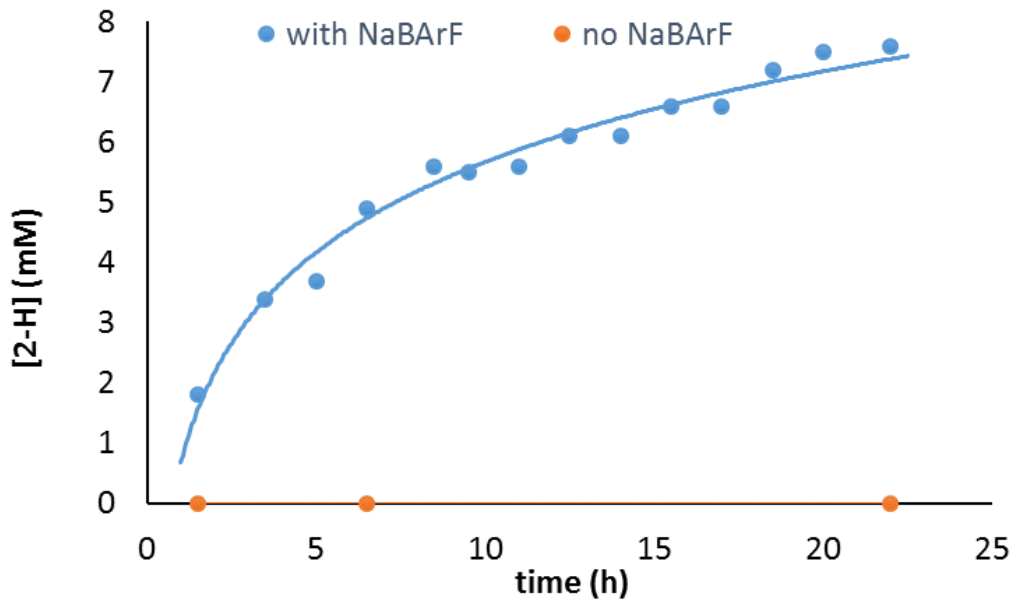

Figure 2.8. Formation of **2-H** in the reaction (eq 7) of **2-Me** (10 mM) with H_2 (1 atm) in C_6D_6, at 25 °C, in the absence and in the presence of $NaBAr^F_4$ (1.2 mM).

Based on microscopic reversibility our results suggest that the reaction of **2-H** with alkanes to give **2-R** plus H_2 should be catalyzed by Na^+ and (perhaps other Lewis acids as well). Since hydrogenolysis of late-metal alkyls is generally thermodynamically quite favorable (for the same reasons and by the same amount that addition of H_2 is thermodynamically

more favorable than addition of R-H[37]) we investigated the reverse of hydrogenolysis (eq 2.8) through H/D exchange experiments.

n-Octane-d_{18} solutions of **2-H** (30 mM) with $NaBAr^F_4$ (4.5 mM) and without $NaBAr^F_4$ were heated to 160 °C. Based on disappearance of the hydride signal in the ^{1}H NMR spectra, conversion of hydride to deuteride occurred in both cases. However, in the case of the solution with $NaBAr^F_4$, but not the solution without $NaBAr^F_4$, extensive incorporation of D into the Phebox and acetate ligands was also observed, manifest by both integration of the ^{1}H NMR signals and by isotopic shifts and splitting/broadening of the signals attributable to the oxazole methyl, benzylic, and acetate protons (Figure 2.9). Interestingly, of the five positions bearing hydrogen, the only position where H/D exchange was not observed was the 5-position (methylene) of the oxazole rings. This is demonstrated by the fact that the ^{1}H NMR signal of this proton remained unchanged as a sharp doublet of doublets (the two hydrogens on each ring are chemically inequivalent), which allowed the integral of this peak to serve as a calibration standard for integration of the other ligand proton signals. We presume that the ligand H/D exchange proceeds via H/D exchange with *n*-octane-d_{18} at the hydride position, followed by exchange (probably intermolecular) with the ligand hydrogens. Thus $NaBAr^F_4$ catalyzes H/D exchange not only at the hydride positions, but at the ligand methyl and aryl positions as well. The more detailed mechanism of these H/D exchanges will be the subject of future study.

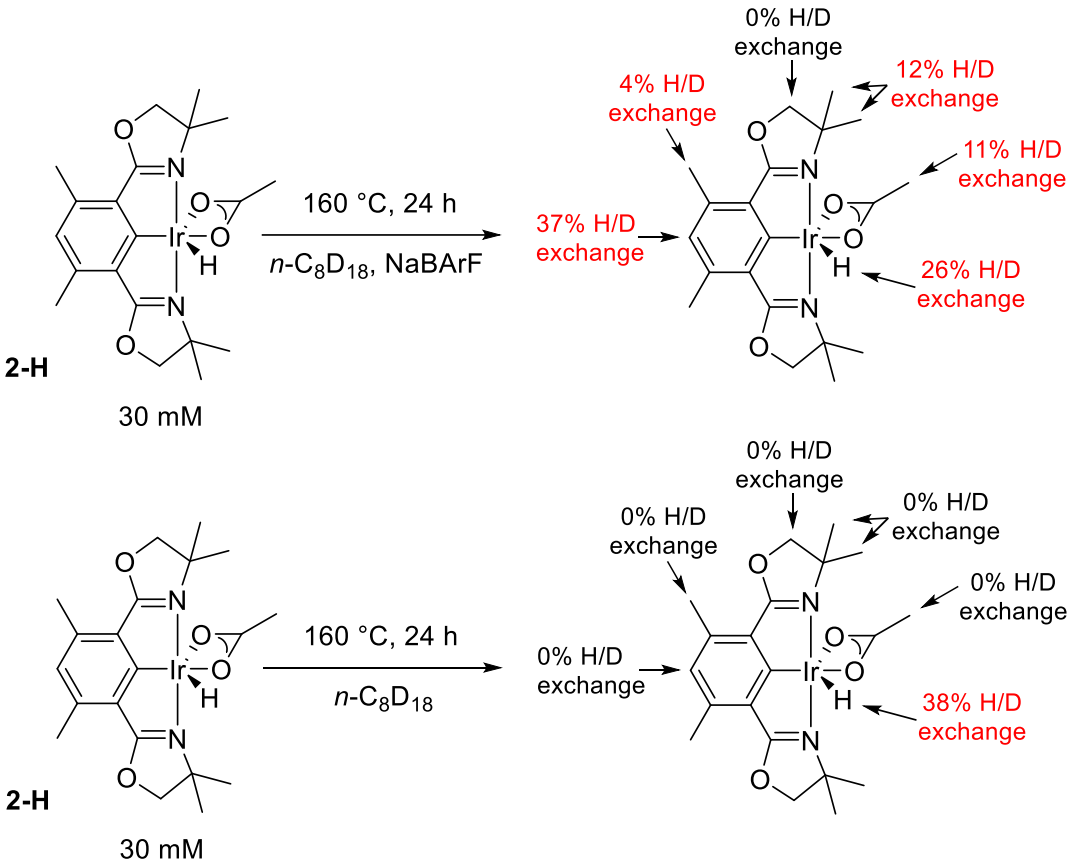

Figure 2.9. H/D exchange of **2-H** with *n*-octane-d_{18} in the presence and in the absence of $NaBAr^F{}_4$ (4.5 mM); percent deuteration at each position of **2-H** is indicated in red.

Hydrogenolysis and C-H activation: DFT calculations. Oxidative addition to Cp*Ir(I) fragments[38-40] are the iconic examples of alkane C-H bond activation, first reported by Bergman in 1982. However, reports[41] of alkane C-H activation by Cp*Ir(III) complexes followed very soon thereafter. Since then, although Ir(I) has perhaps maintained its lead status in this area, C-H activation by Ir(III) has become increasingly well established,[42,43] including within catalytic cycles for hydrogenation and dehydrogenation.[44-47]

DFT calculations suggest that the uncatalyzed hydrogenolysis of **2-Me** proceeds via a CMD-type mechanism. Dechelation of the acetate ligand and addition of H_2 trans to the methyl group gives an intermediate (Phebox)Ir(Me)(κ^1-OAc)(H_2) (**4a**) with a fairly low

free energy, 10.2 kcal/mol relative to **2-Me** (Figure 2.10). Transfer of a proton from the coordinated H_2 to the acetate ligand gives the acetic acid complex (Phebox)Ir(Me)[OC(OH)Me](H) (**5a-syn**), which is also relatively low in free energy (13.2 kcal/mol); this proton transfer is virtually barrierless ($\Delta G^{\ddagger}$ = 0.2 kcal/mol in the reverse, endoergic direction). Rotation around the Ir-O bond of the acetic acid complex would then give the rotamer of (Phebox)Ir(Me)[OC(OH)Me](H) (**5a-anti**), with a free energy of 22.4 kcal/mol. **5a-anti** can undergo protonolysis of the Ir–Me group (the reverse of a CMD activation mechanism); this CMD-type reaction also has a very low barrier ($\Delta G^{\ddagger}$ = 0.6 kcal/mol). The required rotation around the Ir-O bond to give **5a-anti**, however, is sterically very hindered and we are unable to find an accessible intramolecular pathway for this reaction. Alternatively, the isomerization can be achieved via loss of acetic acid and then re-coordination to provide the anti orientation. The coordination of acetic acid could also lead to coordination isomer **5b** which can undergo Ir-Me protonolysis. Likewise, addition of H_2 trans to the Phebox aryl group of **2-Me**, to give **4b** and then **5c**, followed by loss of acetic acid would also give the same intermediate, (Phebox)Ir(Me)(H) (**6**), plus free acetic acid. From either intermediate (**5a-syn** or **5c**), however, loss of acetic acid carries a significant energetic cost; the free energy of **6** plus free acetic acid is calculated as 29.5 kcal/mol. One might envision more facile pathways for the net rotation reaction, **5a-syn** to **5a-anti**, e.g., intramolecular proton transfer (O2-O1) accompanied by slippage of Ir in the reverse direction, but as of yet we have been unable to locate such a TS by computational means. These results are, at least qualitatively, consistent with the experimental observation of a slow hydrogenolysis of **2-Me** in the absence of $NaBAr^F_4$, to give a 3% yield in 24 h at 50 °C, which implies a barrier of $\Delta G^{\ddagger}$ ~ 29 kcal/mol.

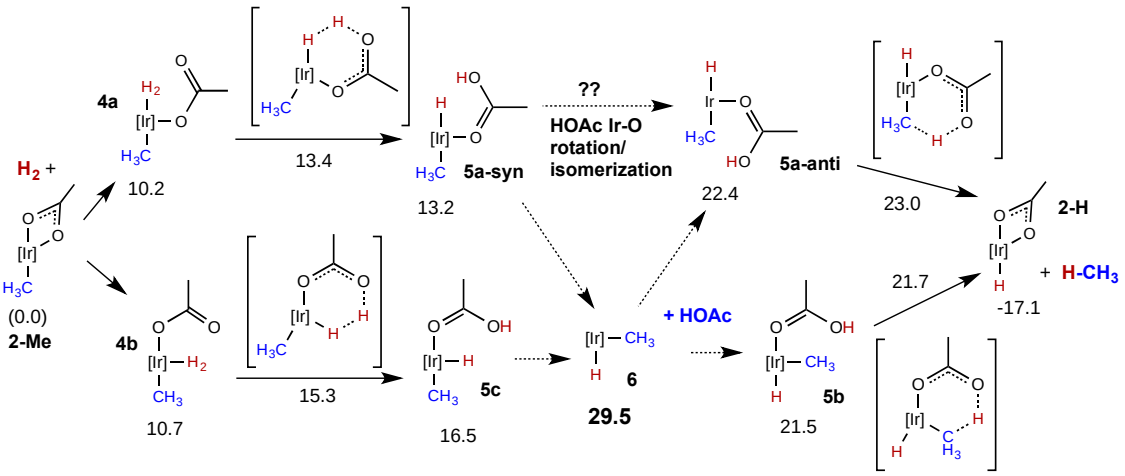

Figure 2.10. CMD-type pathways for hydrogenolysis of the Ir-C bond of **2-Me** (unassisted by Lewis acid); calculated free energies (kcal/mol) of intermediates and transition states indicated.

Two alternative pathways for the uncatalyzed hydrogenolysis of **2-Me**, which do not involve CMD, have also been calculated. Each pathway involves initial coordination of H_2 to the Ir center, producing intermediates **4b** or **4c** respectively, in which CH_3 is coordinated trans to the Phebox aryl and to the acetate group, respectively (Figure 2.11). **4c** is much higher in free energy than isomers **4a** or **4b** (32.2 kcal/mol vs. 10.2 kcal/mol and 10.7 kcal/mol, respectively) consistent with a mutually trans arrangement of the strong-trans-influence aryl and methyl groups. **4c** undergoes oxidative cleavage of the coordinated dihydrogen (Figure 2.11, top path) with virtually no barrier, to give an Ir(V) intermediate, **7** (d_{HH} = 1.44 Å) with free energy 31.3 kcal/mol above reactants (the TS for this reaction is actually lower in free energy than the connected intermediates, although it is a maximum (a first order saddle point) on the electronic potential energy surface). One of the hydride ligands then swings toward the Me group, proceeding through a TS on the potential energy surface with free energy 31.2 kcal/mol above reactants, essentially equal to the free energy of **7**. The TS for hydrogen migration reveals an increased H-H distance, d_{HH} = 1.57 Å, and

incipient C-H bond formation as indicated by a decreased C-H distance (d_{CH} = 1.88 Å) and the Ir-Me bond bending slightly to allow C-H bond formation (Ir-C-H angles = 116.9°, 116.2°, 99.2°). As indicated in Figure 2.11 (upper path), the energy surface is quite flat between the initial dihydrogen adduct **4c** and the C-H bond formation TS.

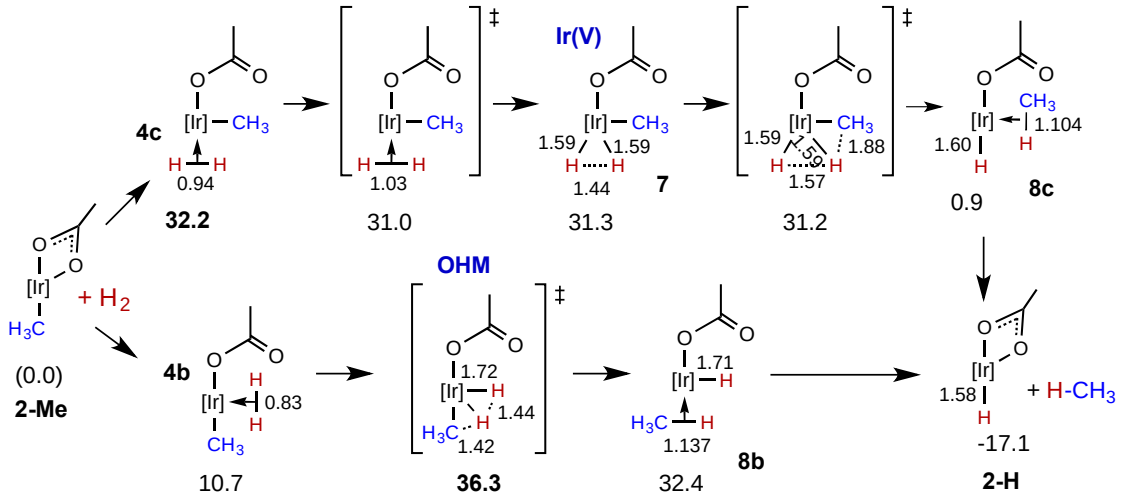

Figure 2.11. Non-CMD (OHM or Ir(V)) pathways for hydrogenolysis of **2-Me** (unassisted by Lewis acid) via H_2 adducts **4b** or **4c**; calculated free energies (kcal/mol) and selected internuclear distances (Å) indicated.

In the case of the other, closely related, pathway, (Figure 2.11, lower path), the H_2 coordinates trans to the Phebox aryl group, rather than trans to the acetate ligand, to give the dihydrogen complex **4b**. This pathway then also proceeds through a species that is Ir(V) in character, but it is a TS, with free energy 36.3 kcal/mol above the reactants. No Ir(V) intermediate was located; thus this appears to be an example of an oxidative hydrogen migration (OHM) pathway.[43]

Thus, both of the calculated non-CMD uncatalyzed pathways (Figure 2.11) appear to have higher overall barriers (>32 kcal/mol and >36 kcal/mol, respectively) than the CMD

pathway of Figure 2.10 (29.5 kcal/mol), even if the CMD pathway must proceed through loss of acetic acid to achieve the net rotation around the Ir-O bond.

We initially considered that a Na^+-catalyzed pathway might proceed analogously to the uncatalyzed pathway, with Na^+ simply favoring the ring-opened intermediates and/or TS's; this was essentially the case for the insertion/β-H elimination reactions discussed above. The situation, however, is apparently not so simple for hydrogenolysis. If we consider the reverse reaction, the CMD activation of methane (**2-H** to **5a-anti** or **5b**), coordination of Na^+ facilitates the dechelation of acetate, but it *strongly lowers the basicity of the unbound O atom*. As a result, the proton transfer from the incoming methane has a TS that is substantially *higher* in free energy (32.3 kcal/mol relative to **2-Me** plus H_2) than the corresponding TS unbound to Na^+ (23.0 kcal/mol; Figure 2.10). Moreover, the step that was apparently rate-limiting in the uncatalyzed case, namely rotation about the Ir-O bond, would still be required subsequent to CMD activation of methane. Thus, rather than introducing a lower barrier to the CMD-type pathway, coordination of Na^+ at the terminal oxygen to promote dechelation is calculated to leave the highest barrier unchanged, while introducing a new, even higher, barrier to the overall reaction.

Thus dechelation of the acetate ligand, required for the CMD pathways of Figure 2.10, is favored by Na^+ coordination but the advantage is more than offset by the resulting decrease in basicity of the ensuing κ^1-acetate terminal oxygen. In the (non-CMD) Ir(V) and OHM pathways (Figure 2.11) however, no such counteracting effect of Na^+ coordination is expected. Coordination of Na^+ to an acetate O atom favors the thermodynamics of dechelation by 5.7 kcal/mol in the case of **4c**, and 8.6 kcal/mol in the case of **4b** (Figure 2.12). Both species then undergo Ir-Me hydrogenolysis via an oxidative hydrogen

migration pathway (the Na^+-coordinated analogue of the Ir(V) intermediate, **7**, in Figure 2.11 is not a stationary point on the potential energy surface). The calculated barriers are approximately equal, with the pathway proceeding through **4b** calculated to have a slightly lower overall free energy barrier of 24.5 kcal/mol. This is ca. 8 kcal/mol lower than the overall barrier of the more favorable of the unassisted *non*-CMD pathways of Figure 2.11. It is also more favorable, by ca. 5 kcal/mol, than the (unassisted) CMD-type pathway (Figure 2.10), which is calculated to be the most favorable pathway in the absence of Na^+ with a barrier of 29.5 kcal/mol.

The sodium cation presumably facilitates the OHM pathway of Figures 2.11 and 2.12 primarily by favoring the κ^1-acetate configuration. In the case of the bottom pathway of Figure 2.12, however, (proceeding via **4b•Na**$^+$) the Na^+ ion appears to play an additional role by interacting with the incipient hydride of the TS connecting **4b•Na**$^+$ with **8b•Na**$^+$. In all the κ^1-acetate complexes shown in Figure 2.2, the Na^+ is positioned over the Phebox phenyl ring (Na^+-centroid distances of ca. 2.5 Å are shown in Figure 2.12), except for **8b•Na**$^+$ and the TS which leads to it. In **8b•Na**$^+$ the calculated Na-H (hydride) distance is particularly short at 2.05 Å. Accordingly, an isomer of **8b•Na**$^+$ in which the Na+ cation is located near the Phebox aryl group (Na^+-centroid distance = 2.50 Å) is 5.9 kcal/mol higher in free energy than **8b•Na**$^+$. In the case of the TS connecting **4b•Na**$^+$ with **8b•Na**$^+$ H-H bonding is still significant and the H atom does not have full hydride character; nevertheless, this TS, as shown in Figure 2.12, is still calculated to be 2.2 kcal/mol lower in free energy than a conformer of this TS (not shown) in which the Na^+ is interacting with the aryl ring (Na^+-centroid distance = 2.53 Å).

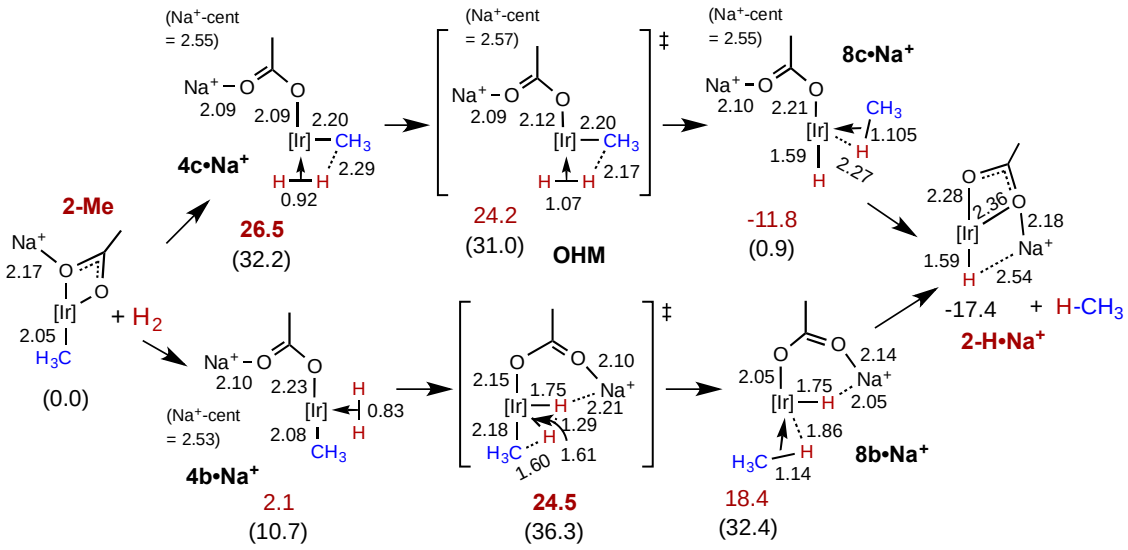

Figure 2.12. Na^+-catalyzed hydrogenolysis of **2-Me** proceeding via H_2 adducts **4b•Na$^+$** or **4c•Na$^+$**; free energies (kcal/mol) and selected internuclear distances (Å) of intermediates and transition states indicated. Energies of analogous species in the unassisted pathway (Figure 2.11) are shown (in parentheses) for comparison. "Na^+-cent" is the calculated distance between the Na^+ cation and the centroid of the Phebox phenyl ring; this is given for all species for which such an interaction is calculated (distance < 3.5 Å).

Thus, while the sodium ion does not promote the more favorable unassisted pathways (CMD, Figure 2.10), it is calculated to lower the barrier to the OHM pathway (Figure 2.11) to a level below that of the unassisted CMD pathway. Results of kinetic isotope experiments, in which **2-Me** reacted with either H_2 or D_2 (eq 2.8), support the proposal that the Na^+-catalyzed and unassisted reactions proceed via qualitatively different pathways (or at least different rate-determining TSs). For the unassisted reaction, the kinetic isotope effect (KIE) of the hydrogenolysis of eq 2.8 is found to be inverse, $k_{H2}/k_{D2} = 0.71\pm0.07$, consistent with a rate-determining step in which the H-H(D-D) bond has been broken and Ir-H(D) and O-H(D) bonds have been formed. The Na^+-catalyzed reaction, by contrast, reveals a normal albeit very small KIE, $k_{H2}/k_{D2} = 1.08\pm0.08$. The directions of both of these KIEs are consistent with the DFT calculations on the respective proposed pathways.[48]

CONCLUSIONS

Transition metal acetate complexes have received great attention in recent years,[49-52] in part thanks to the ability to activate C-H bonds via a CMD mechanism.[8-11] The present system, Nishiyama's Phebox iridium acetate complex, represents an important example of this phenomenon. Here we report that simple Lewis acids, and particularly Na^+, can catalyze two of the most relevant and fundamental organometallic reactions with this complex: olefin insertion and C-H addition (and their respective microscopic reverse reactions). The results of DFT calculations indicate that the Lewis acid catalysts primarily operate via coordination to an acetate oxygen atom which promotes the opening of a vacant coordination site. For C-H addition, the calculations indicate that acetate dechelation by Na^+ promotes a non-CMD, high metal-oxidation-state, pathway. Further investigation is ongoing to determine the scope of the applicability of such Lewis acids in the context of transition metal acetate chemistry, as well as attempts to apply the understanding gained in this work toward the development of new, non-acetate, catalysts.

Experimental

General

Unless specified otherwise, all reactions were conducted under an argon atmosphere using an MBraun glovebox, or Schlenk or vacuum-line techniques. Anhydrous benzene, *p*-xylene, *n*-pentane and THF were purchased from Sigma-Aldrich, stored over molecular sieves in the glovebox and used without further purification. Benzene-d_6, toluene-d_8, *n*-octane-d_{18} and cyclohexane-d_{12} were purchased from Cambridge Isotope Labs, dried over activated alumina and filtered. 1-Pentene, *trans*-2-pentene and 1-octene were purchased

from Sigma-Aldrich, dried over NaK and vacuum-transferred. (Phebox)Ir(OAc)$_2$(OH$_2$) (**1**) was prepared according to published procedures.[53] All other reagents were purchased from commercial suppliers and used without further purification. NMR spectra were acquired on 500 MHz Varian VNMRS NMR spectrometers and ^{1}H and ^{13}C spectra are referenced to residual solvent peaks. Kinetic simulation and fitting was performed using COPASI.[54]

Synthesis and Characterization of Complexes

(Phebox)Ir(OAc)(H) (2-H). **1** (50 mg, 0.0080 mmol) and 5 mL 2-propanol were added to a 50-mL Teflon-stoppered reaction vessel under argon atmosphere and then heated at 100 °C for 2 h. Volatiles were then removed in vacuo. Complex **2** was obtained in 98% yield. Further purification was achieved by recrystallization from diethyl ether/pentane at -32 °C. ^{1}H NMR (C_6D_6, 500 MHz): δ 6.49 (s, 1H), 3.85 (d, *J* = 8.3 Hz, 2H), 3.80 (d, *J* = 8.3 Hz, 2H), 2.64 (s, 6H), 2.05 (s, 3H), 1.33 (s, 6H), 1.29 (s, 6H), -33.80 (s, 1H). ^{13}C NMR (C_6D_6, 125 MHz): δ 185.8, 178.6, 177.2, 139.4, 126.9, 123.0, 81.6, 65.7, 27.3, 26.6, 26.3, 18.9. Anal. Calcd. for **2-H**: C, 43.54; H, 4.93; N. 5.08. Found: C, 43.11; H: 4.74; N, 4.70.

(Phebox)Ir(OAc)(CH$_2$CH$_3$) (2-Et). **2-H** (44 mg, 0.080 mmol) and 5 mL benzene were added to a 25-mL Schlenk flask in the glovebox. The flask was removed from the glovebox and charged with 1 atm of ethylene atmosphere. NaO^{t}Bu (3.8 mg, 0.040 mmol) in benzene solution was added via a syringe dropwise through the septum, at room temperature. The reaction solution was kept at room temperature for 30 min and acetic acid (4.6 µL, 0.080 mmol) was then added via microsyringe. The reaction solution was separated by filtration after 10 minutes. Bright orange powder was obtained after removing the volatiles *in vacuo*. Yield: 42 mg (90%). ^{1}H NMR (C_6D_6, 500 MHz): δ 6.48 (s, 1H), 3.82 (m, 4H), 2.64 (s, 6H), 2.09 (s, 3H), 1.35 (s, 6H), 1.28 (s, 6H), 0.97 (t, *J* = 7.5 Hz, 3H), 0.64 (q, *J* = 7.4 Hz, 2H).

^{13}C NMR (C_6D_6, 125 MHz): δ 184.1, 182.2, 177.2, 139.2, 126.0, 123.2, 82.0, 66.2, 27.2, 27.0, 25.9, 18.9, 15.7, -11.4. Anal. Calcd. for **2-Et**: C, 45.58; H, 5.39; N. 4.83. Found: C, 45.85; H: 5.31; N, 4.55.

(Phebox)Ir(η^2-ethylene)$_2$ (3). 2-H (11 mg, 0.020 mmol) and 2.5 mL benzene were added to a 25-mL Schlenk flask in the glovebox. The flask was removed from the glovebox and charged with 1 atm of ethylene. A benzene solution of NaO^{t}Bu (4.8 mg, 0.050 mmol) was added via syringe dropwise through the septum at room temperature. After 24 h, the volatiles were removed under vacuum and the product was redissolved in toluene (2.5 mL). The clear solution was filtered using a cannula filter. Subsequently, the residue was washed with additional toluene (2.5 mL) and then combined with initial toluene solution. Removal of the volatiles under vacuum resulted in a bright orange powder. Yield: 8.3 mg (76%). ^{1}H NMR (C_6D_6, 500 MHz): δ 6.68 (s, 1H), 3.41 (s, 4H), 3.45-3.32 (m, 4H), 2.66 (s, 6H), 1.65-1.50 (m, 4H), 0.73 (s, 12H). ^{13}C NMR (C_6D_6, 125 MHz): δ 211.1, 178.0, 138.2, 129.0, 126.6, 81.3, 67.8, 31.9, 26.4, 19.0, 10.8. Anal. Calcd. for **3**: C, 48.24; H, 5.71; N. 5.11. Found: C, 47.78; H: 5.40; N, 4.86.

(Phebox)Ir(OAc)(CH$_3$) (2-Me). 3 (55 mg, 0.10 mmol) and 5 mL benzene were added to a 25-mL Schlenk flask in the glovebox. MeI (28 mg, 0.20 mmol) was added via microsyringe at room temperature. After 1 h, all volatiles were removed under vacuum and without further purification, AgOAc (33 mg, 0.2 mmol) in 5 mL THF suspension solution was added to the reaction vessel. The mixture was heated in an oil bath at 50 °C for 2 hours. At the end of reaction, a clear solution was separated by filtration. Subsequent removal of the volatiles in vacuo yielded a residue that was recrystallized from diethyl ether/pentane. Yield: 40 mg (71%). ^{1}H NMR (C_6D_6, 500 MHz): δ 6.44 (s, 1H), 3.82 (d, J = 8.4 Hz, 2H),

3.77 (d, *J* = 8.3 Hz, 2H), 2.60 (s, 6H), 2.00 (s, 3H), 1.26 (s, 6H), 1.25 (s, 6H), 0.37 (s, 3H). ^{13}C NMR (C_6D_6, 125 MHz): δ 185.23, 181.2, 176.9, 139.4, 126.1, 123.1, 82.0, 66.0, 26.8, 26.7, 26.0, 18.9, -25.5. Anal. Calcd. for **2-Me**: C, 44.59; H, 5.17; N. 4.95. Found: C, 45.45; H: 5.55; N, 4.24.

Reactions of 2-H with Ethylene with or without Additive

Without Additive

2-H (2.2 mg, 0.004 mmol), 400 µL of C_6D_6 were added to a sealable NMR tube, which was connected to a Kontes high-vacuum adapter with Tygon tubing. The Kontes valve was attached to a vacuum-gas manifold and the solution was frozen with liquid nitrogen. The headspace of NMR tube was evacuated until the pressure reached 10 mTorr. The headspace was filled with 0.5 atm ethylene and then condensed using liquid nitrogen. After 30 seconds, the NMR tube was sealed using an oxygen torch (the headspace volume was decreased by 50%, which brought the total ethylene pressure to 1 atm). The reaction was conducted at 90 °C and monitored by ^{1}H NMR spectroscopy. 5% **2-Et** and 4% **2-Ph** were formed after 25 h.

NaO^{t}Bu

2-H (2.2 mg, 0.004 mmol), 400 µL of C_6D_6 were added to a J-Young NMR tube in the glovebox. The solution was degassed using one freeze-pump-thaw cycle and charged with 1 atm of ethylene. Then 16 µL of 0.052 M NaO^{t}Bu in C_6D_6 was added and reaction solution was thoroughly mixed. After 1 hour, the volatiles were removed under vacuum and 400 µL of with dioxane (1.17 mM) was added. **2-Et** was obtained in 85% yield and **4** was obtained in 14% yield.

General Procedure with Added Lewis Acid

2-H (2.2 mg, 0.004 mmol), catalyst, 400 µL of C_6D_6, and 10 µL of 0.117 M dioxane in C_6D_6 solution were added to a J-Young NMR tube in a glovebox. The solution was degassed using one freeze-pump-thaw cycle and then charged with 1 atm of ethylene. The reaction was monitored by ^{1}H NMR spectroscopy.

Sodium tetrakis[(3,5-trifluoromethyl)phenyl]borate ($NaBAr^F{}_4$)

Following the general procedure outlined above. $NaBAr^F{}_4$ (0.6 mg, 0.7 µmol) was added to the reaction, it is only partially soluble in benzene (0.2 mM) based on the ^{1}H NMR spectrum. However, sufficient amount of Na^+ was dissolved and the reaction was finished within 5 minutes at room temperature. Yield: 99%.

$NaBAr^F{}_4$ and 15-crown-5

$NaBAr^F{}_4$ (2 mg) was added to a C_6D_6 solution of 15-crown-5 (0.8 mL, 12 mM). After leaving at room temperature overnight, undissolved $NaBAr^F{}_4$ was removed by filtration through Celite. The concentration of $NaBAr^F{}_4$ in solution was determined to be 1 mM by ^{1}H NMR spectroscopy by comparison to an internal standard. Following the general procedure, 0.4 mL of 15-crown-5 (12 mM) and $NaBAr^F{}_4$ (1 mM) in C_6D_6 solution and **2-H** (2.2 mg, 0.004 mmol) were added. Only trace amount (less than 3%) of **2-Et** was detected by ^{1}H NMR spectroscopy after 2 days at room temperature.

Lithium tetrakis(pentafluorophenyl)borate ethyl etherate ($[Li(OEt_2)_3][B(C_6F_5)_4]$)

Following the general procedure outlined above. $[Li(OEt_2)_3][B(C_6F_5)_4]$ (0.6 mg, 0.9 µmol) was added to the reaction solution. The reaction was completed within 5 minutes at room temperature. Yield: 98%.

Triphenylborane

Following the general procedure, 50 µL of 40 mM $B(C_6H_5)_3$ in C_6D_6 solution was added and the reaction was finished after 5 days under 50 °C. Yield: 98%.

Tris(pentafluorophenyl)borane

Following the general procedure outlined above. 20 µL of 40 mM $B(C_6F_5)_3$ in C_6D_6 solution was added to the reaction mixture. The reaction was finished after 2 hours at room temperature. Yield: 99%.

Catalyst	**Additive**	**Temperature (°C)**	**Time**	**Yield**
$NaBAr^F_4$	-	25	5 min	99%
$NaBAr^F_4$	15-crown-5	25	2 days	<3%
$[Li(OEt_2)_3][B(C_6F_5)_4]$	-	25	5 min	98%
$B(C_6H_5)_3$	-	50	5 days	98%
$B(C_6F_5)_3$	-	25	2 hours	99%

Reaction of 2-H with Alkenes Catalyzed by $NaBAr^F_4$

2-H (2.2 mg, 0.004 mmol), $NaBAr^F_4$ (0.6 mg, 0.7 µmol), 400 µL of C_6D_6 and 10 µL of 0.117 M dioxane in C_6D_6 solution were added to a J-Young NMR tube under argon atmosphere in the glovebox. Alkenes were then added and the reaction was monitored by ^{1}H NMR.

Propene

(Phebox)Ir(OAc)($CH_2CH_2CH_3$) (2-Pr). 2-H (2.2 mg, 0.004 mmol), $NaBAr^F_4$ (0.6 mg, 0.7 μmol), 400 μL of C_6D_6 and 10 μL of 0.117 M dioxane in C_6D_6 solution were added to a J-Young NMR tube in the glovebox. The solution was degassed using one freeze-pump-thaw cycle and then charged with 1 atm of propene. The reaction was finished in 15 minutes at room temperature. Yield: 98%. ^{1}H NMR (C_6D_6, 500 MHz): δ 6.49 (s, 1H), 3.82 (m, 4H), 2.65 (s, 6H), 2.08 (s, 3H), 1.82-1.54 (m, 2H), 1.33 (s, 6H), 1.28 (s, 6H), 1.04 (t, *J* = 7.3 Hz, 3H), 0.68-0.44 (m, 2H). ^{13}C NMR (C_6D_6, 125 MHz): δ 184.4, 182.2, 177.2, 139.2, 126.0, 123.1, 82.0, 66.2, 27.1, 27.0, 26.0, 24.3, 19.0, 15.7, -0.7.

1-Pentene

(Phebox)Ir(OAc)($CH_2(CH_2)_3CH_3$) (2-Pe). 1-pentene (2.2 μL, 0.02 mmol). Reaction was finished in 1 hour at room temperature. Yield: 94%. ^{1}H NMR (C_6D_6, 500 MHz): 6.48 (s, 1H), 3.85 (d, *J* = 8.3 Hz, 2H), 3.82 (d, *J* = 8.3 Hz, 2H), 2.64 (s, 6H), 2.07 (s, 3H), 1.75-1.65 (m, 2H), 1.18-1.46 (m, 4H), 1.37 (s, 6H), 1.28 (s, 6H), 0.91 (t, *J* = 6.9 Hz, 3H), 0.59-0.53 (m, 2H). ^{13}C NMR (C_6D_6, 125 MHz): δ 184.3, 182.1, 177.3, 139.3, 126.0, 123.2, 82.0, 66.2, 34.1, 30.9, 27.2, 27.0, 25.9, 23.1, 19.0, 14.6, -3.4.

trans-2-Pentene

(Phebox)Ir(OAc)($CH_2(CH_2)_3CH_3$) (2-Pe). *trans*-2-pentene (2.2 μL, 0.02 mmol). Reaction was finished in 1 hour at room temperature. The linear alkyl insertion product was observed by ^{1}H NMR spectroscopy. Yield: 93%.

1-Octene

(Phebox)Ir(OAc)($CH_2(CH_2)_6CH_3$) (2-Oc). 1-octene (6.3 µL, 0.04 mmol). Reaction was finished in 1 hour at room temperature. Yield: 96%. ^{1}H NMR (C_6D_6, 500 MHz): δ 6.49 (s, 1H), 3.86 (d, *J* = 8.3 Hz, 2H), 3.82 (d, *J* = 8.3 Hz, 2H), 2.64 (s, 6H), 2.08 (s, 3H), 1.76-1.66 (m, 2H), 1.47-1.39 (m, 4H), 1.39 (s, 6H), 1.29 (s, 6H), 1.26–1.19 (m, 6H), 0.85 (t, *J* = 6.9 Hz, 3H), 0.63–0.56 (m, 2H). ^{13}C NMR (C_6D_6, 125 MHz): δ 184.3, 182.2, 177.3, 139.3, 1260, 123.2, 82.0, 66.2, 32.4, 31.9, 31.3, 30.2, 30.0, 27.2, 27.0, 25.9, 23.2, 19.0, 14.4, -3.3.

Typical Procedure for Kinetics Experiments

$NaBAr^F{}_4$ as catalyst

A C_6D_6 (1.6 mL) stock solution of **2-H** (8.8 mg, 0.016 mmol) and 40 µL of 0.117 M dioxane was prepared in the glovebox. $NaBAr^F{}_4$ (0.6 mg) was added to the solution and then filtered after 30 minutes. The concentration of **2-H** (10 mM) and $NaBAr^F{}_4$ (0.18 mM) was determined by ^{1}H NMR spectroscopy. For each kinetic run, a 0.4 mL sample of stock solution was transferred to a J-Young NMR tube in the glovebox. The solution was degassed using one freeze-pump-thaw cycle, charged with 1 atm of alkene gas, and then quickly frozen in liquid nitrogen until NMR data acquisition was started. Two different alkenes, ethylene and propene, were used as the substrate and the reactions were conducted at two different temperatures, 25 °C and 10 °C. (The reaction at 25 °C with ethylene was complete in 4 minutes and the data collected is not enough for a plot).

Tris(pentafluorophenyl)borane as catalyst

Stock solutions of **2-H**, tris(pentafluorophenyl)borane and dioxane in C_6D_6 were prepared. For each kinetic run, the appropriate amount of each reagent was added via syringe to a J. Young NMR tube. The solution was degassed using one freeze-pump-thaw cycle, charged

with 1 atm of ethylene, and then quickly frozen in liquid nitrogen until NMR data acquisition was started. All data was collected at 25 °C.

β-Hydride Elimination Reactions of 2-Alkyl Catalyzed by $NaBAr^F_4$

2-H (2.2 mg, 0.004 mmol), $NaBAr^F_4$ (0.6 mg, 0.7 μmol), 400 μL of C_6D_6, and alkene were added to a J-Young NMR tube in the glovebox. After 1 hour at room temperature, the reaction solution was filtered through cotton wool and transferred to a second J-Young NMR tube. All volatiles were removed under vacuum and 400 μL of cyclohexane-d_{12} and 10 μL of 0.117 M dioxane in cyclohexane-d_{12} solution were added. The reaction was conducted at high temperature and monitored by ^{1}H NMR spectroscopy.

*(Phebox)Ir(OAc)($CH_2(CH_2)_6CH_3$) (**2-Oc**)*

The reaction was performed following the general procedure outlined above. The β-hydride elimination reaction was conducted at 55 °C. Kinetic simulation and fitting was performed using COPASI (**Figure 2.13**) and the following reaction scheme.

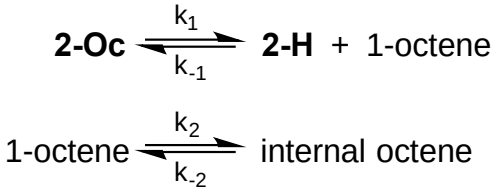

Based upon known thermodynamic data,[55] the equilibrium constant for 1-octene isomerization with all linear internal octenes is calculated to be 253. With $K_2 = k_2/k_{-2}$ fixed at that value, the data can be successfully modeled with a value of $K_1 = k_1/k_{-1} = 1.4 \times 10^{-5}$ M, the equilibrium constant for β-hydride elimination by **2-Oc** at 55 °C. The combination of reactions introduces too many degrees of freedom into the fitting process to allow us to

meaningfully determine individual rate constants, but a good fit was obtained using the following rate constants: k_1 = 0.082 s^{-1}, k_{-1} = 5.8 × 10^3 M^{-1} s^{-1} (K_1 = 1.4 × 10^{-5} M), k_2 = 0.025 s^{-1}, k_{-2} = 9.6 × 10^{-5} s^{-1} (K_2 = 253).

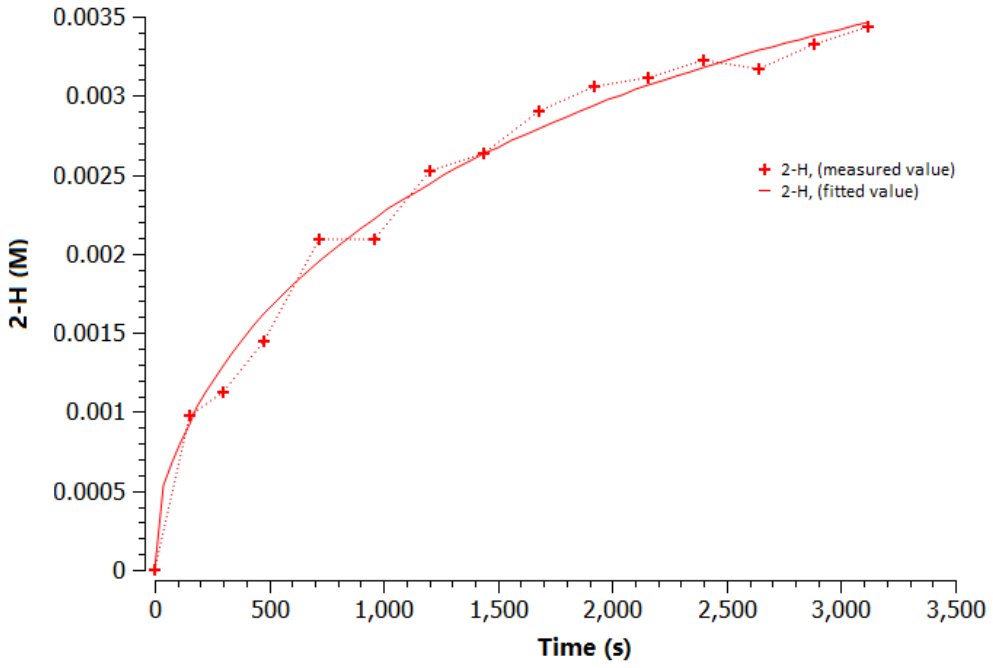

Figure 2.13. Result of kinetic fitting and simulation for β-hydride elimination of **2-Oc** and 1-octene isomerization to internal octenes. Reaction conditions: 10 mM [Ir], 0.5 mM $NaBAr^F{}_4$, 0.4 mL cyclohexane-d_{12}, 55 °C.

*(Phebox)Ir(OAc)($CH_2(CH_2)_3CH_3$) (**2-Pe**)*

Following the general procedure, *trans*-2-pentene (2.2 μL, 0.02 mmol) was added. β-Hydride elimination was observed at 70 °C. After 40 minutes, the reaction reaches equilibrium and the pentene observable in the ^{1}H NMR spectrum is only 2-pentenes (**Table 2.1**, **Figure 2.14**). Again, the combination of reactions introduces too many degrees of freedom to allow meaningful determination of individual rate constants, but a good fit was

obtained with the following: k_1 = 0.53 s^{-1}, k_{-1} = 1.6 × 10^4 M^{-1} s^{-1} (K_1 = 3.3 × 10^{-5} M), k_2 = 0.016 s^{-1}, k_{-2} = 3.4 × 10^{-4} s^{-1} (K_2 = 47)

Table 2.1 Concentration of species at equilibrium and equilibrium constant at 70 °C

[2-Pe]	**[2-H]**	**[2-pentenes]**	**K_{eq} = [2-pentene][2-H]/[2-Pe]**
5.7 mM	2.9 mM	2.0 mM	1.0 × 10^{-3} M

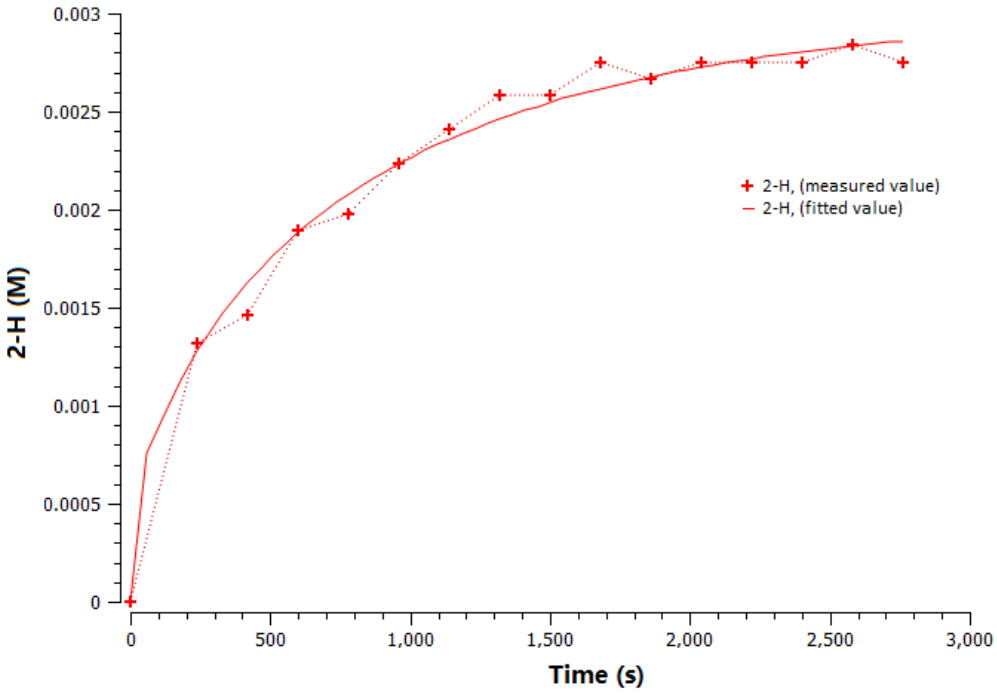

Figure 2.14. Result of kinetic fitting and simulation for β-hydride elimination of **2-Pe**. Reaction conditions: 8.6 mM [Ir], 0.4 mM $NaBAr^F{}_4$, 0.4 mL cyclohexane-d_{12}, 70 °C.

Reaction of 2-Oc with ethylene

Without additive

2-Oc (2.7 mg, 0.004 mmol) and 400 µL of cyclohexane-d_{12} were added to a sealable NMR tube in the glove box. The NMR tube was connected to a Kontes high-vacuum adapter via Tygon tubing and then attached to a vacuum-gas manifold. The solution was frozen with liquid nitrogen and the headspace of NMR tube was evacuated until 10 mTorr was reached. The headspace was backfilled with 0.5 atm of ethylene. The NMR tube was then half immersed in liquid nitrogen to condense the ethylene. After 30 seconds, the NMR tube was sealed using an oxygen torch (the volume of the headspace decreased by 50% resulting in an ethylene pressure of 1 atm). The NMR tube was carefully warmed to room temperature, and then placed inside a GC oven and heated to 125 °C for 13 h. 9% **2-Et** and 13% **2-Vinyl** were detected by ^{1}H NMR spectroscopy.

$NaBAr^F{}_4$ as catalyst

2-Oc (10.8 mg, 0.016 mmol), $NaBAr^F{}_4$ (0.6 mg, 0.7 µmol), 0.5 µL dioxane and 1.6 mL of C_7D_8 were added to a small vial under argon atmosphere in glovebox and filtered after 30min. ^{1}H NMR spectrum showed the stock solution with 10 mM **2-Oc** and 0.38 mM $NaBAr^F{}_4$. 400 µL of stock solution was added to a sealable NMR tube, which is then connected to a Kontes high-vacuum adapter via a length of Tygon tubing. The Kontes valve was attached to a vacuum-gas manifold and the solutions inside were frozen with liquid nitrogen. The headspace of NMR tube was evacuated down to 10 mTorr and then placed under 0.5 atm ethylene. The NMR tube was half immersed in liquid nitrogen, allowing the ethylene to condense. After 30 seconds, the NMR tube was sealed with an oxygen torch (this decrease the volume by 50% and brought the total pressure to 1 atm). The sealed NMR tube was kept frozen in liquid nitrogen until NMR data acquisition could begin. Reaction

was monitored by ^{1}H NMR at -15 °C (**Fig. 2.15**). The reaction was over in 45 minutes with 10 mM **2-Et** and 6.5 mM 1-octene formed.

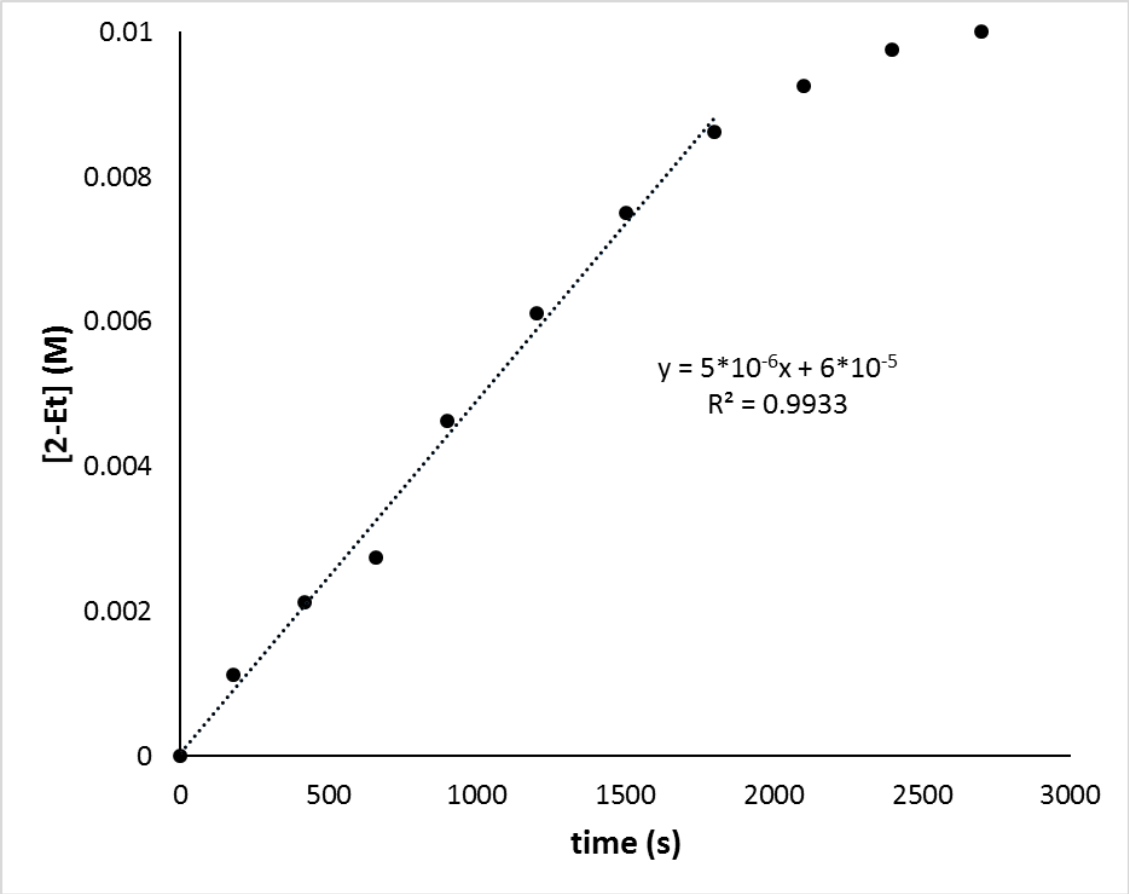

Figure 2.15. Plot of [**2-Et**] vs. time under ethylene atmosphere. Reaction conditions: 1 atm C_2H_4, 10 mM **2-Oc**, 0.38 mM $NaBAr^F_4$ in toluene-d_8, -15 °C.

Typical Procedure for Hydrogenolysis of 2-Alkyl Catalyzed by $NaBAr^F_4$

(Phebox)Ir(OAc)(alkyl) (0.004 mmol), 0.6 mg $NaBAr^F_4$, 400 µL of C_6D_6, and 10 µL of 0.117 M dioxane in C_6D_6 solution were added to a J-Young NMR tube in a glovebox. The solution was degassed using one freeze-pump-thaw cycle and then charged with 1 atm of hydrogen gas. The reaction was conducted at room temperature and monitored periodically by ^{1}H NMR spectroscopy.

Kinetic Isotope Effect (KIE) Experiments

Without additive

400 µL of 10 mM of **2-Me** in *p*-xylene-d_{10} solution was added to a sealable NMR tube, which was then connected to a Kontes high-vacuum adapter via Tygon tubing. The Kontes valve was attached to a vacuum-gas manifold and the solution was frozen with liquid nitrogen. The headspace of NMR tube was evacuated to 10 mTorr pressure and then 1 atm of hydrogen or deuterium was added. The NMR tube was half immersed in liquid nitrogen for 1 minute and then sealed with an oxygen torch. The sealed NMR tube was carefully warmed to room temperature, and then heated in a GC oven at 85 °C. The NMR tube was rotated inside the oven to allow efficient gas-liquid mixing. The reaction was monitored by ^{1}H NMR spectroscopy over several hours. Initial reaction rates were calculated (See **Figure 2.16 (a)**) and the ratio of k_H/k_D was found to be 0.71±0.07.

$NaBAr^F{}_4$ as catalyst

400 µL of a C_6D_6 stock solution with **2-Me** (10 mM), and $NaBAr^F{}_4$ (1.2 mM) was added to a J-Young NMR tube in a glovebox. The solution was degassed using one freeze-pump-thaw cycle and then charged with 1 atm of hydrogen or deuterium. Each reaction was monitored by ^{1}H NMR spectroscopy at room temperature. Initial reaction rates for both of the reactions were calculated (See **Figure 2.16 (b)**) and the ratio of k_H/k_D was found to be 1.08±0.08.

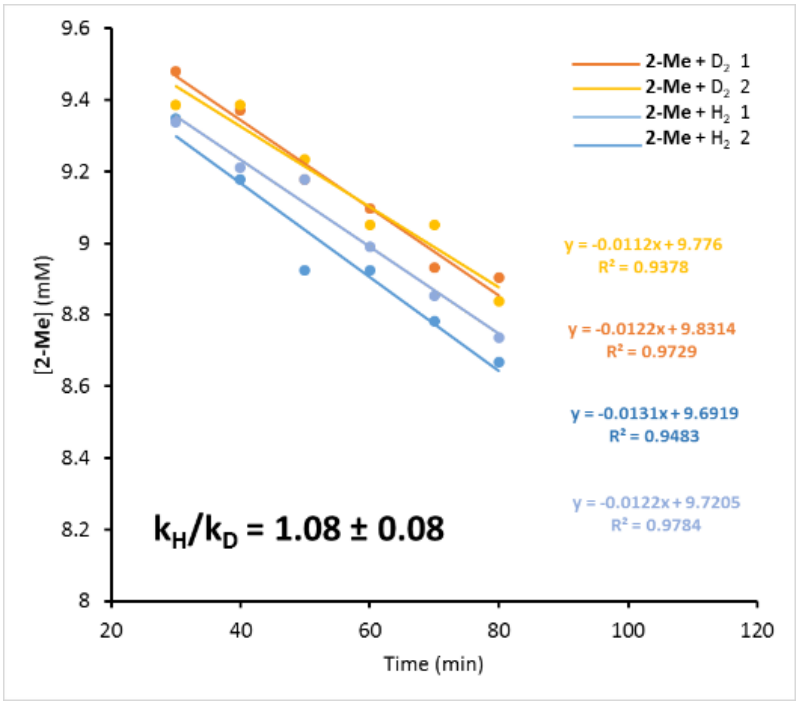

(a)

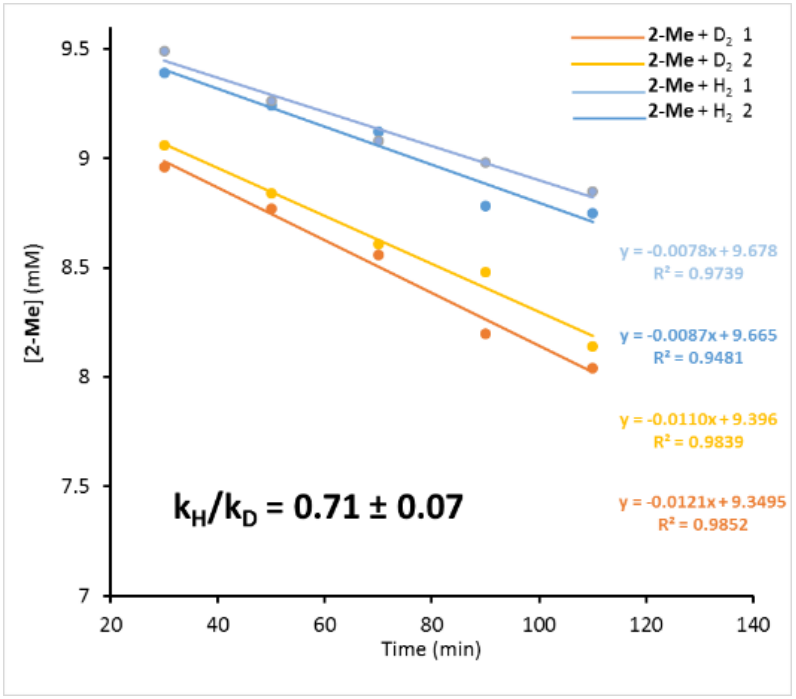

(b)

Figure 2.16. Hydrogenolysis of **2-Me**, plots of [**2-Me**] vs time. (a) 1 atm H_2 (blue) or D_2 (orange and yellow), 10 mM **2-Me** in C_8D_{10}, 85 °C (b) 1 atm H_2 (blue) or D_2 (orange and

yellow), 10 mM **2-Me**, 1.2 mM $NaBAr^F{}_4$ in C_6D_6, 25 °C. Error determined from averaged repeat experiments.

Typical Procedure for H/D Exchange Reaction of Hydride of 2-H by *n*-Octane-d_{18}

2-H (1.8 mg, 0.003 mmol), 0.4 mg $NaBAr^F{}_4$, 100 µL of *n*-octane-d_{18} were added to a sealable glass tube in a glovebox. The tube was then connected to a Kontes high-vacuum adapter via Tygon tubing and attached to a vacuum line. The solution was frozen in liquid nitrogen, and the headspace of the tube was evacuated down to 10 mTorr. With the bottom of the tube still immersed in liquid nitrogen, the tube was sealed using an oxygen torch. The sealed tube is allowed to reach room temperature, then heated inside a GC oven for the desired amount of time. After cooling to room temperature, the reaction solution was transferred to a J-Young NMR tube inside an argon glovebox, all the volatiles were then removed under vacuum and 400 µL of C_6D_6 was added. ^{1}H NMR spectra were used to analyze H/D exchange result.

General information for X-ray structure determination

Single-crystal X-ray diffraction data were collected on a Bruker Smart APEX CCD diffractometer with graphite monochromatized Mo Ka radiation (l = 0.71073Å) at 100 K. The crystals were immersed in oil and placed on a glass needle in the cold stream. The data were corrected for Lorenz effects, polarization, and absorption, the latter by a multi-scan method using program SAINT.[56] The structures were solved by direct methods using program SHELXS.[57] Using program SHELXL,[5 58] all non-hydrogen atoms were refined based upon Fobs and all hydrogen atom coordinates were calculated with idealized geometries.

Table 2.2. Crystal data and structure refinement for **2-Et**.

Identification code	Ir-OAc-Et_ordered	
Empirical formula	C22 H31 Ir N2 O4	
Formula weight	579.69	
Temperature	100(2) K	
Wavelength	0.71073 Å	
Crystal system	Orthorhombic	
Space group	P b c a	
Unit cell dimensions	a = 12.5997(7) Å	α= 90°.
	b = 18.2207(10) Å	β= 90°.
	c = 19.5033(11) Å	γ= 90°.
Volume	4477.5(4) $Å^3$	
Z	8	
Density (calculated)	1.720 Mg/m^3	
Absorption coefficient	5.993 mm^{-1}	
F(000)	2288	
Crystal size	0.600 x 0.200 x 0.100 mm^3	
Theta range for data collection	2.088 to 31.505°.	
Index ranges	-18<=h<=18, -26<=k<=26, -28<=l<=28	
Reflections collected	57464	
Independent reflections	7465 [R(int) = 0.0400]	
Completeness to theta = 25.242°	100.0 %	
Absorption correction	Numerical	
Max. and min. transmission	0.6944 and 0.1994	
Refinement method	Full-matrix least-squares on F^2	
Data / restraints / parameters	7465 / 0 / 270	
Goodness-of-fit on F^2	1.008	
Final R indices [I>2sigma(I)]	R1 = 0.0279, wR2 = 0.0664	
R indices (all data)	R1 = 0.0404, wR2 = 0.0729	
Extinction coefficient	n/a	
Largest diff. peak and hole	2.511 and -0.831 $e.Å^{-3}$	

Table 2.3. Crystal data and structure refinement for **3**.

Identification code	twin5	
Empirical formula	C22 H31 Ir N2 O2	
Formula weight	547.69	
Temperature	100(2) K	
Wavelength	0.71073 Å	
Crystal system	Triclinic	
Space group	P -1	
Unit cell dimensions	a = 9.3340(10) Å	α= 111.002(2)°.
	b = 11.4364(12) Å	β= 109.988(2)°.
	c = 15.3376(16) Å	γ= 120.760(2)°.
Volume	992.95(18) $Å^3$	
Z	2	
Density (calculated)	1.832 Mg/m^3	
Absorption coefficient	6.743 mm^{-1}	
F(000)	540	
Crystal size	0.180 x 0.130 x 0.045 mm^3	
Theta range for data collection	1.881 to 31.039°.	
Index ranges	-13<=h<=13, -16<=k<=16, -22<=l<=22	
Reflections collected	21258	
Independent reflections	21258 [R(int) = ?]	
Completeness to theta = 25.242°	100.0 %	
Absorption correction	Semi-empirical from equivalents	
Max. and min. transmission	0.4334 and 0.2536	
Refinement method	Full-matrix least-squares on F^2	
Data / restraints / parameters	21258 / 0 / 251	
Goodness-of-fit on F^2	1.004	
Final R indices [I>2sigma(I)]	R1 = 0.0669, wR2 = 0.1555	
R indices (all data)	R1 = 0.0736, wR2 = 0.1596	
Extinction coefficient	n/a	
Largest diff. peak and hole	3.701 and -4.885 $e.Å^{-3}$	

Reference

(1) Kumar, A.; Goldman, A. S. In *The Privileged Pincer-Metal Platform: Coordination Chemistry & Applications*; van Koten, G., Gossage, R. A., Eds.; Springer International Publishing: Cham, 2016, p 307.

(2) Choi, J.; MacArthur, A. H. R.; Brookhart, M.; Goldman, A. S. *Chem. Rev.* **2011**, *111*, 1761.

(3) Dobereiner, G. E.; Crabtree, R. H. *Chem. Rev.* **2010**, *110*, 681.

(4) Ito, J.-i.; Kaneda, T.; Nishiyama, H. *Organometallics* **2012**, *31*, 4442.

(5) Allen, K. E.; Heinekey, D. M.; Goldman, A. S.; Goldberg, K. I. *Organometallics* **2013**, *32*, 1579.

(6) Kumar, A.; Goldman, A. S. In *Top. Organomet. Chem.*; van Koten, G., Gossage, R. A., Eds.; Springer International Publishing: 2016; Vol. 54, p 307.

(7) Davies, D. L.; Donald, S. M. A.; Macgregor, S. A. *J. Am. Chem. Soc.* **2005**, *127*, 13754.

(8) Gorelsky, S. I.; Lapointe, D.; Fagnou, K. *J. Am. Chem. Soc.* **2008**, *130*, 10848.

(9) Lapointe, D.; Fagnou, K. *Chem. Lett.* **2010**, *39*, 1118.

(10) Ackermann, L. *Chem. Rev.* **2011**, *111*, 1315.

(11) Gorelsky, S. I. *Coord. Chem. Rev.* **2013**, *257*, 153.

(12) Pahls, D. R.; Allen, K. E.; Goldberg, K. I.; Cundari, T. R. *Organometallics* **2014**, *33*, 6413.

(13) Allen, K. E.; Heinekey, D. M.; Goldman, A. S.; Goldberg, K. I. *Organometallics* **2014**, *33*, 1337.

(14) Williams, D. B.; Kaminsky, W.; Mayer, J. M.; Goldberg, K. I. *Chem. Commun.* **2008**, 4195.

(15) Roddick-air-stable.

(16) Owens, C. P.; Varela-Alvarez, A.; Boyarskikh, V.; Musaev, D. G.; Davies, H. M. L.; Blakey, S. B. *Chem. Sci.* **2013**, *4*, 2590.

(17) Zhou, M.; Hintermair, U.; Hashiguchi, B. G.; Parent, A. R.; Hashmi, S. M.; Elimelech, M.; Periana, R. A.; Brudvig, G. W.; Crabtree, R. H. *Organometallics* **2013**, *32*, 957.

(18) Zhou, M.; Johnson, S. I.; Gao, Y.; Emge, T. J.; Nielsen, R. J.; Goddard, W. A.; Goldman, A. S. *Organometallics* **2015**, *34*, 2879.

(19) Shin, K.; Park, S.-W.; Chang, S. *J. Am. Chem. Soc.* **2015**, *137*, 8584.

(20) Choi, J.; Goldman, A. S. *Top. Organomet. Chem.* **2011**, *34*, 139.

(21) Kumar, A.; Zhou, T.; Emge, T. J.; Mironov, O.; Saxton, R. J.; Krogh-Jespersen, K.; Goldman, A. S. *J. Am. Chem. Soc.* **2015**, *137*, 9894.

(22) PyBoxIrEthene2.

(23) SeeSI.

(24) Kundu, S.; Choliy, Y.; Zhuo, G.; Ahuja, R.; Emge, T. J.; Warmuth, R.; Brookhart, M.; Krogh-Jespersen, K.; Goldman, A. S. *Organometallics* **2009**, *28*, 5432.

(25) Punji, B.; Emge, T. J.; Goldman, A. S. *Organometallics* **2010**, *29*, 2702.

(26) FilteredNaBArf-insoluble.

(27) More, M. B.; Ray, D.; Armentrout, P. B. *J. Am. Chem. Soc.* **1999**, *121*, 417.

(28) Zhao, Y.; Truhlar, D. G. *J. Chem. Phys.* **2006**, *125*, 194101/1.

(29) Andrae, D.; Haeussermann, U.; Dolg, M.; Stoll, H.; Preuss, H. *Theor. Chim. Acta* **1990**, *77*, 123.

(30) Iron, M. A.; Lucassen, A. C. B.; Cohen, H.; van der Boom, M. E.; Martin, J. M. L. *J. Am. Chem. Soc.* **2004**, *126*, 11699.

(31) Ditchfield, R.; Hehre, W. J.; Pople, J. A. *J. Chem. Phys.* **1971**, *54*, 724.

(32) Hariharan, P. C.; Pople, J. A. *Mol. Phys.* **1974**, *27*, 209.

(33) Raghavachari, K.; Binkley, J. S.; Seeger, R.; Pople, J. A. *J. Chem. Phys.* **1980**, *72*, 650.

(34) OtherFunctionalsInsertn.

(35) NaOBondCH3CO2Na.

(36) Na+benzene.

(37) Labinger, J. A.; Bercaw, J. E. *Organometallics* **1988**, *7*, 926.

(38) Janowicz, A. H.; Bergman, R. G. *J. Am. Chem. Soc.* **1982**, *104*, 352.

(39) Hoyano, J. K.; Graham, W. A. G. *J. Am. Chem. Soc.* **1982**, *104*, 3723.

(40) Arndtsen, B. A.; Bergman, R. G.; Mobley, T. A.; Peterson, T. H. *Acc. Chem. Res.* **1995**, *28*, 154.

(41) Burger, P.; Bergman, R. G. *J. Am. Chem. Soc.* **1993**, *115*, 10462.

(42) Ir(V)examples2016See.

(43) OxgaardOHM2refs.

(44) BurgessHallIrV.

(45) Cheng, C.; Kim, B. G.; Guironnet, D.; Brookhart, M.; Guan, C.; Wang, D. Y.; Krogh-Jespersen, K.; Goldman, A. S. *J. Am. Chem. Soc.* **2014**, *136*, 6672−6683.

(46) Mazuela, J.; Norrby, P.-O.; Andersson, P. G.; Pàmies, O.; Diéguez, M. *J. Am. Chem. Soc.* **2011**, *133*, 13634.

(47) Rimoldi, M.; Fodor, D.; van Bokhoven, J. A.; Mezzetti, A. *Chem. Commun.* **2013**, *49*, 11314.

(48) H2IsotopeEffects.

(49) Daugulis, O.; Do, H.-Q.; Shabashov, D. *Acc. Chem. Res.* **2009**, *42*, 1074.

(50) Cook, A. K.; Sanford, M. S. *J. Am. Chem. Soc.* **2015**, *137*, 3109.

(51) Davies, H. M. L.; Morton, D. *J. Org. Chem.* **2016**, *81*, 343.

(52) He, J.; Wasa, M.; Chan, K. S. L.; Shao, Q.; Yu, J.-Q. *Chem. Rev.* **2016**.

(53) Ito, J.-i.; Shiomi, T.; Nishiyama, H. *Adv. Synth. Catal.* **2006**, *348*, 1235.

(54) Hoops, S.; Sahle, S.; Gauges, R.; Lee, C.; Pahle, J.; Simus, N.; Singhal, M.; Xu, L.; Mendes, P.; Kummer, U. *Bioinformatics* **2006**, *22*, 3067.

(55) NIST-Jan17 In *NIST Chemistry WebBook, NIST Standard Reference Database Number 69, Eds. P.J. Linstrom and W.G. Mallard, National Institute of Standards and Technology, Gaithersburg MD, 20899, http://webbook.nist.gov, (retrieved January 10, 2017).*

(56) Bruker-AXS. SADABS, Bruker area detector scaling and absorption correction, v2.05, Bruker-AXS Inc., Madison, Wisconsin, 2003; SAINTplus, Bruker area detector data reduction program, v6.45, Bruker-AXS Inc., Madison, Wisconsin, 2003.

(57) Sheldrick, G. M. SHELX86, Program for the Solution of Crystal Structures, University of Göttingen, Germany, 1986.

(58) Sheldrick, G. M. SHELXL97, Program for Crystal Structure Refinement, University of Göttingen, Germany, 1997.

Chapter 3 Hydrocarbon Functionalization co-Catalyzed by (Phebox)Ir(OAc)(H) and Sodium Cation

Part of this chapter is reproduced with permission from

β-Hydride Elimination and C–H Activation by an Iridium Acetate Complex, Catalyzed by Lewis Acids. Alkane Dehydrogenation Cocatalyzed by Lewis Acids and [2,6-Bis(4,4-dimethyloxazolinyl)-3,5-dimethylphenyl]iridium

Yang Gao, Changjian Guan, Meng Zhou, Akshai Kumar, Thomas J. Emge, Ashley M. Wright, Karen I. Goldberg, Karsten Krogh-Jespersen, and Alan S. Goldman

J. Am. *Chem. Soc.,* **2017**, 139, 6338−6350

Introduction

Catalytic dehydrogenation of alkanes and alkyl groups is of great interest with respect to the synthesis of fuels and both commodity and fine chemicals. Notably, alkane dehydrogenation to loss H_2 is a thermodynamically uphill process and hence requires the use of a hydrogen acceptors or the immediate removal of H_2 by physical methods. Tremendous effort has been put into study of iridium catalyzed alkane dehydrogenation since Crabtree reported the first example of alkane dehydrogenation using a cationic iridium species. Among those successfully established catalysis systems where pincer-ligated iridium catalysts predominate, oxidative addition of C-H bond of alkane to Ir(I) species and subsequent β-hydride elimination is usually involved.

In the early study of alkane dehydrogenation by Crabtree, *t*-Butyl ethylene (TBE) was found to be an effective hydrogen acceptor,[1-4] and has been used as the most commonly used acceptor for alkane transfer dehydrogenation since then. Goldman reported that norbornene (NBE) is also very effective in the catalysis system with PCP-ligated-iridium catalysts.[5,6] Both TBE and NBE are bulky and hence only weakly coordinate to the iridium center; in contrast, ethylene or propene was found to be a strong π-bonding ligand and inhibit catalytic activity. Only a few examples with these small olefins as the acceptor have been reported. Goldman and Brookhart have shown that propene can be used as the acceptor in dehydroaromatization reaction.[7] Brookhart and co-workers have also demonstrated that ethylene can be applied as both an acceptor and a dienophile in the synthesis of piperylene,[8] toluene[8] and *p*-xylene.[9] Very recently, Goldman and co-workers have reported the transfer dehydrogenation of gas-phase light alkanes with ethylene and propylene catalyzed by solid-phase (^{iPr}PCP)Ir(C_2H_4).[10] Notably, similar to the acceptorless

alkane dehydrogenation, all of those ethylene or propylene involved catalysis systems require high operating temperatures (200-250 °C). It is challenging to avoid catalyst decomposition under these severe reaction conditions.

Several years ago, Goldberg and co-worker reported that an pincer-ligated iridium(III) complex, (Phebox)Ir$(OAc)_2(OH_2)$ (**1**) (Phebox = 2,6-bis(4,4-dimethyloxazolinyl)-3,5-dimethylphenyl) was able to dehydrogenate alkane and converted itself to an Ir(III) hydride complex (Phebox)Ir(OAc)(H) (**2-H**) at 200 °C.[11] Remarkably, this Ir(III) mediated alkane dehydrogenation is not inhibited by N_2, water or excess amount of olefin, which have been found to hinder the C-H activation at Ir(I) center. At first, we tested the reactivity of **1** in *n*-dodecane acceptorless dehydrogenation. Surprisingly, 20 mM dodecenes were obtained after 12 h with 1 mM **1** under refluxing condition (*n*-dodecane bp 216 °C). In the presence of $NaBAr^F{}_4$, under otherwise the same reaction condition, the initial reaction rate was increased by 8 folds. We have also established the transfer dehydrogenation using olefin as acceptor co-catalyzed by $NaBAr^F{}_4$ and **2-H**. Experimental data suggest that in this co-catalyst system, the dehydrogenation of alkene is more favorable than that of alkane.

Results and Discussion

(Phebox)Ir(III) Catalyzed Acceptorless Dehydrogenation of *n*-Dodecane

n-Dodecane, due to its high boiling point (216 °C), was employed in the study of acceptorless dehydrogenation (eq 3.1). 1 mM **1** in *n*-dodecane solution was prepared and heated at 250 °C under Argon flow. Interestingly, there were no dehydrogenation products observed until the reaction was heated for a while. After 3 h at reflux, no dodecenes were

detected by GC chromatography, however, 2.2 mM and 43 mM dodecenes were produced after 6 h and 27 h, respectively (entry 1, Table 3.1).

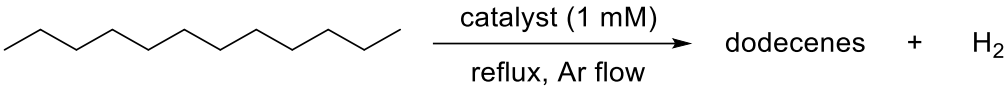

(3.1)

It can be easily imagined that **1** would be transformed to a new species (Phebox)Ir(OAc)(H) (**2-H**) along with 1 eq of HOAc and H_2O under the reaction condition according to the reaction between 1 and *n*-octane (eq 3.2) reported by Goldberg and coworker[11]. To test whether HOAc is necessary for the catalysis or not, compound **2-H** was synthesized independently and 1 mM of that in *n*-dodecane solution was prepared and heated at 250 °C under argon flow. 3.1 mM dodecenes were formed immediately after 1 h at reflux (entries 4, Table 3.1). The higher initial reaction rate with **2-H** in the absence of HOAc indicates that HOAc may adversely affect the reactivity, not merely innocent.

To further test that, a solution of 1.0 mM **1** and 5.0 Mm HOAc in *n*-dodecane was prepared and heated at 250 °C under argon flow. The reaction was nearly inhibited with only 5.7 mM olefins produced after heating for 27 h (entries 3, Table 3.1). This result, together with the early observation of high activity of **2-H**, indicates that **2-H** may be the true catalyst. Excess amount of water has been reported to facilitate the reaction between **1** and alkane to generate **2-H**.[11] The reactions with **1** or **2-H**, in the presence of H_2O, were performed. It was observed that the reaction using **1** in the presence of H_2O has a higher initial reaction rate than that in the absence of H_2O (entries 1 and 2, Table 3.1), while the reactions with **2-H** in the presence or in the absence of H_2O have similar reaction rate (entries 3 and 4, Table 3.1). The different effects of water on the reactions started with different pre-catalysts are consistent with the hypothesis of **2-H** as the true catalyst.

Table 3.1. Acceptorless Dehydrogenation of *n*-Dodecane by Ir(III)[a]

entry	catalyst	additive	Dodecenes/mM				
			1 h	3 h	6 h	27 h	72 h
1	**1**	-	0	0	2.2	43	
2	**1**	H_2O (3.7 M)	0	3.1	8.3	55	
3	**1**	HOAc (5.0 mM)	0	0	0	5.7	
4	**2-H**	-	3.1	7.2	16	53	78
5	**2-H**	H_2O (3.7 M)	4.3	12.8	21	50	78
6	**2-H**	$NaBAr^F_4$ (0.45 mM)	24			47 (24 h)	
7	**2-H**	$NaBAr^F_4$ (0.45 mM) H_2O (3.7 M)	28			60 (24 h)	92

[a] Conditions: catalyst = 1.0 mM, *n*-dodecane = 1.5 mL, *n*-dodecane b.p. = 216 °C, oil bath temp = 250 °C

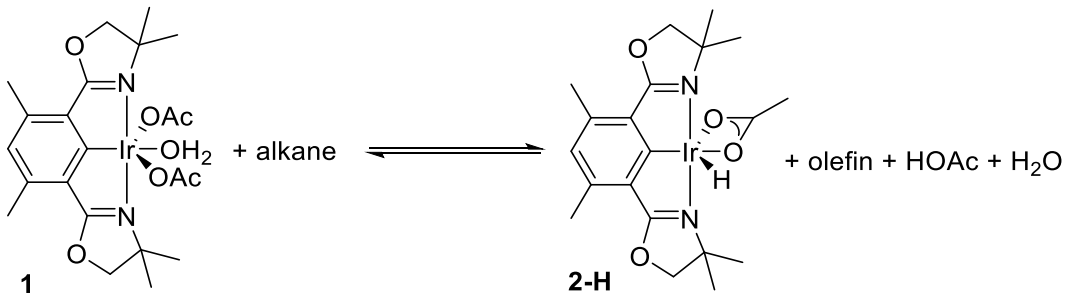

(3.2)

The proposed mechanism for **2-H** catalyzed acceptorless alkane dehydrogenation is comprised by two steps, alkane C-H addition to form **2-Alkyl** intermediate and subsequent

β-hydride elimination of it leading to the olefin product and regenerating **2-H** (Scheme 3.1). Note that both steps have been studied and found to be catalyzed by $NaBAr^F{}_4$.[12] Refluxing a *n*-dodecane solution of **2-H** (1.0 mM) in the presence of $NaBAr^F{}_4$ yields 24 mM dodecenes after 1 h, however, the reaction rate leveled off significantly in the run with $NaBAr^F{}_4$, yielding 47 mM and 78 mM dodecenes after 24 h and 72 h respectively (entry 7, Table 3.1). This is comparable to results obtained with (^{R4}PCP)Ir derivatives, which are the most effective molecular catalysts for acceptorless dehydrogenation of *n*-alkanes reported to date. For example, (^{Ad4}PCP)IrH_2 (1 mM) yields a total of 71 mM dodecene after 72 h and (^{iPr4}PCP)IrH_2 (1 mM) affords 61 mM after 48 h.[13] We suspect that the very similar turnover numbers of all these catalysts at longer reaction times indicates that the rate of olefin formation is not limited primarily by the activity of the respective catalyst. Rather, as the rate of back reaction increases with increasing concentration of olefin, the catalysts can only maintain equilibrium concentrations of olefin and H_2, which correspond to increasingly low concentrations of H_2 and commensurately slow rates of H_2 being purged from solution.

Scheme 3.1. Proposed Mechanism for 2-H Catalyzed Alkane Acceptorless Dehydrogenation

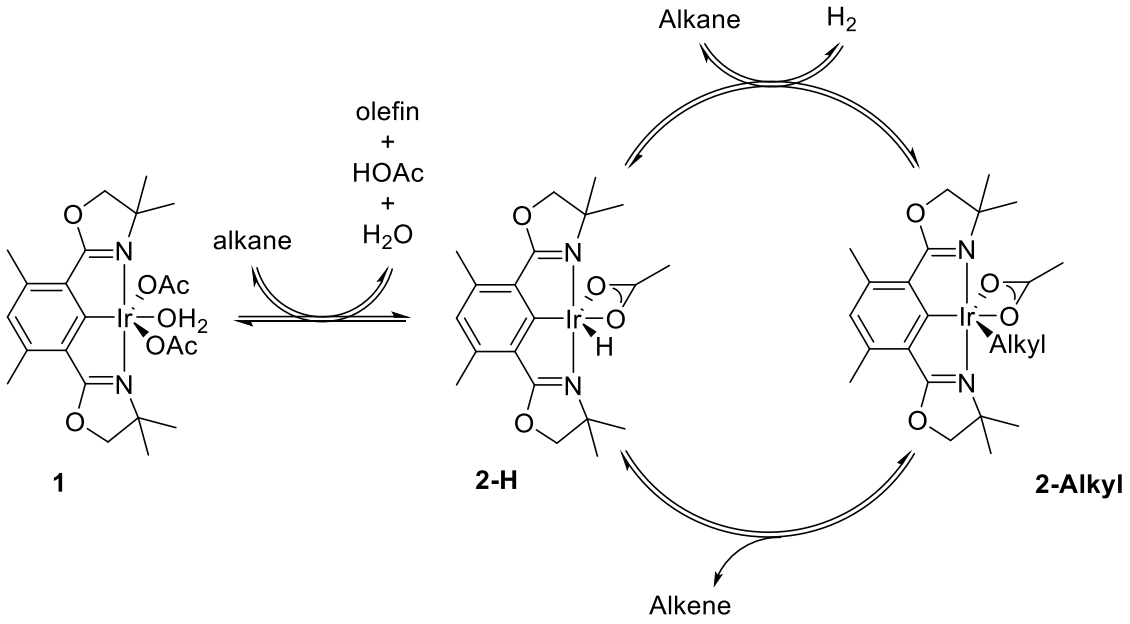

Design of Transfer Dehydrogenation Using Olefin as an Acceptor

Ir(III)-catalyzed alkane dehydrogenation with olefin as acceptor has been tried. At first, complex **2-H** was tested as a catalyst in neat *n*-octane at 200 °C in the presence of acceptor without any other additive. Different kinds of olefins were used as acceptor, including both bulky olefin, such as TBE and NBE, and linear alkenes. No dehydrogenation products were observed in any of these cases (eq 3.3). When **2-H** (2.0 mM) in *n*-octane/1-hexene (1:1) solution was heated in the presence of $NaBAr^F{}_4$ (5.0 mM) at 150 °C, surprisingly, 63 mM 2,4-hexadiene isomers were obtained as the major dehydrogenation products along with formation of 4.0 mM octenes after 2 h (eq 3.4). Hexane was also observed after reaction, suggesting that it is a hexene disproportionation reaction co-catalyzed by **2-H** and Na^+. At

the meantime, a small portion of C_{12} olefins (18 mM) was obtained as well, probably from the dimerization of hexenes. **2-H** in neat 1-hexene solution in the presence of $NaBAr^F{}_4$ was prepared and 1-hexene isomerization reaction was immediately observed at room temperature with 98% conversion after 3 h. When the same reaction solution was heated to 150 °C, hexene disproportionation reaction was performed with slightly better result, 126 mM hexadiene isomers formed after 2 h. 20 mM C_{12} olefins was observed as well. Notably, in the absence of Na^+, under the otherwise same condition, no dehydrogenation reaction was observed, instead, a slow 1-hexene isomerization reaction was detected with 8% yield of internal hexenes (Scheme 3.2). To avoid the dehydrogenation and dimerization, TBE was also tried as an acceptor. When the solution of **2-H** (2.0 mM), $NaBAr^F{}_4$ (5.0 mM) and TBE (800 mM) in *n*-octane was heated at 180 °C, 2 TONs and 5 TONs were observed after 8 h and 24 h, respectively.

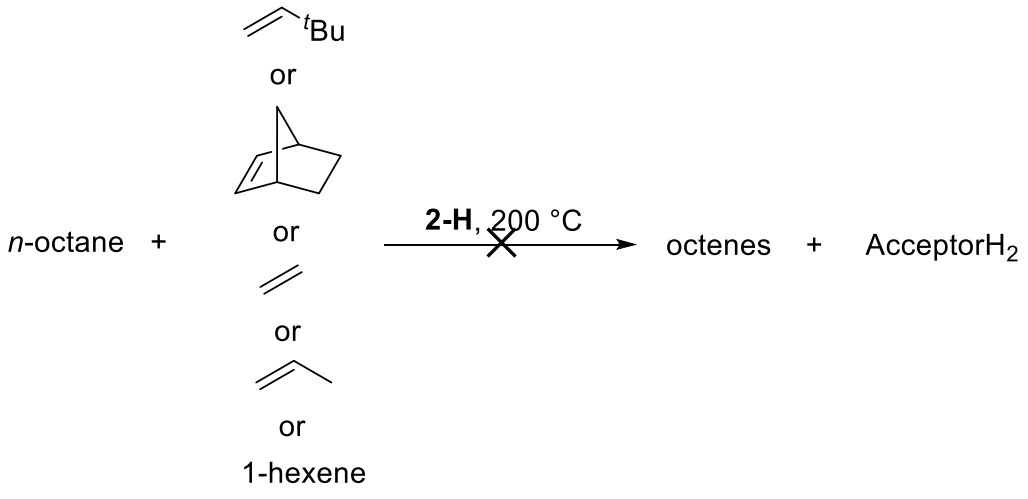

(3.3)

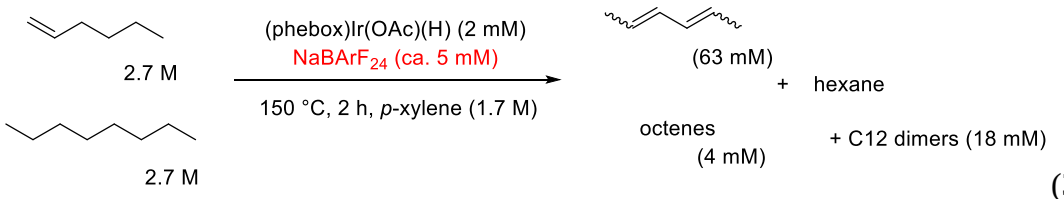

(3.4)

Scheme 3.2. Na^+ Effect on 2-H Catalyzed Hexene Reactions

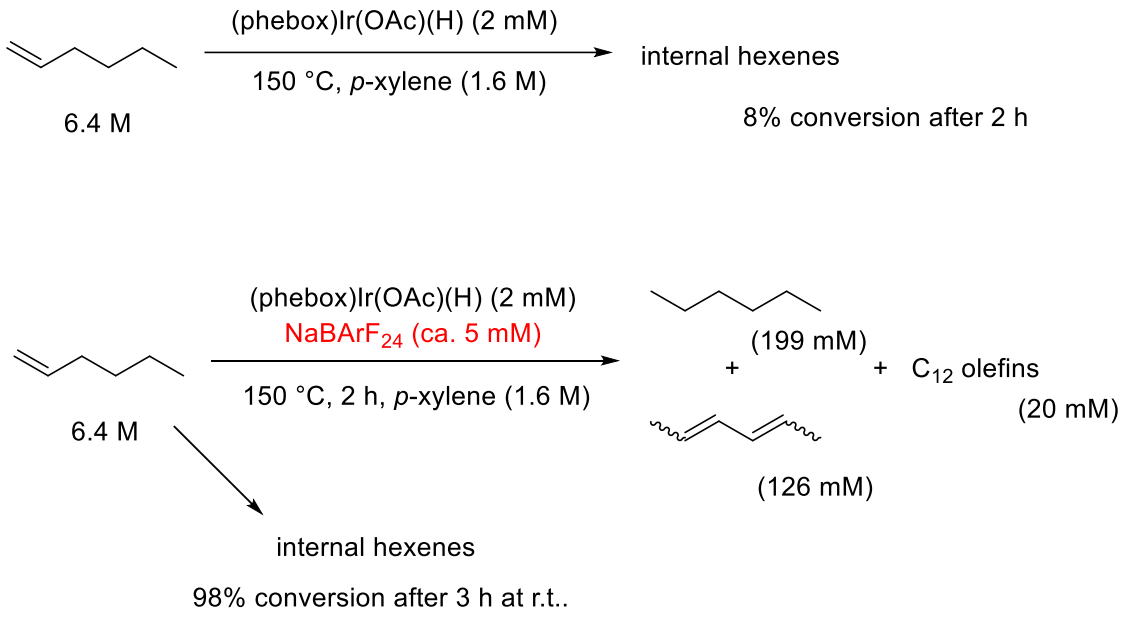

Two different mechanisms were proposed for the hexene disproportionation reaction (Scheme 3.3). The first mechanism includes two cycles, Ir(III) catalyzed dehydrogenation of hexenes cycle and hexenes hydrogenation cycle. The hydrogen generated from hexenes dehydrogenation reacted with another eq of hexene immediately to form hexane. The second possible pathway started with the insertion of hexene into **2-H** to form **2-Hexyl**, which subsequently reacted with another hexene to generate hexane and **2-Hexenyl** as the intermediate. β-Hydride elimination of **2-Hexenyl** led to the regeneration of **2-H** along with formation of hexadiene. A solution of **2-H** (10 mM) and $NaBAr^F_4$ (6.0 mM) in 1-hexene was heated at 150 °C for 30 min. The resting state was characterized as **2-Hexyl** by ^1H NMR spectroscopy.

Scheme 3.3. Proposed Mechanisms for Hexene Disproportionation Reaction

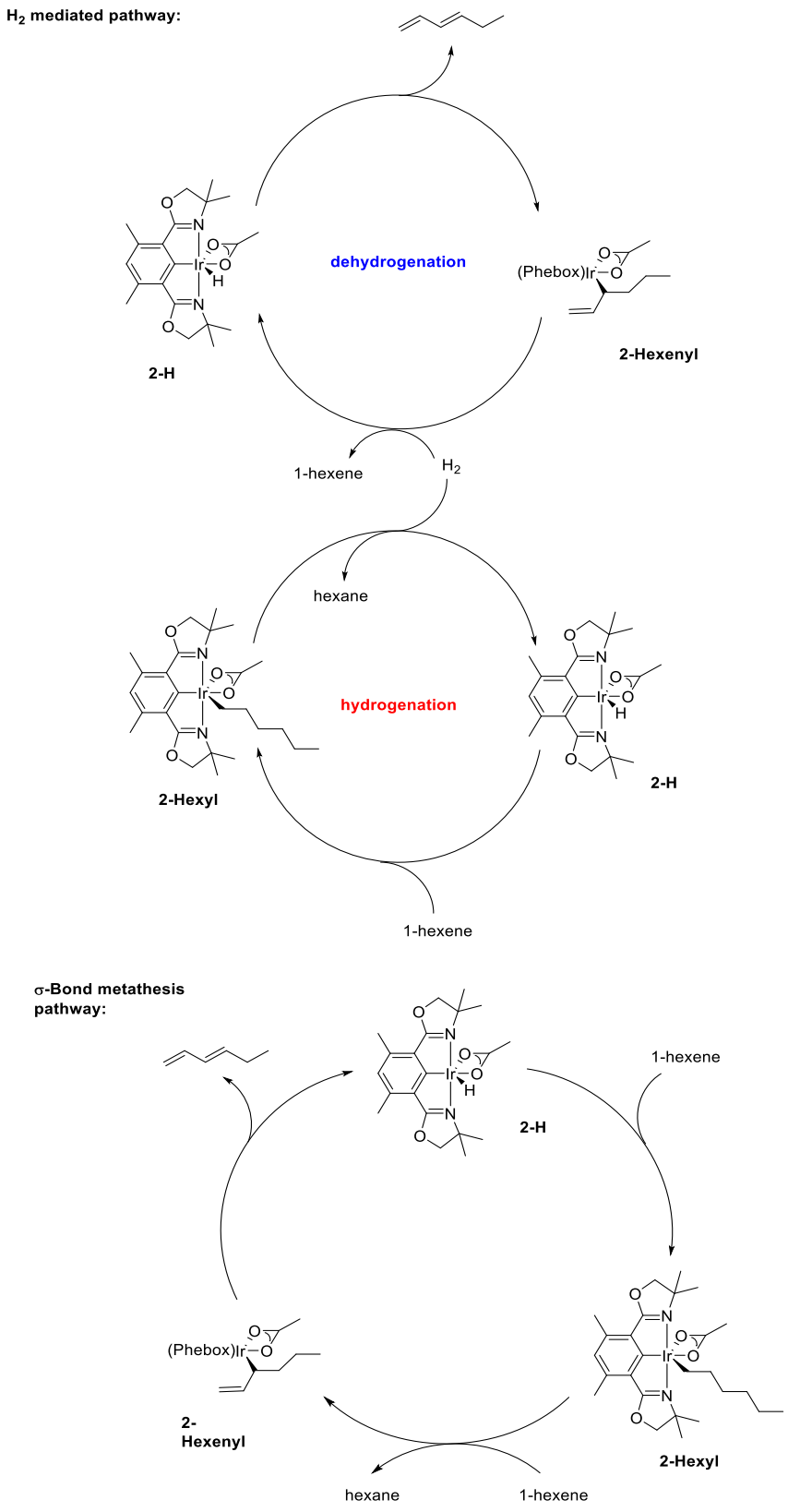

The key difference between two possible mechanisms is the pathway to generate **2-Hexenyl** from **2-Hexyl**. As shown in Scheme 3.4, **2-Hexyl**, generated from hexene insertion into **2-H**, could directly react with another eq of hexene to form **2-Hexenyl** via the σ-bond metathesis; or it could go through a H_2 catalyzed pathway, with **2-H** formed as the intermediate. However, both **2-Hexyl** and **2-Hexenyl** can easily go through the β-H elimination to form **2-H**, which makes it difficult to control the amount of **2-H** (or H_2) in the reaction between **2-Hexyl** and 1-hexene. (Phebox)Ir(OAc)(Me), **2-Me** is an ideal reactant, considering the inaccessibility of β-H elimination. Ito and Nishiyama have reported that the reaction between (phebox)Ir(OAc)$_2$(OH$_2$) (**1**) and toluene happened at the meta and para phenyl position to form the corresponding iridium tolyl complexes (**2-^{m}Tolyl** and **2-^{p}Tolyl**) with 85% yield (eq 3.5).[14] A few years later, Zhou and Goldman reported that the C-H activation happened at the benzyl position selectively when mesitylene was used to react with **1** (eq 3.6).[15] However, there was no evidence whether the C-H activation of *p*-xylene by phebox ligated iridium complex happened at aryl or benzyl position. When 10 mM **1** and 40 mM K_2CO_3 in *p*-xylene solution was heated at 140 °C for 24 h, (Phebox)Ir(OAc)(Xylyl) (**2-Xylyl**) was formed in 70% yield. C-H activation at benzyl position was preferred with no significant (<10%) product from aryl C-H activation.

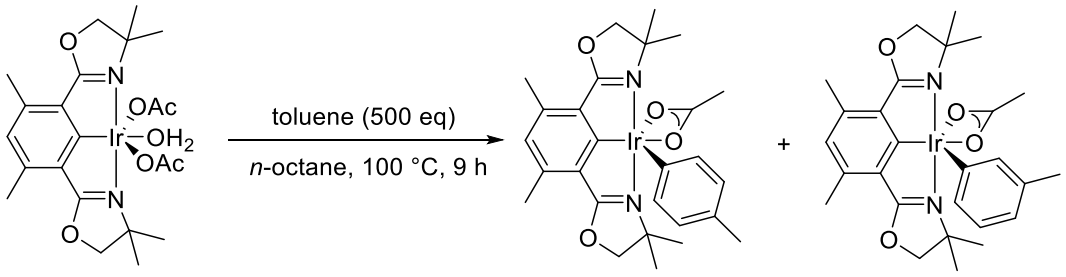

(3.5)

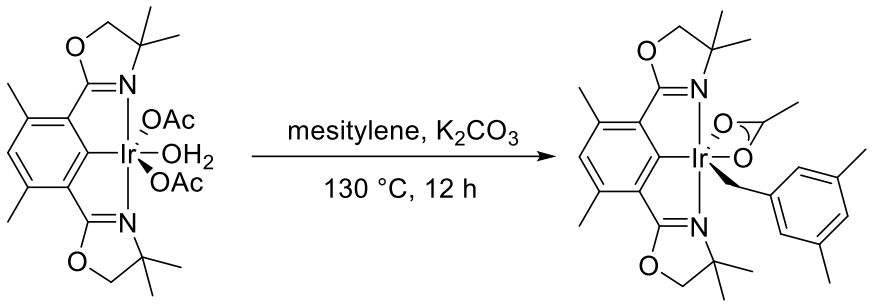

(3.6)

10 mM **2-Me** in *p*-xylene-d_{10} solution was prepared and heated at 140 °C, a new species, confirmed as **2-Xylyl**, was formed slowly with 12% yield after 14 h (eq 3.7, Table 3.2). This result suggests that σ-bond metathesis pathway is accessible since neither **2-Me** nor **2-Xylyl** can undergo β-hydride elimination to generate **2-H**. When $NaBAr^F_4$ (1.0 mM) was present, under the otherwise same reaction condition, the reaction rate was enhanced with 22% conversion after 2 h. To test the H_2 mediated pathway, the mixture of **2-H** (2.5 mM) and 2-Me (10 mM) in *p*-xylene-d_{10} solution was prepared. In the absence of $NaBAr^F_4$, 1.6 mM **2-Xylyl** was formed at 140 °C after 14 h, 33% larger compared to the reaction without **2-H**, suggesting that H_2 mediated pathway is accessible but non-dominant. When $NaBAr^F_4$ (1.0 mM) was added to another same reaction solution and heated at 140 °C, the reaction was ca. 3 times faster compared to the reaction in the presence of $NaBAr^F_4$ and no **2-H.** Clearly, the H_2 mediated pathway is more favorable in the presence of $NaBAr^F_4$, opposed to the case without $NaBAr^F_4$.

Scheme 3.4. Different Pathways from Conversion of 2-Hexyl to 2-Hexenyl

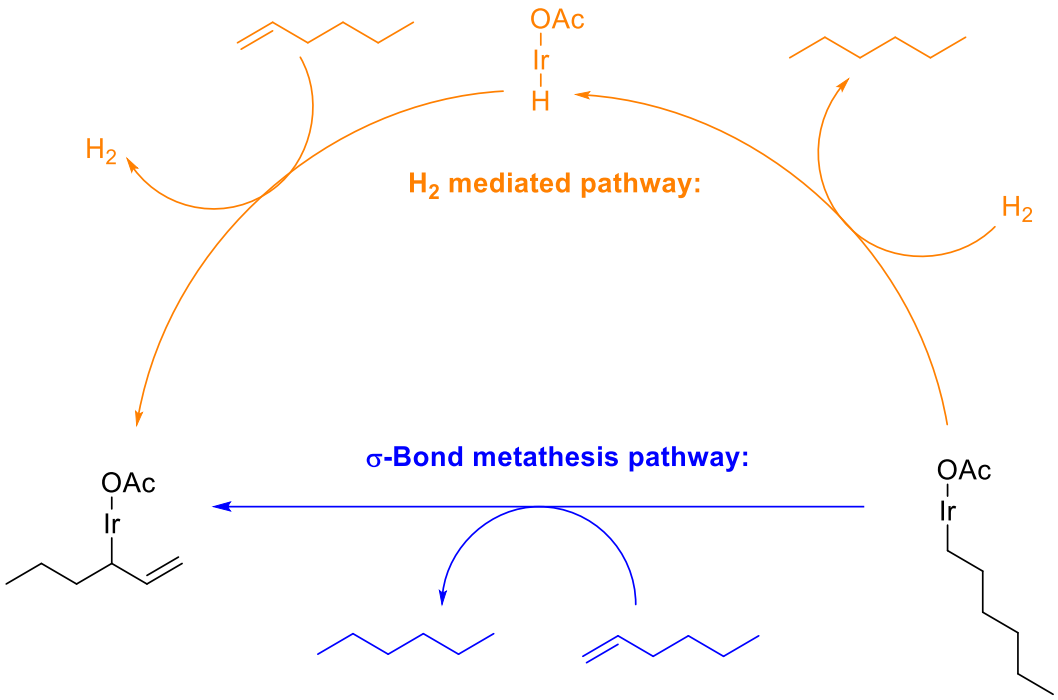

Ir = (Phebox)Ir

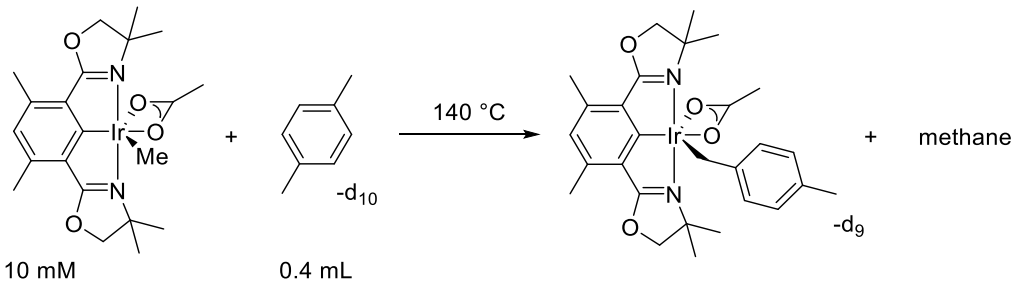

10 mM 0.4 mL (3.7)

Table 3.2. Reactions between 2-Me and *p*-Xylene-d_{10} with or without Additives

entry	additive	**2-Xylyl**/mM		
		0.5 h	2 h	14 h
1	-	0.1	0.1	1.2
2	2-H (2.5 mM)	0.1	0.2	1.6
3	$NaBAr^F{}_4$ (1.0 mM)	1.0	2.2	-
4	2-H (2.5 mM) $NaBAr^F{}_4$ (1.0 mM)	3.1	7.1	-

Norbornene (NBE) Isomerization Reaction Co-catalyzed by 2-H and Lewis Acids

NBE, as one of the most common acceptors for transfer alkane dehydrogenation, was also tried in our (Phebox)Ir(III) catalyzed transfer dehydrogenation system. When THF (0.30 M) and NBE (0.31 M) in *p*-xylene solution was heated at 180 °C in the presence of catalytic amount of **2-H** (1.5 mM) and $LiB(C_6F_5)_4 \cdot 2.5Et_2O$ (11 mM), no dehydrogenation reaction was observed, instead, NBE was detected to convert into a new species, identified as nortricyclane (Tricyclo[2.2.1.0(2.6)]heptane) by both GC-MS and NMR spectroscopy, with 57% conversion after 14 h (eq 3.8). When **2-H** (1.5 mM) and NBE (300 mM) in *p*-xylene solution was heated at 180 °C in the absence of Lewis acid, no reaction was observed, suggesting that Lewis acid is crucial for the catalysis. In addition, the reaction was tried in the absence of Ir(III) complex. No isomerization product was obtained when $NaBAr^F{}_4$, $LiB(C_6F_5)_4 \cdot 2.5Et_2O$ or HOAc was tried as the catalyst, ruling out the acid-catalyzed mechanism.[16,17]

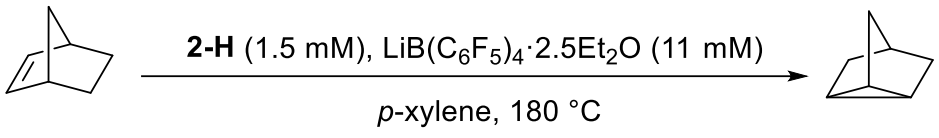

(3.8)

$NaBAr^F_4$ was found to catalyze the reaction between **2-H** and norbornene to form **2-Norbonyl** at room temperature (eq 3.9). The crystal structure of **2-Norbonyl** shown in Figure 3.1 suggests an exo isomer of **2-Norbonyl**. When the solution of $NaBAr^F_4$ (1 mM) and **2-Norbonyl** (10 mM) in *p*-xylene-d_{10} solution was heated at 135 °C, β-hydride elimination was first observed with generation of **2-H** (3.0 mM) after 30 min. Longer heating led to the disappearance of both **2-H** and **2-Norbonyl**, along with growth of several new species including **2-Xylyl** and two unknown species with two new hydride peaks observed from ^{1}H NMR spectrum (eq 3.9). When the reaction was performed in neat NBE under 180 °C, **2-Norbonyl** was the major product after 30 min and another new species grew and became the major one after 2 h. The new species was believed to form via stoichiometric σ-bond metathesis between **2-Norbonyl** and NBE and was proposed as **2-Norbovinyl** by both ^{1}H NMR and ^{13}C NMR spectra. In ^{1}H NMR spectrum, only one doublet (1H, 4.73 ppm) was observed in the region of olefin protons, except the signals assigned to phebox ligand.

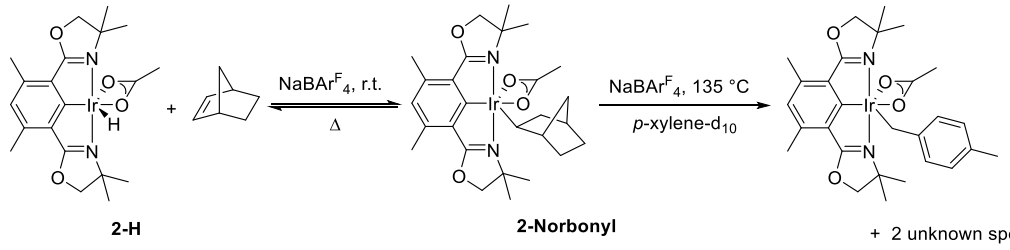

(3.9)

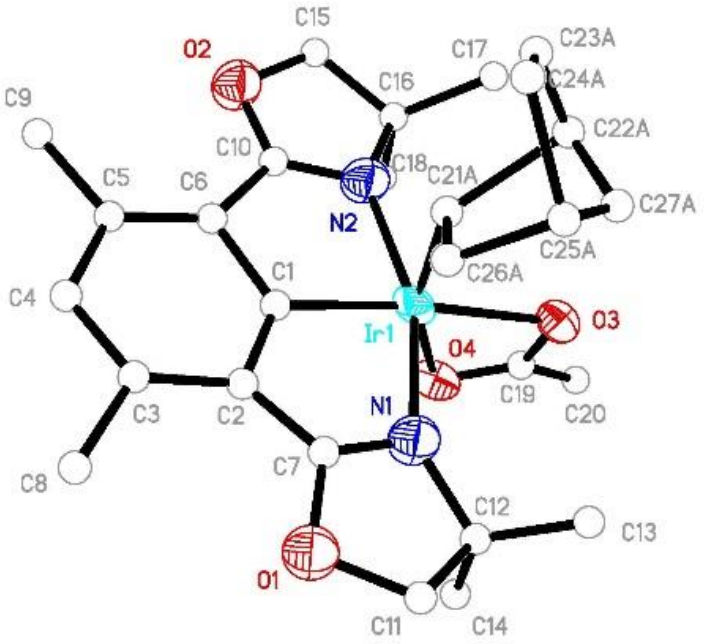

Figure 3.1. Crystal structure of complex **2-Norbonyl**, ORTEP diagram shown at 50% probability level. Hydrogen atoms omitted for clarity.

Two different mechanisms were proposed for this Ir(III)-catalyzed NBE isomerization reaction (Figure 3.2). The first possible pathway started with the insertion of **2-H** into NBE to form the endo isomer of **2-Norbonyl** and subsequent γ-hydride elimination led to the formation of product and regeneration of **2-H**. Or **2-Norbonyl** could react with another eq of NBE to form **2-Norbonenyl** intermediate which then transformed to **2-Nortricyclyl** and generate the product via stoichiometric σ-bond metathesis with another eq of NBE.

Attempts to synthesize **2-Norbonenyl** have been made but failed. A C_6D_6 solution of **2-H** (10 mM) and norbornadiene (75 mM) was prepared and no reaction was observed at room temperature. When catalytic amount of $NaBAr^F{}_4$ (2.0 mM) was added to the solution, the

color of solution changed immediately, but no insertion product was observed. Instead, a new species with a norbornadiene ligand and a hydride ligand was observed in ^{1}H NMR spectrum, obtained with 15% conversion (eq 3.10). The signal of acetate ligand disappeared in the ^{1}H NMR spectrum, indicating that it was replaced by the norbornadiene ligand. The reaction solution was started to heat at 150 °C. After 1 h, the reaction solution turned into black color, with ^{1}H NMR spectrum shown as a mess. This result suggests that the co-existence of norbornadiene with $NaBAr^{F}_{4}$ would lead to the decomposition of **2-H** at high temperature.

When norbornadiene (5.0 mM), **2-H** (5.0 mM) and $NaBAr^{F}_{4}$ (3.0 mM) were added to the NBE (450 mM) in *p*-xylene-d_{10} solution, NBE isomerization reaction stopped after 20% conversion and solution color turned into black, which was clearly different from the catalysis without norbornadiene, orange color with more than 60% conversion. This result goes against the mechanism with **2-Norbonenyl** intermediate, which could be assumed to undergo β-hydride elimination easily under the reaction condition to generate norbornadiene and hence kill the catalysis. To date the mechanism for Ir(III)-catalyzed NBE isomerization has not been understood thoroughly and need further study.

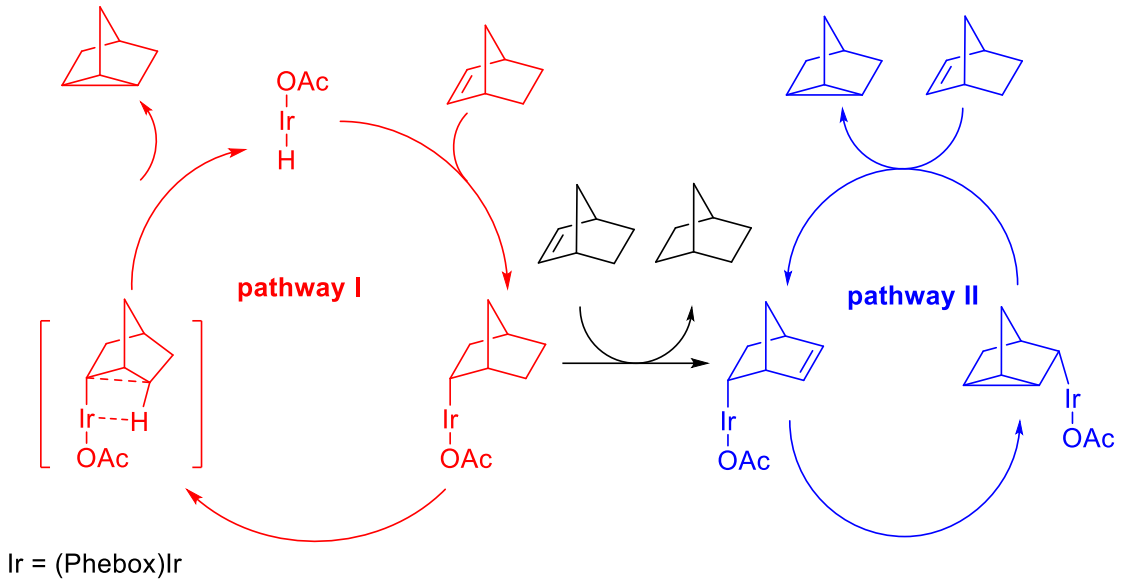

Figure 3.2. Proposed two pathways for Ir(III)-catalyzed NBE isomerization.

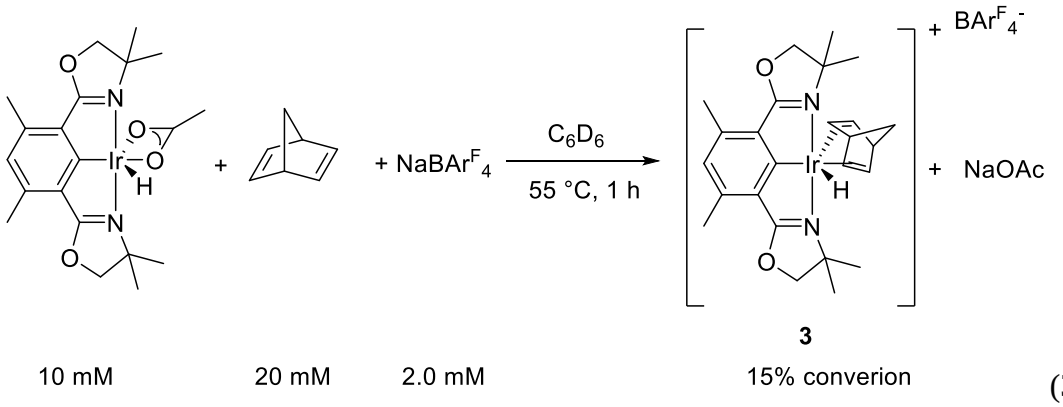

(3.10)

Ethylene Oligomerization-dehydrogenation Reaction co-Catalyzed by 2-H and Na^+

As mentioned before, not only dehydrogenation products were observed, but a small portion of dimerization products were obtained as well, in the case of 1-hexene reaction catalyzed by **2-H** and Na^+. The formation of C_{12} dimers suggests that Na^+ may also promote the olefin insertion into Ir-C bond of **2-Alkyl**. Ethylene, which would not be

dehydrogenated to form diene, makes it a potential substrate to help establish and understand the Ir(III) and Na^+ co-catalyzed oligomerization-dehydrogenation system.

A *p*-xylene solution of **2-H** (5.0 mM) under ethylene (4 atm), in the absence of $NaBAr^F_4$, was first prepared and heated at 175 °C. After 72 h, a very slow reaction was observed with butene (7.0 mM) formed as the major products along with a few oligomers (5.0 mM), as determined by GC chromatography (entry 1, Table 3.3). Notably, there was no formation of ethane after reaction, suggesting that it was only an ethylene oligomerization reaction. When an identical solution in the presence of $NaBAr^F_4$ (8.0 mM) was heated at 175 °C, the yield of oligomers was much higher and the major products were shifted from C_4 olefins to C_{10} and C_{12} olefins. (eq 3.11) 134 mM C_{10} and C_{12} olefins were obtained after 24 h (entry 3, Table 3.3). Ethane was also obtained during the reaction, indicating that both the oligomerization and dehydrogenation happened.

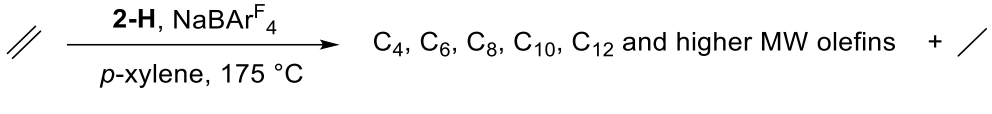

(3.11)

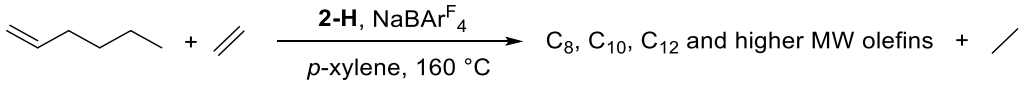

(3.12)

Table 3.3. Ethylene Oligomerization-dehydrogenation Catalyzed by 2-H[a]

entry	**Temp**	**2-H** (mM)	additive	time	Na^+ (mM)	olefin distribution (mM)				
						C_4	C_6	C_8	C_{10}, C_{12}	$C_{>12}$
1	175 °C	5.0	-	72 h	-	7.0	4.0	1.0	0	0
2	175 °C	5.0	-	2 h	9.0	8.0	3.0	14	40	2
3	175 °C	5.0	-	24 h	9.0	6.0	9.0	16	134	18
4	175 °C	5.0	-	72 h	9.0	4.0	7.0	21	160	44
5	160 °C	2.0	1-hexene	2 h	6.0	-	198	97	33	
6	160 °C	2.0	1-hexene	4 h	6.0	-	0	143	159	
7	160 °C	2.0	1-hexene	6 h	6.0	-	0	87	209	
8	160 °C	2.0	1-butene	2 h	6.0	89	7.0	83	6.0	
9	160 °C	2.0	1-butene	4 h	6.0	28	12	108	51	
10	160 °C	2.0	1,3-butadiene	2 h	6.0	0	244	129	8.0	

A *p*-xylene solution of **2-H** (2.0 mM) and $NaBAr^F_4$ (6.0 mM) with added 1-hexene (300 mM) was prepared, octenes (97 mM) was observed as the primary products after 2 h at 160 °C, under 4 atm ethylene (entry 5, Table 3.3). After a longer time (6 h) at 160 °C, C_{10} and higher MW olefins were observed as the major product with 100% conversion of hexenes and decreased amount of C_8 olefins (entry 7, Table 3.3). Ethane was also observed, together with former observation, suggesting that it was an O-D reaction between ethylene and hexenes. (eq 3.12) When 1-butene was introduced to the solution, the O-D reaction between ethylene and butenes was observed as well (entry 8 and 9, Table 3.3). 7.0 mM C6 olefins and 83 mM C8 olefins were observed after 2 h at 160 °C.

The reaction between 1,3-butadiene (300 mM) and ethylene (4 atm) was also tried and all butadiene was consumed in 2 h at 160 °C with formation of both C6 and C8 olefins (entry 10, Table 3.3), faster than the reaction between 1-butene and ethylene (entry 8) with 40% 1-butene left under the same reaction condition. In addition, the comparison of GC spectra of reactions after 2 h with these two different substrate shows that the reaction with 1-butene generated 3 times more ethane than the reaction with butadiene.

Scheme 3.5. The O-D reaction between 1,3-butadiene and ethylene

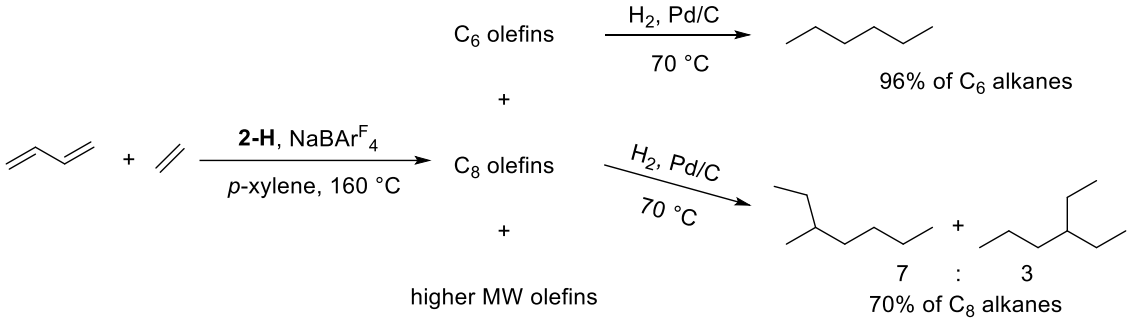

In the reaction between butadiene and ethylene, 2,4-hexadiene was found to comprise 87% of the C6 olefins produced as determined by GC chromatography. The reaction solution was hydrogenated after reaction and 96% of the C_6 alkanes was determined as *n*-hexane. Differently, branched C_8 alkanes were identified as the major components after hydrogenation by ^{13}C NMR spectroscopy and GC chromatography. 3-Methylheptane and 3-ethylhexane were obtained with ratio of 7:3 and comprised 70% of all C_8 alkanes (Scheme 3.5). The ^{1}H NMR spectrum of C_8 olefin products showed that the ratio of alkenyl protons to alkyl protons is roughly 3:13, indicating that most of the C_8 olefin products were dienes.

A pathway for the ethylene O-D reaction was proposed and shown in Scheme 3.6. Firstly, butenes were produced via ethylene dimerization, and then dehydrogenated to butadiene with formation of ethane. The oligomerization between butadiene and ethylene proceeds with linear C_6 olefins formed, which were subsequently converted to branched C_8 olefins by reacting with another eq of ethylene. It could be imagined that the C_{10} and higher MW oligomers would be highly branched and hence impede the further oligomerization, leading to the result of C_{10} and C_{12} olefins as the major products. We also considered another possibility that the chain growing of monoenes is much faster than the dehydrogenation. Since most of C_6 olefins formed were linear olefins, linear C_8 olefins would be expected to be produced as the major C_8 products as well, which, however is not the case. Besides, the reaction of butadiene with ethylene was found to be faster than that of 1-butene with ethylene, with the same product patterns. All these evidences suggest that chain growing started from butadiene instead of butenes.

Scheme 3.6. Proposed pathway for the ethylene O-D reaction

Conclusions

In summary, Ir(III) complex (Phebox)Ir(OAc)(H) (**2-H)** and $NaBAr^F_4$ were shown to co-catalyze acceptorless *n*-alkane dehydrogenation and transfer dehydrogenation (alkene disproportionation). Norbornene was tried as a H_2 acceptor but failed. Instead, isomerization of norbornene to nortricyclane was discovered co-catalyzed by **2-H** and Lewis acid. Not only was olefin insertion into Ir-H bond of **2-H** facilitated by Na^+, but also olefin insertion into Ir-C bond of **2-Alkyl** was discovered to be promoted by Na^+. Based on that, an ethylene oligomerization-dehydrogenation reaction was developed, co-catalyzed by **2-H** and $NaBAr^F_4$. Mechanistic study suggests that dimerization of ethylene is the first step, followed by butene dehydrogenation to produce butadiene, which continues to couple with ethylene, forming higher MW olefins. Current efforts are focused on understanding the olefin insertion into Ir-C bond mechanism and developing other possible systems of catalytic alkane/alkene functionalization.

Experimental

General

All reactions were conducted under an argon atmosphere using an MBraun glovebox, or Schlenk or vacuum-line techniques unless specified otherwise. Anhydrous benzene, *p*-xylene and THF were purchased from Sigma-Aldrich, stored over molecular sieves in the glovebox and used without further purification. *n*-Dodecane and *n*-octane were purchased from Sigma-Aldrich, dried over activated alumina and filtered. 1-Hexene, *tert*-butyl ethylene (TBE) and norbornene were purchased from Sigma-Aldrich, dried over NaK and vacuum-transferred. Benzene-d_6, toluene-d_8 and *p*-xylene-d_{10} were purchased from Cambridge Isotope Labs, dried over activated alumina and filtered. All other reagents were purchased from commercial suppliers and used without further purification. NMR spectra

were acquired on 400 MHz and 500 MHz Varian VNMRS NMR spectrometers and ^{1}H and ^{13}C spectra are referenced to residual solvent peaks. The signal of the residual protio methyl group of *p*-xylene-d_{10} was set at δ 20.90 in the ^{13}C NMR spectrum.

Synthesis and Characterization of Complexes

(Phebox)Ir(OAc)($CH_2(CH_2)_4CH_3$) (2-Hexyl). 2-H (2.2 mg, 0.004 mmol), $NaBAr^F_4$ (0.6 mg, 0.7 μmol), 400 μL of C_6D_6, 1-hexene (4.0 μL, 0.03 mmol) and 10 μL of 0.117 M dioxane in C_6D_6 solution were added to a J-Young NMR tube under argon atmosphere in the glovebox. Reaction was finished in 30 min at room temperature. Yield: 94%. ^{1}H NMR (C_6D_6, 500 MHz): δ 6.50 (s, 1H), 3.94-3.72 (m, 4H), 2.64 (s, 6H), 2.06 (s, 3H), 1.77-1.62 (m, 2H), 1.47-1.11 (m, 18H), 0.90-0.77 (m, 3H), 0.63-0.52 (m, 2H).

(Phebox)Ir(OAc)(Norbonyl) (2-Norbonyl). 2-H (2.2 mg, 0.004 mmol), $NaBAr^F_4$ (0.6 mg, 0.7 μmol), 400 μL of C_6D_6, norbornene (2.0 mg, 0.03 mmol) and 10 μL of 0.117 M dioxane in C_6D_6 solution were added to a J-Young NMR tube under argon atmosphere in the glovebox. Reaction was finished in 30 min at room temperature. Yield: 94%. ^{1}H NMR (C_6D_6, 500 MHz): δ 6.47 (s, 1H), 3.91-3.84 (m, 3H), 3.80 (d, *J* = 8.3 Hz, 1H), 2.64 (s, 3H), 2.63 (s, 3H), 2.22 (t, *J* = 3.8 Hz, 1H), 2.06 (s, 3H), 1.78-1.69 (m, 1H), 1.56 (d, *J* = 9.2 Hz, 2H), 1.49 (s, 3H), 1.44 (s, 3H), 1.30 (ddd, *J* = 16.3, 11.3, 4.6 Hz, 1H), 1.21 (s, 3H), 1.20 (s, 3H), 1.15-1.08 (m, 3H), 0.99 (ddd, *J* = 12.2, 7.0, 5.0 Hz, 1H), 0.89-0.79 (m, 2H). ^{13}C NMR (125 MHz, Benzene-d_6) δ 183.8, 182.8, 177.6, 177.6, 139.6, 139.4, 135.5, 126.2, 126.2, 123.1, 82.1, 82.0, 66.5, 66.4, 40.8, 39.2, 38.2, 37.6, 31.6, 29.7, 27.9, 26.4, 25.9, 25.8, 19.1, 19.0, 11.0.

[(Phebox)Ir(nbde)(H)][BAr$^{F}_{4}$] (3). 2-H (2.2 mg, 0.004 mmol), NaBAr$^{F}_{4}$ (0.6 mg, 0.7 μmol), 400 μL of C_6D_6 and norbornadiene (2.8 μL, 0.03 mmol) were added to a J-Young NMR tube under argon atmosphere in the glovebox. 20% conversion was observed after 30 min at room temperature. ^{1}H NMR (500 MHz, C_6D_6) δ 6.42 (s, 1H), 5.46 (q, *J* = 1.9 Hz, 2H), 3.85 (dt, *J* = 3.5, 1.6 Hz, 2H), 3.78-3.64 (m, 4H), 3.36 (d, *J* = 4.5 Hz, 2H), 2.30 (d, *J* = 1.3 Hz, 6H), 0.99 (d, *J* = 1.6 Hz, 6H), 0.83 (dq, *J* = 9.1, 1.5 Hz, 1H), 0.56 (d, *J* = 1.6 Hz, 6H), 0.41 (dt, *J* = 9.0, 1.6 Hz, 1H), -19.82 (t, *J* = 1.5 Hz, 1H).

(Phebox)Ir(OAc)(Xylyl) (2-Xylyl). 1 (4.0 mg, 0.006 mmol), K_2CO_3 (2.0 mg, 0.014 mmol) and 400 μL of *p*-xylene were added to a J-Young NMR tube under argon atmosphere in the glovebox. The reaction solution was heated in an oil bath at 140 °C. The product in *p*-xylene solution was separated by filtration after 28 h. Reddish-orange powder was obtained after removing the volatiles in vacuo. ^{1}H NMR (C_6D_6, 400 MHz) δ 6.86 (d, *J* = 8.0 Hz, 2H), 6.79 (d, *J* = 7.8 Hz, 2H), 6.52 (s, 1H), 3.80 (d, *J* = 8.1 Hz, 2H), 3.69 (d, *J* = 8.2 Hz, 2H), 2.71 (s, 2H), 2.66 (s, 6H), 2.04 (s, 3H), 2.03 (s, 3H), 1.24 (s, 6H), 1.20 (s, 6H). ^{13}C NMR (C_6D_6, 75 MHz) δ 185.3, 181.7, 177.1, 147.2, 139.6, 132.0, 128.8, 128.2, 126.5, 123.2, 82.0, 66.0, 27.4, 25.9, 25.7, 21.4, 19.0, -2.8.

(Phebox)Ir(OAc)(Norbovinyl) (2-Norbovinyl). 2-H (2.2 mg, 0.004 mmol) and 20 mg of norbornene were added to a sealable tube, which was connected to a Kontes high-vacuum adapter with Tygon tubing. The Kontes valve was attached to a vacuum-gas manifold and the mixture was frozen with liquid nitrogen. The headspace of NMR tube was evacuated until the pressure reached 10 mTorr. The tube was sealed using an oxygen torch under vacuum. After 10 h at 180 °C, the volatiles were removed under vacuum and 400 μL C_6D_6 was added. Yield: 95%. ^{1}H NMR (500 MHz, C_6D_6) δ 6.48 (s, 1H), 4.73 (d, *J* = 3.0 Hz, 1H),

3.93-3.72 (m, 4H), 2.90-2.84 (m, 1H), 2.77 (d, *J* = 3.0 Hz, 1H), 2.62 (d, *J* = 2.3 Hz, 6H), 2.05 (s, 3H), 1.59-1.46 (m, 2H), 1.42 (s, 3H), 1.41 (d, *J* = 2.3 Hz, 1H), 1.37 (s, 3H), 1.24 (s, 3H), 1.22 (s, 3H), 1.06 (d, *J* = 7.0 Hz, 1H), 0.97 (tt, *J* = 8.9, 2.6 Hz, 1H), 0.88 (q, *J* = 7.0 Hz, 1H), 0.81 (td, *J* = 9.7, 2.9 Hz, 1H).

3-Ethylhexane. 3-Ethyl-3-hexanol (13 mg, 0.1 mmol), H_2SO_4 (2.5 μL, 0.05 mmol) and 1.0 mL of C_6D_6 were added to a 2.5 mL vial. After 2 h at room temperature, the reaction was quenched with 100 μL of K_2CO_3 (50 mM) in water solution. The organic layer was washed with saturated brine, dried over magnesium sulfate. After filtration, 400 μL solution and 10 mg Pd/C powder were transfer to a J-Young NMR tube. The solution was degassed using one freeze-pump-thaw cycle and then charged with 1 atm of hydrogen. The reaction was conducted at room temperature for 5 days. Yield: 90%. ^{1}H NMR (500 MHz, C_6D_6) δ 1.33-1.12 (m, 9H), 0.90 (t, *J* = 7.0 Hz, 3H), 0.85 (t, *J* = 7.5 Hz, 6H). ^{13}C NMR (125 MHz, C_6D_6) δ 40.5, 35.6, 25.8, 20.3, 14.8, 11.1.

Acceptorless Dehydrogenation of *n*-Dodecane Catalyzed by 2-H

Following a procedure outlined in the literature,[18] 1.5 mL catalyst (1 mM) in *n*-dodecane solution and additive were charged into a reaction vessel. Reactions were refluxed in oil bath at 250 °C (*n*-dodecane boiling point: 216 ˚C) under argon atmosphere and monitored by GC.

Typical Procedure for Attempted Transfer Dehydrogenation of *n*-Octane with Different Acceptor

A stock solution of **2-H** (2.0 mM), H_2 acceptor and *p*-xylene in *n*-octane was prepared in the glovebox. 100 μL of stock solution and $NaBAr^F_4$ (0.6 mg, 7.0 mM) were added to a

sealable tube, which was connected to a Kontes high-vacuum adapter with Tygon tubing. The Kontes valve was attached to a vacuum-gas manifold and the mixture was frozen with liquid nitrogen. The headspace of tube was evacuated until the pressure reached 10 mTorr. The tube was sealed using an oxygen torch under vacuum. The sealed tube was allowed to reach room temperature and heated inside a GC oven for the desired amount of time. Products were analyzed by GC chromatography.

Typical Procedure for Transfer Dehydrogenation Using 1-Hexene as Acceptor

A stock solution of **2-H** (2.0 mM), 1-hexene and reactant was prepared in *p*-xylene in the glovebox. 100 µL of stock solution and $NaBAr^F{}_4$ (0.6 mg, 7.0 mM) were added to a sealable tube, which was connected to a Kontes high-vacuum adapter with Tygon tubing. The Kontes valve was attached to a vacuum-gas manifold and the mixture was frozen with liquid nitrogen. The headspace of tube was evacuated until the pressure reached 10 mTorr. The tube was sealed using an oxygen torch under vacuum. The sealed tube was allowed to reach room temperature and heated inside a GC oven for the desired amount of time. Products were analyzed by GC chromatography.

Reactions between 2-Me and *p*-xylene-d_{10}. A stock solution of **2-H** (10 mM) in *p*-xylene-d_{10} was prepared in the glovebox. 400 µL of stock solution and additives (1.0 mM $NaBAr^F{}_4$, 2.5 mM **2-H**) were added to a J-Young NMR tube and heated in an oil bath at 140 °C. The reactions were monitored by ^{1}H NMR spectroscopy.

NBE Isomerization Reaction. A stock solution of 300 mM THF, 310 mM NBE, 1.5 mM **2-H** and 11 mM $LiB(C_6F_5)_4 \cdot 2.5Et_2O$ in *p*-xylene was prepared in the glovebox. 100 µL of stock solution was added to a sealable tube, which was connected to a Kontes high-vacuum adapter with Tygon tubing. The Kontes valve was attached to a vacuum-gas manifold and

the mixture was frozen with liquid nitrogen. The headspace of tube was evacuated until the pressure reached 10 mTorr. The tube was sealed using an oxygen torch under vacuum. The sealed tube was allowed to reach room temperature and heated inside a GC oven for the desired amount of time. Products were analyzed by GC chromatography.

Ethylene O-D Reaction. A stock solution of **2-H** (5.0 mM) in *p*-xylene was prepared in the glovebox. 100 μL stock solution and $NaBAr^{F}_{4}$ (0.8 mg, 9.0 mM) were added to a 5 mL sealable glass ampule, which was connected to a Kontes high-vacuum adapter with Tygon tubing. The Kontes valve was attached to a vacuum-gas manifold and the solution was frozen with liquid nitrogen. The headspace of ampule was evacuated until the pressure reached 10 mTorr. The headspace was filled with 2 atm ethylene and then condensed using liquid nitrogen. After 30 seconds, the ampule was sealed using an oxygen torch (the headspace volume was decreased by 50%, which brought the total ethylene pressure to 4 atm). The sealed ampule was allowed to reach room temperature and heated inside a GC oven for the desired amount of time. Products were analyzed by GC chromatography.

Typical Procedure for Ethylene O-D Reaction with Other Olefin

A stock solution of **2-H** (2.0 mM) and olefin (300 mM) in *p*-xylene was prepared in the glovebox. 100 μL stock solution, $NaBAr^{F}_{4}$ (0.8 mg, 9.0 mM) and olefin were added to a 5 mL sealable glass ampule, which was connected to a Kontes high-vacuum adapter with Tygon tubing. The Kontes valve was attached to a vacuum-gas manifold and the solution was frozen with liquid nitrogen. The headspace of ampule was evacuated until the pressure reached 10 mTorr. The headspace was filled with 2 atm ethylene and then condensed using liquid nitrogen. After 30 seconds, the ampule was sealed using an oxygen torch (the headspace volume was decreased by 50%, which brought the total ethylene pressure to 4

atm). The sealed ampule was allowed to reach room temperature and heated inside a GC oven for the desired amount of time. Products were analyzed by GC chromatography.

Typical Procedure for Olefin Hydrogenation Reaction After O-D Reaction

Follow the procedure above and after reaction, the solution in ampule was frozen in liquid N_2 and carefully cracked open. The solution was transferred to a J-Young NMR tube, together with Pd/C powder (5 mg). The solution was degassed using one freeze-pump-thaw cycle and then charged with 1 atm of hydrogen. The reaction was heated in an oil bath at 60 °C for 2 to 5 days.

Reference

(1) Burk, M. J.; Crabtree, R. H.; Parnell, C. P.; Uriarte, R. J. *Organometallics* **1984**, *3*, 816.

(2) Crabtree, R. H.; Mihelcic, J. M.; Quirk, J. M. *J. Am. Chem. Soc.* **1979**, *101*, 7738.

(3) Crabtree, R. H.; Mellea, M. F.; Mihelcic, J. M.; Quirk, J. M. *J. Am. Chem. Soc.* **1982**, *104*, 107.

(4) Burk, M. J.; Crabtree, R. H.; McGrath, D. V. *J. Chem. Soc., Chem. Commun.* **1985**, 1829.

(5) Liu, F.; Pak, E. B.; Singh, B.; Jensen, C. M.; Goldman, A. S. *J. Am. Chem. Soc.* **1999**, *121*, 4086.

(6) Kundu, S.; Choliy, Y.; Zhuo, G.; Ahuja, R.; Emge, T. J.; Warmuth, R.; Brookhart, M.; Krogh-Jespersen, K.; Goldman, A. S. *Organometallics* **2009**, *28*, 5432.

(7) Ahuja, R.; Punji, B.; Findlater, M.; Supplee, C.; Schinski, W.; Brookhart, M.; Goldman, A. S. *Nature Chem.* **2011**, *3*, 167.

(8) Kundu, S.; Lyons, T. W.; Brookhart, M. *ACS Catal.* **2013**, *3*, 1768.

(9) Lyons, T. W.; Guironnet, D.; Findlater, M.; Brookhart, M. *J. Am. Chem. Soc.* **2012**, *134*, 15708.

(10) Kumar, A.; Zhou, T.; Emge, T. J.; Mironov, O.; Saxton, R. J.; Krogh-Jespersen, K.; Goldman, A. S. *J. Am. Chem. Soc.* **2015**, *137*, 9894.

(11) Allen, K. E.; Heinekey, D. M.; Goldman, A. S.; Goldberg, K. I. *Organometallics* **2013**, *32*, 1579.

(12) Gao, Y.; Guan, C.; Zhou, M.; Kumar, A.; Emge, T. J.; Wright, A. M.; Goldberg, K. I.; Krogh-Jespersen, K.; Goldman, A. S. *J. Am. Chem. Soc.* **2017**, *139*, 6338.

(13) Punji, B.; Emge, T. J.; Goldman, A. S. *Organometallics* **2010**, *29*, 2702.

(14) Ito, J.-i.; Kaneda, T.; Nishiyama, H. *Organometallics* **2012**, *31*, 4442.

(15) Zhou, M.; Johnson, S. I.; Gao, Y.; Emge, T. J.; Nielsen, R. J.; Goddard, W. A.; Goldman, A. S. *Organometallics* **2015**, *34*, 2879.

(16) Von Ragué Schleyer, P. *J. Am. Chem. Soc.* **1958**, *80*, 1700.

(17) Bowring, M. A.; Bergman, R. G.; Tilley, T. D. *Organometallics* **2011**, *30*, 1295.

(18) Zhu, K.; Achord, P. D.; Zhang, X.; Krogh-Jespersen, K.; Goldman, A. S. *J. Am. Chem. Soc.* **2004**, *126*, 13044.

Chapter 4 Selective Dehydrogenative Coupling of Ethylene to Butadiene via an Iridacyclopentane Complex

Majority of this chapter is reproduced with permission from

Selective Dehydrogenative Coupling of Ethylene to Butadiene via an Iridacyclopentane Complex

Yang Gao, Thomas J. Emge, Karsten Krogh-Jespersen, and Alan S. Goldman

J. Am. *Chem. Soc.*, **2018**, *140*, 2260-2264

Introduction

1,3-Butadiene is a "platform chemical", with ca. 10 M tons per annum produced for the manufacture of rubbers, polymers and chemicals.[1] Until recently demand for butadiene was largely met through its production as a side-product from the cracking of naphtha, driven primarily by demand for ethylene.[2] The recent abundance of ethane-rich shale gas, however, has shifted the production of ethylene toward the cracking of ethane; this has led to tightening supplies of butadiene while demand continues to increase with growth of the global economy. As a result there is renewed interest in the development of methods for the on-purpose production of butadiene from inexpensive feedstock.[3-5] On the supply side of this calculus, the same abundance of ethane that has led to decreased butadiene production from naphtha makes ethylene an attractive potential feedstock for butadiene.

Herein we report the discovery of a catalyst for the selective formation of butadiene from ethylene, a reaction with little if any precedent. We show that this dehydrogenative coupling proceeds via an iridacyclopentane intermediate that undergoes β-H elimination, a reaction step which also has limited precedent.

Results and Discussion

As part of our studies of pincer-ligated iridium catalysts for the dehydrogenation of alkanes we recently reported the synthesis of a new Phebox complex (Phebox = 3,5-dimethylphenyl-2,6-bis-(oxazolinyl)) (Phebox)Ir(C_2H_4)$_2$ (**1**).[6] In the course of testing this complex for activity for catalytic alkane dehydrogenation (which was not detected), using ethylene as a potential hydrogen acceptor, the formation of butadiene was observed. For example, upon heating a toluene-d_8 solution of **1** (5.0 mM) under ethylene (2 atm) at 100 °C for 4 h, 1,3-butadiene (8.0 mM) and ethane (3.0 mM) were observed in solution by ^{1}H

NMR spectroscopy (eq 4.1). Surprisingly, only a minimal concentration of butenes (<1.0 mM) was observed in the ^{1}H NMR spectrum, comprising only 8% of C_4 products (entry 1, Table 4.1) as determined by gas chromatography.

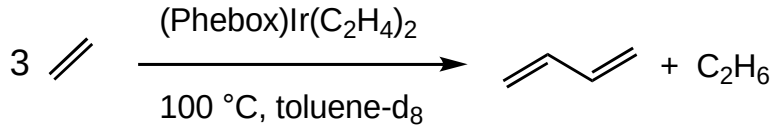

(4.1)

When an identical solution was heated for a longer time (16 h) the yield of butadiene was higher but the amount of butene as a percentage of C_4 products was significantly greater at 21% (entry 2, Table 4.1). The latter observation indicates that the butadiene observed at the shorter reaction time was not a secondary product formed by the dehydrogenation of butene; it is instead consistent with the converse possibility that the butenes observed are formed as secondary products from butadiene hydrogenation.

Table 4.1. Dehydrogenative Ethylene Coupling Catalyzed by 1[a]

entry	temp/°C	time	$P_{C_2H_4}$	butadiene/mM (% total olefins)	butenes/ mM	C_6/mM
1	100	4 h	2 atm	8.0 (92%)	<1.0	0
2	100	16 h	2 atm	15 (68%)	4.1	2.2
3	100	12 h	8 atm	23 (88%)	2.1	1.3
4	100	12 h	12 atm	20 (90%)	2.2	0
5	100[b]	6 h	8 atm	6.1 (47%)	6.2	0.7
6	110	18 h	8 atm	65 (62%)	28	12
7	110	18 h	12 atm	70 (71%)	20	8.2
8	110	21 h	12 atm	67 (62%)	30	12
9	110[c]	21 h	12 atm	101 (76%)	21	11

[a]**1** (5 mM) in toluene-d_8. To promote gas-liquid mixing the NMR tube was shaken periodically (entries 1-5, sealed NMR tube in an oven equipped with an internal rotator; entries 6-9, high-pressure J-Young tube manually shaken every 1 h). [b]73 mM added butadiene. [c]Volatiles removed every 5.5 h followed by recharging with toluene-d_8 and ethylene.

Under higher pressures of ethylene (8 atm and 12 atm; entries 3 and 4) greater yields of butadiene were obtained, with a relatively lower yield of butenes. When butadiene was added initially to the solution (entry 5), the net production of butadiene was much less, while the production of butene was significantly greater, consistent with the proposal that the butene is formed from butadiene. Accordingly, when the reaction is taken to higher

conversion (with slightly longer times and a slightly higher temperature of 110 °C) significant yields of butene are obtained (entries 6-8). The formation of C_6 olefins is also observed at later times suggesting that these are also secondary products.

By removing the volatiles periodically (every 5.5 h) and replacing solvent and ethylene, greater total yields of butadiene and selectivity were achieved. After 21 h (4 cycles) a total of 101 mM butadiene had been produced, comprising 76% of the total olefins (entry 9, Table 4.1).

To our knowledge the direct catalytic coupling of ethylene to butadiene under mild conditions (or perhaps under any conditions) is effectively unprecedented.[7] We therefore considered alternative pathways proceeding through dimerization and subsequent butene dehydrogenation[8-10]. In that context we prepared a toluene-d_8 solution of **1** with added isotopically unlabeled 1-butene (30 mM) to which 2 atm ethylene-d_4 was added. After 2 h at 100 °C, 3.2 mM butadiene had formed all of which was butadiene-d_6, while the concentration of unlabeled 1-butene was unchanged. An analogous experiment was conducted with ethylene-$^{13}C_2$ and unlabeled 1-butene (3.6 mM). After 3 h at 100 °C, 7.1 mM butadiene had formed, of which 7.0 mM was butadiene-$^{13}C_4$, as determined by ^{1}H NMR spectroscopy. Thus the formation of butadiene does not proceed via free 1-butene.

In the course of the catalytic runs (5.0 mM **1**, ethylene, toluene-d_8, 100 °C), ^{1}H NMR spectroscopy revealed the presence of a new species **2**, along with **1**. The ratio of **2** to **1** reached a steady state within ca. 4 h. It was found to be independent of ethylene pressure over a range from 2 atm – 8 atm, with [**2**]/[**1**] = 1.6 ± 0.1.

The ^{1}H NMR spectral data for **2** indicates C_s symmetry, in contrast with the C_{2v} symmetry of **1**. A set of four multiplets is observed in the ^{1}H NMR spectrum; their assignment to a 1,4-butanediyl ligand is supported by HCOSY NMR spectroscopy. A broad singlet indicative of an ethylene ligand, is observed at δ 2.86 ppm (4H) with a corresponding signal at δ 53.19 ppm in the ^{13}C NMR spectrum. Signals in the ^{13}C NMR spectrum at δ 40.6, δ 36.4, δ 29.9 and δ 2.7 ppm are attributable to the butanediyl group. Based on this data, complex **2** is proposed to be an iridacyclopentane ethylene complex. We were unable to isolate **2** from the mixture with **1,** and attempts to grow X-ray-quality crystals directly from the mixture were unsuccessful.

Addition of acetic acid (20 mM) to the C_6D_6 solution of **1** and **2** (3:7), immediately afforded a 3:7 mixture of (phebox)Ir(OAc)(ethyl) (**3**)[6] and (phebox)Ir(OAc)(*n*-butyl) (**4**) (Figure 4.1). When an identical solution of **1** and **2** was exposed to 1 atm CO, the signals attributable to the ethylene ligands of both compounds quickly disappeared from the ^{1}H NMR spectrum. The products were identified, on the basis of their ^{1}H and ^{13}C NMR spectra, as (Phebox)Ir(CO) (**5**) and **6**, the product of substitution of the ethylene ligand of **2** by CO. We were able to obtain X-ray-quality crystals of complex **6** from this mixture, which confirmed our assignment of complex **6** (Figure 4.1), and by inference, our assignment of **2**.

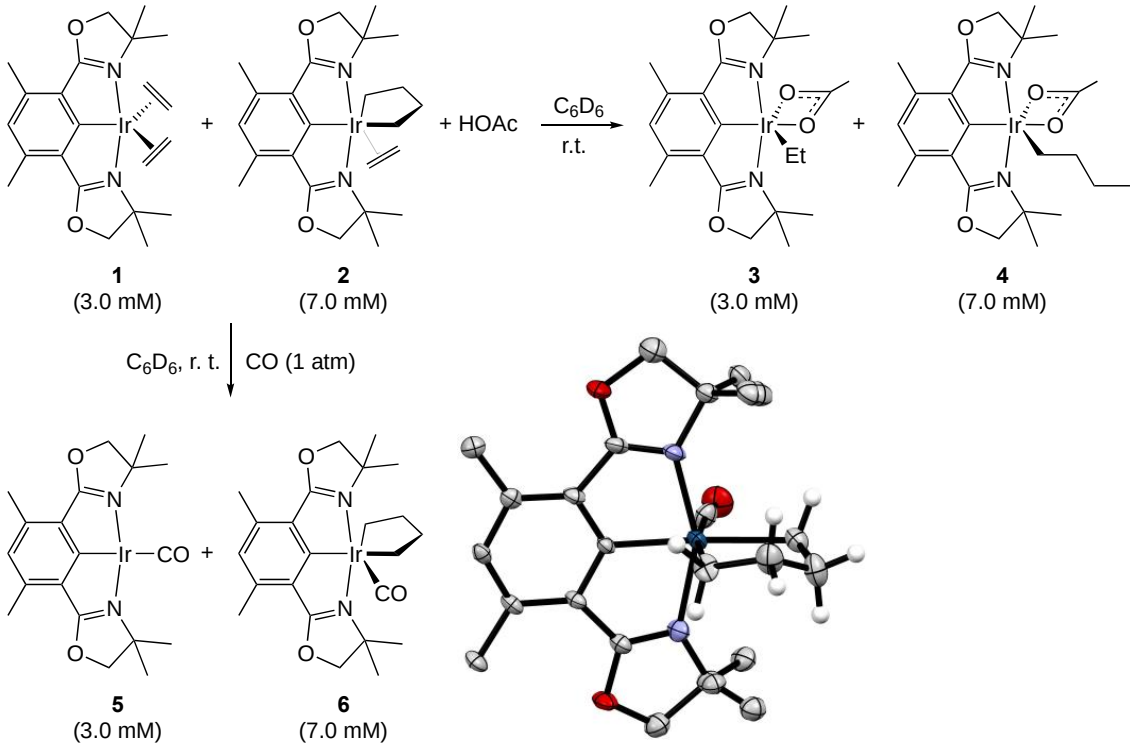

Figure 4.1. Characterization of **2** by reaction with HOAc to yield **4** and reaction with CO to yield **6**. Solid-state molecular structure of complex **6**. H atoms other than those of the iridacyclopentane ring omitted for clarity.

When a mixture of **1** (3.0 mM) and **2** (7.0 mM) in *p*-xylene-d_{10} solution was heated under argon (1 atm) at 90 °C, **1** was observed as the major species after 1 h. Further heating led to the decomposition of **1** with release of ethylene and the formation of only trace amounts (< 0.5 mM) of C_4 hydrocarbons (eq 4.2).

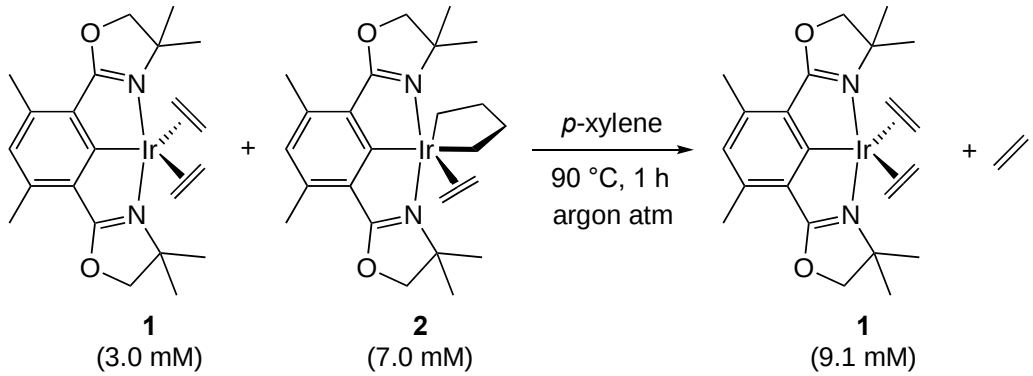

(4.2)

The formation of a metallacyclopentane represents a coupling of ethylene units, obviously suggesting the possibility that the iridacyclopentane is an intermediate in the catalytic formation of butadiene (eq 4.1). Nonetheless, *a priori* it remained quite plausible that **2** is an out-of-cycle species rather than an actual intermediate in the catalytic cycle for butadiene formation. To test this possibility, we synthesized a mixture of **1** and **2** with $^{13}C_2H_4$, which resulted in full ^{13}C-labeling of the 1,4-butanediyl unit of **2** and the ethylene ligands of both **1** and **2**. The mixture of **1**-$^{13}C_4$ (3.0 mM) and **2**-$^{13}C_6$ (7.0 mM) in *p*-xylene-d_{10} was then exposed to unlabeled ethylene (2 atm) at room temperature. The ethylene-$^{13}C_2$ ligands of both complexes were rapidly substituted by unlabeled ethylene ligand. No loss of ^{13}C labeling of the 1,4-butanediyl group was observed, consistent with the higher temperatures required for interconversion of **1** and **2**. Upon heating this mixture of unlabeled **1** and $^{13}C_4$-butanediyl labeled **2** at 100 °C for 30 min under an atmosphere of unlabeled C_2H_4, fully labeled ($^{13}C_4$) butadiene (1.7 mM) was observed in the ^1H NMR spectrum, along with some unlabeled butadiene (0.6 mM). The formation of the $^{13}C_4$-labeled butadiene under an atmosphere of unlabeled C_2H_4, particularly as the major product, rules out the possibility that this butadiene formed via conversion of **2** to **1**, as the latter undergoes rapid exchange with free ethylene.

The formation of metallacyclopentanes from reactions of transition metal complexes with ethylene[11-16] and other olefins[16-18] is well precedented. Metallacyclopentanes are believed to be critical intermediates in the selective trimerization and tetramerization of ethylene to give 1-hexene and 1-octene respectively.[19-23] They have been reported to decompose to give 1-butene,[24-26] or even to catalyze the dimerization of ethylene to give 1-butene.[13,27] We are aware, however, of only very limited examples of reactions of

metallacyclopentanes to give butadiene. Gas-phase cationic metallacyclopentanes have been reported to give the corresponding metal butadiene complexes.[28,29] Whitesides reported decomposition of platinacyclopentanes to give primarily butenes but also traces of butadiene.[25,26] Itoh observed formation of Ru(II) η^4-butadiene complexes, and proposed it to proceed via the decomposition of in-situ generated ruthena(IV)cyclopentane intermediates.[30] Berke and Chirik have reported reactions with ethylene to give Re and Mo butadiene complexes respectively; both reactions were proposed to proceed via a metallacyclopentane intermediate.[31,32] Most closely related to the present chemistry, Carmona has reported the apparent interconversion of a butene-1-yl iridium hydride with an iridacyclopentane, and formation of small amounts (<10%) of an η^4-butadiene complex after 2 days at 150 °C.[33] With respect to catalytic transformations we are aware only of Bercaw's report of a titanocene complex affording extremely slow rates, 1-2 turnovers/year at 25 °C.[7]

To determine the mechanism of eq 4.1, and in particular the formation of butadiene derived from the 1,4-butanediyl unit of **2**, we have conducted a computational investigation (DFT) employing the M06-L functional, the SDD effective core potential on Ir, and valence basis sets of triple-zeta plus polarization quality (M06-L/SDD(+f+spdf)/6-311G(d,p)); bulk solvation effects were included via a continuum dielectric model (CPCM/*p*-xylene; see SI for full computational details). Complex **1** was calculated to undergo conversion to iridacyclopentane **2** via a concerted mechanism with activation parameters $\Delta H^{\ddagger}$ = 26.7 kcal/mol and $\Delta S^{\ddagger}$ = -1.7 eu ($\Delta G^{\ddagger}$ = 27.2 kcal/mol at T = 298 K) to afford the 16-electron iridacyclopentane **7**, followed by rapid coordination of ethylene to give **2** (Figure 4.2). At 100 °C these activation parameters correspond to a rate of 7.6 x 10^{-4} s^{-1} or a half life of ca.

900 s, in good agreement with the observation, noted above, that the reaction of **1** at 100 °C took several hours to reach a steady state ratio of **1** to **2**.

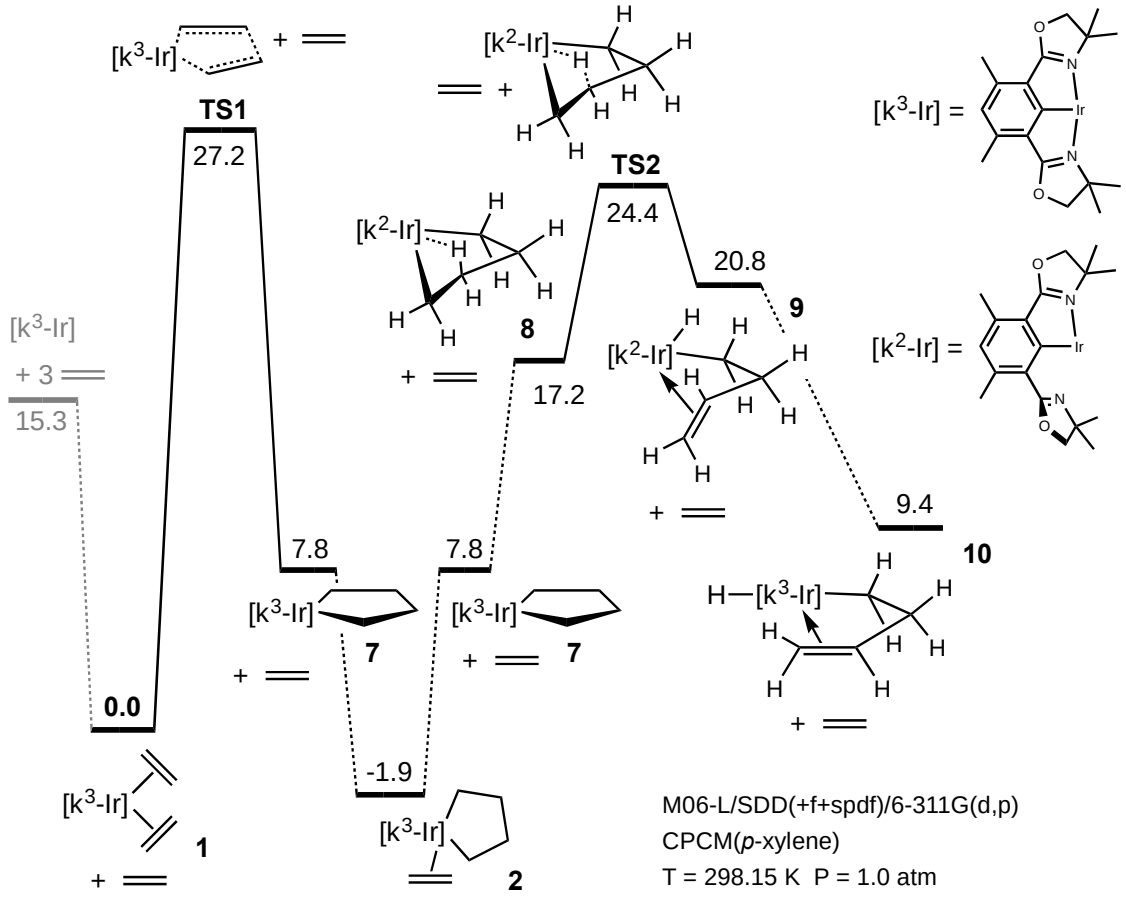

Figure 4.2. Free energy profile for ethylene coupling and β-H elimination of the resulting iridacyclopentane

As first noted by Whitesides,[24,25] a key, characteristic, property of metallacyclopentanes is their resistance toward undergoing β-hydride elimination. Nevertheless, systems in which butene is apparently formed via metallacyclopentanes have been reported, consistent with the occurrence of β-H-elimination, followed by C-H elimination.[24,25,34]

In the case of iridacyclopentane **2**, DFT calculations revealed an unanticipated pathway for β-H-elimination. Loss of ethylene from **2** returns the 16-electron intermediate **7**, which

shows signs of steric crowding including a short distance of 1.97 Å between the H atoms at C2 of the iridacyclopentane ring and an oxazoline methyl group. This is followed by the formation of an agostic interaction with a C(2)-H bond (d_{Ir-H} = 2.11 Å)[35], requiring the formation of a strongly puckered iridacyclopentane ring. Formation of this agostic complex (**8**, Figures 4.2 and 4.3) would be sterically prohibitive but for an accompanying rotation around an oxazoline-aryl bond and thus loss of an N-Ir bond, i.e. κ^3-κ^2 partial dechelation of the Phebox ligand. The free energy of **8** is 17.2 kcal/mol above **1**, or 9.4 kcal/mol above the non-agostic iridacyclopentane **7** (note that this energy includes the loss of an Ir-N bond).

It is perhaps noteworthy that upon dechelation to give **8** the resulting "open" coordination site is not in fact very "open". The pendant oxazolinyl group necessarily remains close to the metal center, probably too close to allow coordination of another ligand (even one as small as ethylene), but not so close as to prevent puckering of the iridacyclopentane ring or slippage of the resulting butenyl vinyl group into the vacant coordination site.

$\Delta G^{\ddagger}$ for β-H elimination from agostic complex **8** is 7.2 kcal/mol (**TS2**), corresponding to an overall barrier of 26.3 kcal/mol from **2.** The β-H elimination from **8**, which requires surprising little geometric rearrangement (Figure 4.3), leads to a 3-buten-1-yl hydride complex, **9**, with the Phebox ligand still bound in a κ^2 configuration. Intermediate **9** may be described as approximately square pyramidal with C1 of the 3-buten-1-yl group in the apical position (Figure 4.3). Migration of the hydride from a basal position to the vacant coordination site, accompanied by migration of the C-C double bond to the position formerly occupied by the hydride, along with coordination of the dangling oxazolinyl N atom, would give the 18-electron κ^3-Phebox complex **10** with a free energy 1.6 kcal/mol above **7.**

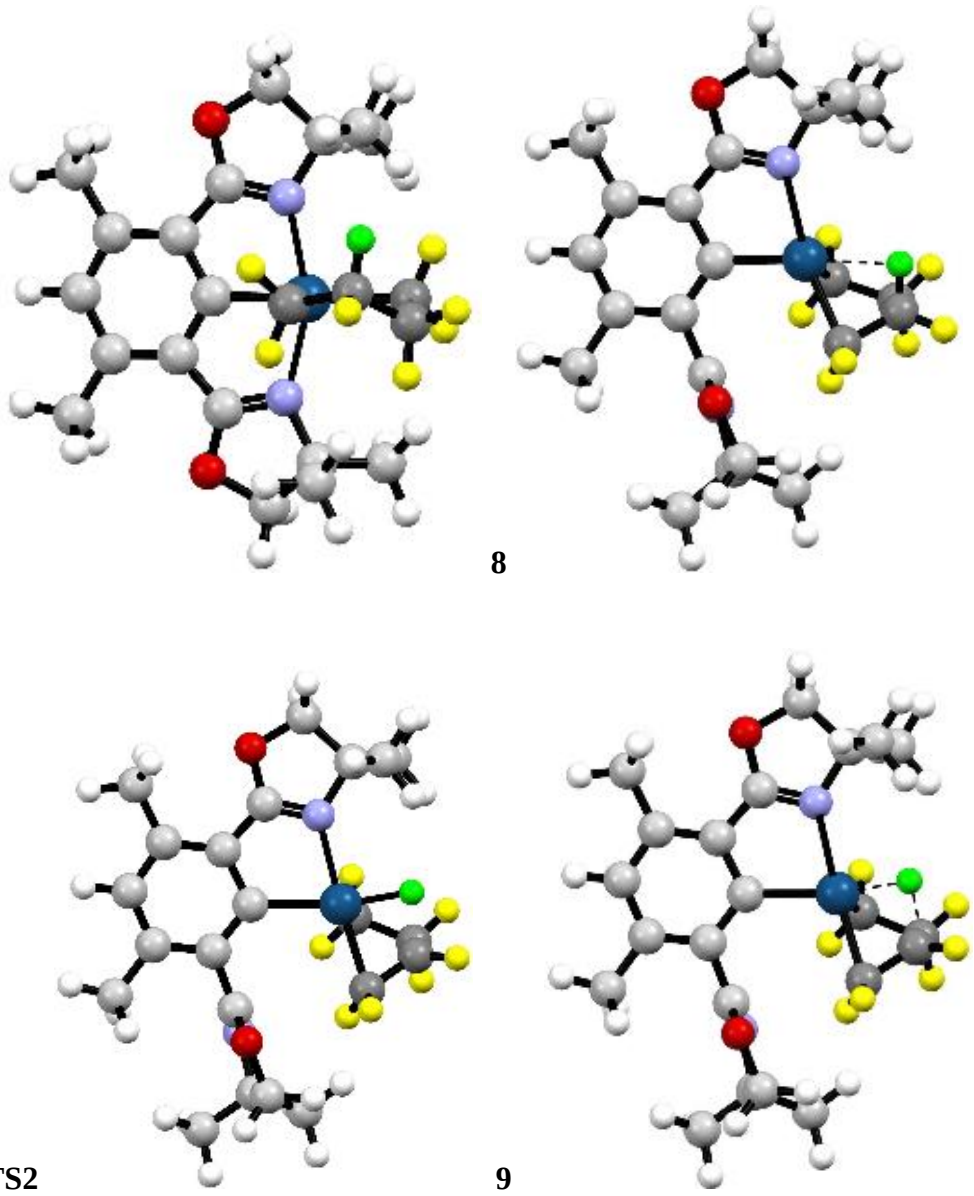

Figure 4.3. DFT structures of complex **7**, agostic iridacyclopentane complex **8**, TS for β-H-elimination **TS2**, and initial product of β-H-elimination **9**, highlighting the distortion required to allow the agostic interaction and the geometrical similarity of **8**, **TS2**, and **9**. (H atom undergoing migration to Ir shown in green, other 1,4-butanediyl H atoms shown in yellow.)

Decoordination of the C-C double bond of **10**, or decoordination of the C-C double bond and re-coordination of the oxazoline N atom directly from **9**, gives κ^3-Phebox complex **11**

(Figure 4.4). Complex **11** could then undergo C-H elimination to give 1-butene. However, the calculations predict that the C-H elimination transition state **TS3** is 4.6 kcal/mol higher in free energy than **TS4** for β-H elimination (Pathway B, shown in blue, Figure 4.4). An even more favorable pathway, however, is calculated to proceed via insertion of ethylene into the Ir-H bond of **11** (following ethylene coordination via **TS5** to give **12**; Pathway A, shown in red). The free energies of TS4 and TS5 are probably not significantly different within the accuracy limits of the calculation, and the relative probability of **11** undergoing ethylene coordination and insertion (Pathway A), as opposed to β-H elimination (Pathway B), may depend on ethylene concentration. Regardless, via either Pathway A or B, butadiene is formed via β-H-elimination of the 3-buten-1-yl group. By the Pathway B, (Phebox)IrH_2 (**14**) is produced, which is expected to undergo facile insertion of ethylene into an Ir-H bond. The two pathways thereby converge at (Phebox)IrH(Et) (**15**); elimination of ethane from **15** and coordination of two ethylene molecules then completes the catalytic cycle.

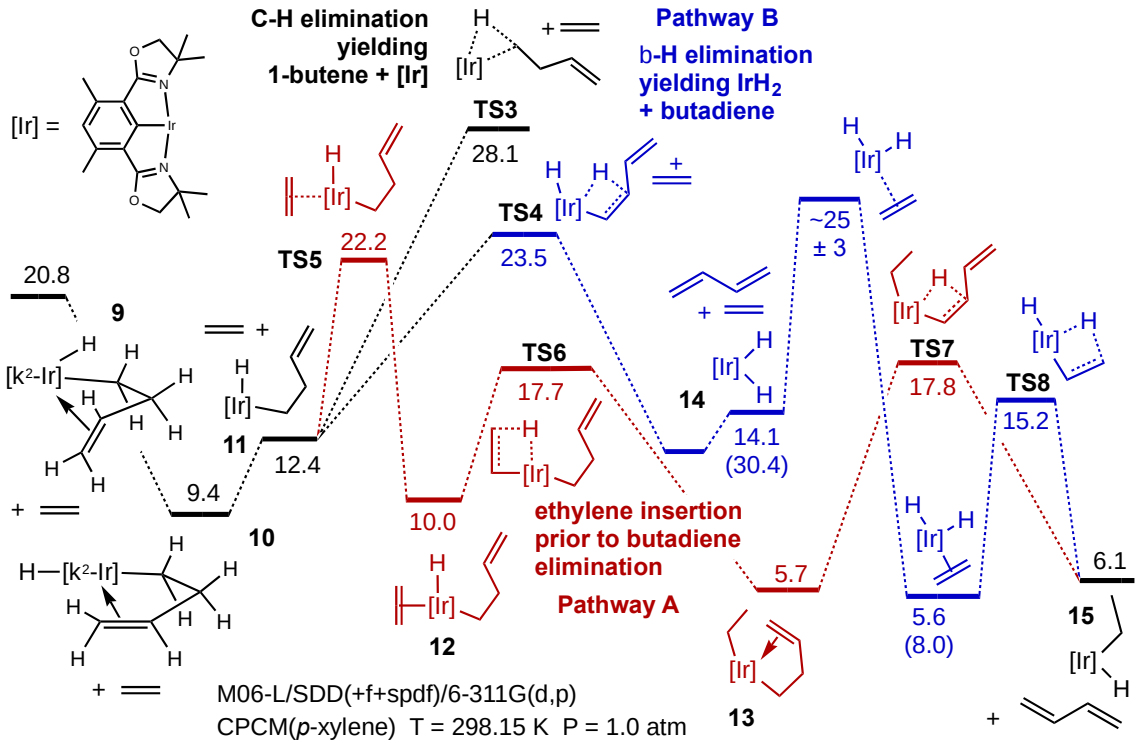

Figure 4.4. Free energy profile for butadiene formation following β-H elimination by iridacyclopentane **2**.

A caveat to the above discussion is that the Pathway B, by proceeding via dihydride **14**, allows the possibility that **14** will hydrogenate the butadiene product to give 1-butene. This is consistent with the observation discussed above that higher pressures of ethylene lead to higher ratios of butadiene to 1-butene.

Alternative mechanisms were also investigated computationally. Ethylene C-H addition to (Phebox)Ir^{I} followed by insertion of a second ethylene molecule into the resulting Ir–C bond was calculated to have a prohibitively high barrier with an insertion TS free energy 41.3 kcal/mol above **1**; this is in accord with our experimental results demonstrating that the iridacyclopentane is a true intermediate. We also considered that β-elimination by iridacyclopentane **7** might lead to butadiene formation, but this step was also calculated to

have a TS prohibitively high in free energy, 55.9 kcal/mol above **1**. Finally, the free energy of the TS for β-H-elimination from **7** with κ^3-Phebox coordination maintained was located 81.6 Kcal/mol above **1**.

Experimental

General

All reactions were conducted under an argon atmosphere using an MBraun glovebox, or Schlenk or vacuum-line techniques unless specified otherwise. Anhydrous benzene and *p*-xylene were purchased from Sigma-Aldrich, stored over molecular sieves in the glovebox and used without further purification. Benzene-d_6, toluene-d_8 and *p*-xylene-d_{10} were purchased from Cambridge Isotope Labs, dried over activated alumina and filtered. (Phebox)Ir(η^2-ethylene)$_2$ (**1**) was prepared according to published procedures.[1] All other reagents were purchased from commercial suppliers and used without further purification. Medium-walled NMR tubes (maximum pressure: 150 psi) and heavy-walled Wilmad quick pressure valve NMR tubes (maximum pressure: 200 psi) were purchased from Sigma-Aldrich. NMR spectra were acquired on 500 MHz Varian VNMRS NMR spectrometers and ^{1}H and ^{13}C spectra are referenced to residual solvent peaks. The signal of the residual protio methyl group of *p*-xylene-d_{10} was set at δ 20.90 in the ^{13}C NMR spectrum.

Synthesis and Characterization of Complexes

(Phebox)Ir(C_4H_8)(C_2H_4) (2). 1 (2.2 mg, 4.0 μmol) and 0.4 mL *p*-xylene (2.0 mM) in C_6D_6 solution were added to a J-Young NMR tube in the glovebox. The solution was degassed with one freeze-pump-thaw cycle, charged with 1 atm of ethylene and heated at 70 °C for 18 h. NMR yield: 71%. ^{1}H NMR (C_6D_6, 500 MHz): δ 6.66 (s, 1H, Ar–*H*), 3.74 (t, *J* = 7.1

Hz, 2H, C*H*$_2$CH$_2$CH$_2$CH$_2$), 3.55 (d, *J* = 8.2 Hz, 2H, OC*H*$_2$), 3.48 (d, *J* = 8.2 Hz, 2H, OC*H*$_2$), 2.86 (br s, 4H, C$_2$*H*$_4$ ligand), 2.64 (s, 6H, Ar–C*H*$_3$), 2.60-2.50 (m, 2H, CH$_2$*CH*$_2$CH$_2$CH$_2$), 2.22-2.12 (m, 2H, CH$_2$CH$_2$C*H*$_2$CH$_2$), 1.53 (t, *J* = 6.8 Hz, 2H, CH$_2$CH$_2$CH$_2$C*H*$_2$), 1.13 (s, 6H, C(C*H*$_3$)$_2$), 0.82 (s, 6H, C(C*H*$_3$)$_2$). ^{13}C NMR (C$_6$D$_6$, 125 MHz): δ 204.8, 178.0, 139.7, 127.0, 126.7, 81.6, 67.7, 53.2, 40.6, 36.4, 29.9, 27.9, 27.4, 19.1, 2.7.

(Phebox)Ir(η^2-ethylene-^{13}C$_2$)$_2$ (1-^{13}C$_4$). (Phebox)Ir(OAc)(H) (4.4 mg, 8.0 μmol), NaO^{t}Bu (2.2 mg, 24 μmol) and 0.5 mL *p*-xylene were added to a J-Young NMR tube in the glovebox. The solution was degassed with one freeze-pump-thaw cycle and charged with 1 atm of ethylene-^{13}C$_2$. After heating at 40 °C for 4 h, the volatiles were removed under vacuum and the product was re-dissolved in toluene (1 mL). Bright orange powder was obtained after filtration and removal of solvent under vacuum. Yield: 3.2 mg (73%). ^{1}H NMR (*p*-xylene-d$_{10}$, 500 MHz): 6.61 (s, 1H), 3.57 (s, 4H), 3.45-3.03 (m, $^1J^{13}_{C\text{-}H}$ = 151.6 Hz, 4H), 2.65 (s, 4H), 1.60-1.18 (m, 4H), 0.82 (s, 12H). ^{13}C NMR of ethylene-^{13}C$_2$ ligand (*p*-xylene-d$_{10}$, 125 MHz): δ 32.8 (d, *J* = 41.7 Hz), 11.6 (d, *J* = 41.9 Hz).

(Phebox)Ir(C$_4$H$_8$-^{13}C$_4$)(C$_2$H$_4$-^{13}C$_2$) (2-^{13}C$_6$). Following the procedure above to synthesize **2, 1-^{13}C$_4$** (10 mM) in *p*-xylene-d$_{10}$ solution (0.4 mL) was heated under ethylene-^{13}C$_2$ (1 atm) at 70 °C for 18 h. NMR yield: 70%. ^{13}C NMR of ^{13}C labeled ligand (*p*-xylene-d$_{10}$, 125 MHz): δ 54.1, 41.3 (ddd, *J* = 36.7, 32.3, 4.2 Hz), 37.2 (dd, *J* = 36.9, 31.9 Hz), 31.2 – 29.8 (m), 3.5 (dd, *J* = 32.0, 4.3 Hz).

(Phebox)Ir(C$_4$H$_8$-^{13}C$_4$)(C$_2$H$_4$) (2-^{13}C$_4$). 2-^{13}C$_6$ (7.0 mM) and **1-^{13}C$_4$** (3.0 mM) in *p*-xylene-d$_{10}$ solution (0.4 mL) was added to a J-Young NMR tube in the glovebox. The solution was degassed with one freeze-pump-thaw cycle and charged with 1 atm of ethylene. **2-^{13}C$_4$** (7.0 mM) and **1** (3.0 mM) formed at room temperature. ^{13}C NMR of ^{13}C

labeled ligand (*p*-xylene-d_{10}, 125 MHz): δ 41.3 (ddd, *J* = 36.6, 32.3, 4.2 Hz), 37.2 (dd, *J* = 36.8, 32.1 Hz), 31.6 – 29.6 (m), 3.5 (dd, *J* = 32.0, 4.3 Hz).

1,3-Butadiene-$^{13}C_4$. 2-$^{13}C_6$ (7.0 mM) and **1-$^{13}C_4$** (3.0 mM) in *p*-xylene-d_{10} solution (0.4 mL) was added to a medium-walled and sealable NMR tube, which was connected to a Kontes high-vacuum adapter with Tygon tubing. The Kontes valve was attached to a vacuum-gas manifold and the solution was frozen with liquid nitrogen. The headspace of the NMR tube was evacuated until the pressure reached 10 mTorr. The headspace was filled with 1 atm of ethylene-$^{13}C_2$ and then condensed using liquid nitrogen. After 30 seconds, the NMR tube was sealed using an oxygen torch (the headspace volume was decreased by 50%, which brought the total ethylene pressure to 2 atm). The sealed NMR tube was allowed to reach room temperature, then heated and rotated in a GC oven at 100 °C for 1 h. ^{13}C NMR (*p*-xylene-d_{10}, 125 MHz,): δ 143.3 – 142.1 (m), 122.7 – 121.1 (m).

(Phebox)Ir(OAc)($CH_2(CH_2)_2CH_3$) (4). Following a procedure outlined in the literature,[6] a C_6D_6 solution (0.4 mL) of (Phebox)Ir(OAc)(H) (10 mM) and $NaBAr^F{}_4$ (0.5 mM) was added to a J-Young NMR tube in the glovebox. The solution was degassed with one freeze-pump-thaw cycle and charged with 1 atm of butene. The reaction finished in 15 minutes at room temperature. NMR yield: 98%. ^1H NMR (C_6D_6, 500 MHz): δ 6.48 (s, 1H), 3.86 – 3.80 (m, 4H), 2.64 (s, 6H), 2.07 (s, 3H), 1.69 (m, 2H), 1.41 (m, 2H), 1.36 (s, 6H), 1.28 (s, 6H), 0.98 (m, 3H), 0.63 – 0.51 (m, 2H). ^{13}C NMR (C_6D_6, 125 MHz): δ 184.3, 182.1, 177.3, 139.3, 126.0, 123.2, 82.0, 66.2, 33.7, 27.2, 27.0, 25.9, 24.6, 19.0, 14.6, -3.8.

(Phebox)Ir(C_4H_8)(CO) (6). A C_6D_6 solution (0.4 mL) of **2** (7.0 mM) and **1** (3.0 mM) was added to a J-Young NMR tube in the glovebox. The solution was degassed with one freeze-

pump-thaw cycle and charged with 1 atm of CO. **6** (7.0 mM) and **5** (3.0 mM) were formed at room temperature. ^{1}H NMR of **6** (C_6D_6, 500 MHz): δ 6.61 (s, 1H), 3.70 – 3.58 (m, 4H), 3.24 (t, *J* = 7.1 Hz, 2H), 2.58 (s, 7H), 2.47 (m, 2H), 2.14 (m, 2H), 1.18 (s, 6H), 1.13 (s, 6H), 1.02 (t, *J* = 6.8 Hz, 2H). ^{13}C NMR of 6 (C_6D_6, 125 MHz): δ 194.7, 178.6, 175.6, 140.4, 127.4, 127.0, 81.4, 67.1, 39.3, 36.9, 32.7, 28.4, 28.3, 19.1, 1.2.

(Phebox)Ir(CO) (5). A C_6D_6 solution (0.4 mL) of **6** (7.0 mM) and **5** (3.0 mM) was added to a J-Young NMR tube in the glovebox. After heating at 90 °C for 1 h, the volatiles were removed under vacuum and the products were re-dissolved in C_6D_6. **5** (8.2 mM) was obtained with free Phebox-H (1.5 mM) as the side product. ^{1}H NMR (C_6D_6, 500 MHz): δ 6.40 (s, 1H), 3.73 (s, 4H), 2.30 (s, 6H), 1.17 (s, 12H). ^{13}C NMR (C_6D_6, 125 MHz): δ 199.8, 199.3, 177.7, 135.5, 131.6, 129.3, 80.5, 65.8, 28.1, 19.0.

Dehydrogenative Coupling of Ethylene Catalyzed by 1, with or without Additive

With ethylene (2 atm or 8 atm)

400 µL of **1** (5.0 mM) and *p*-xylene (internal standard, 3.0 mM) in toluene-d_8 solution was added to a medium-walled and sealable NMR tube, which was connected to a Kontes high-vacuum adapter with Tygon tubing. The Kontes valve was attached to a vacuum-gas manifold and the solution was frozen with liquid nitrogen. The headspace of the NMR tube was evacuated until the pressure reached 10 mTorr. The headspace was filled with 1 or 4 atm ethylene which was condensed by immersion in liquid nitrogen. After 30 s, the NMR tube was sealed using an oxygen torch (the headspace volume was decreased by 50%, which brought the total ethylene pressure to 2 atm or 8 atm). The sealed NMR tube was allowed to reach room temperature, then heated while being rotated in a GC oven to promote gas-liquid mixing.

^{1}H NMR spectroscopy was used to determine the concentration of different C4 olefins in solution, with *p*-xylene as internal standard (one example shown in Figure 4.5). Based on partial vapor pressures, the amount of C4 olefin in the head space was calculated to be only ca. 5% of that in solution at 25 °C, and was neglected. To determine the percentage of butadiene in all products, an aliquot was removed from the NMR tube with a 1-µL GC syringe and analyzed by GC (one example shown in Figure 4.8).

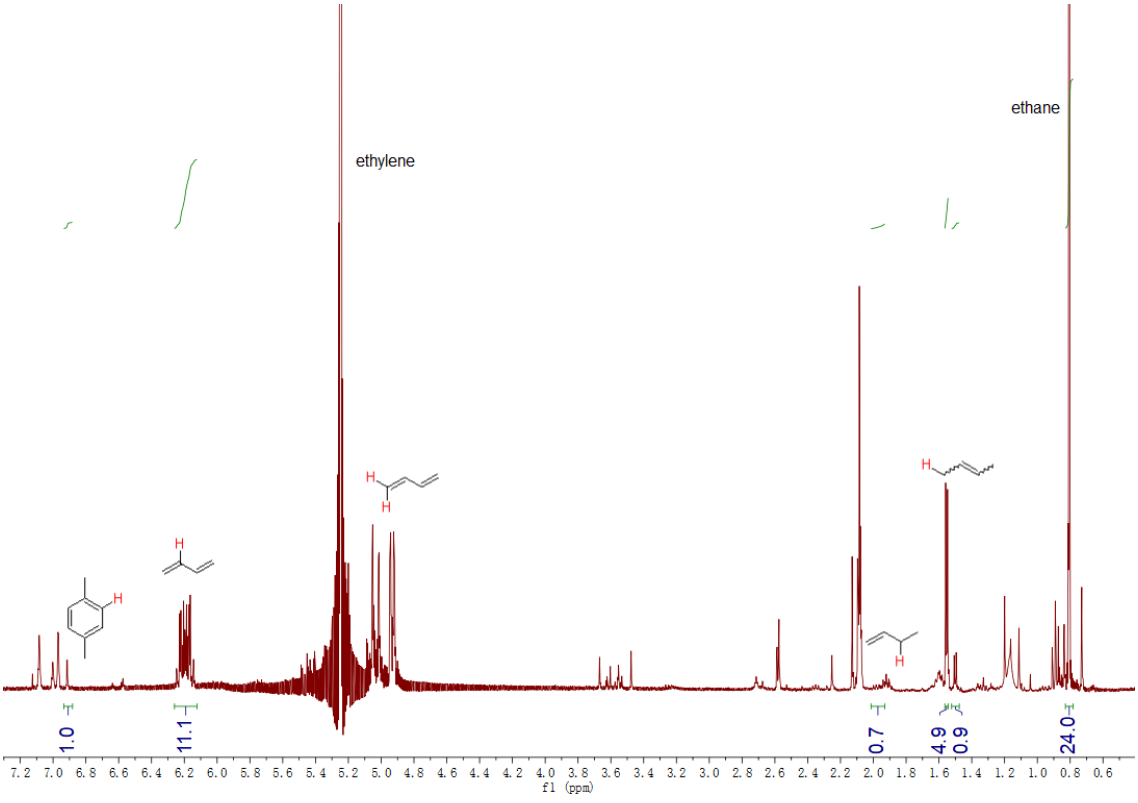

Figure 4.5. ^{1}H NMR spectrum obtained after catalysis. Reaction condition: [**1**] = 5.0 mM, 12 atm of C_2H_4, 3.0 mM *p*-xylene in toluene-d_8, 110 °C, 15 h.

With ethylene (12 atm)

200 µL of **1** (5.0 mM) and *p*-xylene (internal standard, 3.0 mM) in toluene-d_8 solution was transferred to a heavy-walled NMR tube fitted with a re-sealable Teflon valve in a glovebox.

The solution was degassed with a freeze-pump-thaw cycle and charged with 12 atm ethylene. The NMR tube was heated in an oil bath and shaken every 1 hour to promote gas-liquid mixing. The solution was analyzed by both ^{1}H NMR spectroscopy and GC.

In the presence of 1-butene

200 µL of **1** (5.0 mM) and *p*-xylene (internal standard, 3.0 mM) in toluene-d_8 solution was transferred to a heavy-walled NMR tube fitted with a re-sealable Teflon valve in a glovebox. The solution was degassed with a freeze-pump-thaw cycle and charged with 2 psi of 1-butene. After shaking to promote gas-liquid mixing, the NMR tube was charged with 8 atm ethylene. The concentration of 1-butene in solution was determined to be 7.7 mM by ^{1}H NMR spectroscopy. The NMR tube was heated in an oil bath and shaken every 1 hour to promote gas-liquid mixing. After 2 h at 100 °C, 8.8 mM butadiene had formed which was no different from an identical solution to which 1-butene had not been added. There was no change in the concentration of 1-butene, indicating that the butadiene was not formed from 1-butene.

In the presence of 1,3-butadiene

200 µL of **1** (5.0 mM) and *p*-xylene (internal standard, 3.0 mM) in toluene-d_8 solution and 20 µL of 1,3-butadiene (ca. 15 wt. %) in hexane solution was added to a heavy-walled NMR tube fitted with a re-sealable Teflon valve in a glovebox. The solution was degassed with a freeze-pump-thaw cycle and charged with 8 atm ethylene. The NMR tube was heated in an oil bath and shaken every 1 hour to promote gas-liquid mixing.

In the presence of 1-butene under ethylene-d_4

200 µL of a toluene-d_8 solution of **1** (5.0 mM) and *p*-xylene (internal standard, 3.0 mM) was transferred to a heavy-walled NMR tube fitted with a re-sealable Teflon valve in a glovebox. The solution was removed from the glovebox and degassed with a freeze-pump-thaw cycle and charged with 8 psi of 1-butene. After shaking to promote gas-liquid mixing, the NMR tube was charged with 2 atm ethylene-d_4. The concentration of 1-butene in solution was determined to be 30 mM by ^{1}H NMR spectroscopy. The NMR tube was heated in an oil bath and shaken every 1 hour to promote gas-liquid mixing. After 2 h, the reaction solution was first analyzed by ^{1}H NMR spectroscopy. The concentration of 1-butene was unchanged and no ^{1}H NMR signal attributable to butadiene was observed. An aliquot was removed from the NMR tube with a 1-µL GC syringe and analyzed by GC. The observation of 3.2 mM butadiene indicates that the product was butadiene-d_6.

In the presence of 1-butene under ethylene-$^{13}C_2$

400 µL of a *p*-xylene-d_{10} solution of **1-$^{13}C_4$** (10 mM), 1-butene (3.7 mM) and benzene (internal standard, 3.0 mM) was transferred to a J-Young NMR tube in a glovebox. The solution was removed from the glovebox and degassed with a freeze-pump-thaw cycle and charged with 1 atm of ethylene-$^{13}C_2$. After shaking to promote gas-liquid mixing, the NMR tube was heated in an oil bath and shaken every 1 hour to promote gas-liquid mixing. After 3 h at 100 °C, the reaction solution was monitored by ^{1}H NMR spectroscopy (Table 4.2).

Table 4.2. Reaction results in the presence of 1-butene under ethylene-$^{13}C_2$

time	1-butene (mM)	butadiene (mM)	butadiene-$^{13}C_4$ (mM)
0 h	3.7	0	0
3 h	3.6	0.1	7.0

Ratio of 2 to 1 during reaction. Following the procedure in the section above (*"With ethylene (2 atm or 8 atm)"*), reaction solutions with 2 atm, 4 atm, 6 atm and 8 atm ethylene were prepared, heated at 100 °C and monitored by ^{1}H NMR spectroscopy every 25 min. The ratio of 2 to 1 was found to reach a steady state after 150 min (Table 4.3).

Table 4.3. Ratio of **2** to **1** in the reaction under different pressure of ethylene.

$P_{C_2H_4}$	2 atm	4 atm	6 atm	8 atm
[2]/[1]	1.50	1.63	1.56	1.70

Gas Chromatographic Analysis Method.

GC analyses (FID detection) were performed on a Varian 430-GC instrument fitted with Agilent J&W GS-GasPro column (60 m length, 0.32 mm ID) using the following method:

Starting temperature: 40 °C

Time at starting temp: 1.4 min

Ramp1: 8 °C/min up to 150 °C with hold time 3 min

Ramp2: 20 °C/min up to 260 °C with hold time 30 min

Flow rate (carrier): 1.4 mL/min (N_2)

Split ratio: 25

Injector temperature: 250 °C

Detector temperature: 260 °C

Representative GC Traces

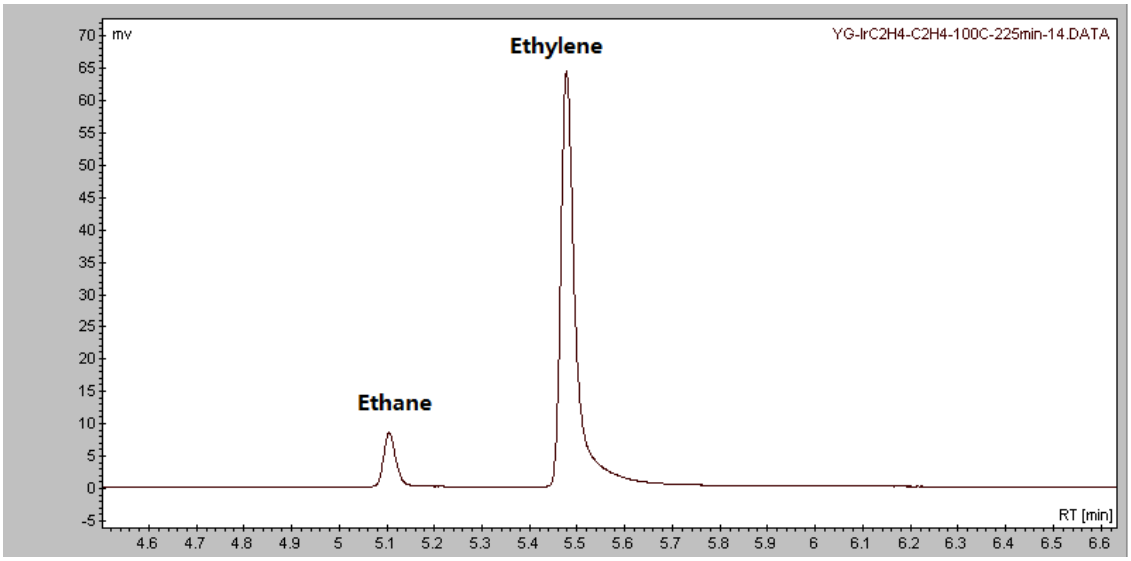

Figure 4.6. GC trace showing the separation of C_2 species during ethylene dehydrogenative coupling catalyzed by **1** (5.0 mM); 2 atm C_2H_4, toluene-d_8, 100 °C, 225 min.

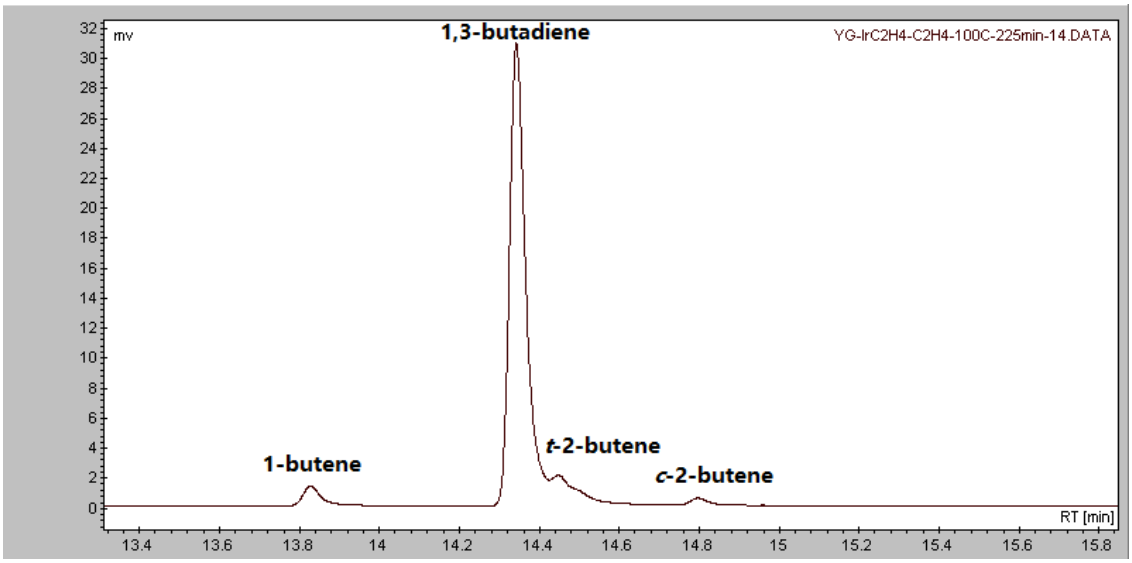

Figure 4.7. GC trace showing the separation of C_4 species during ethylene dehydrogenative coupling catalyzed by **1** (5.0 mM); 2 atm C_2H_4, toluene-d_8, 100 °C, 225 min.

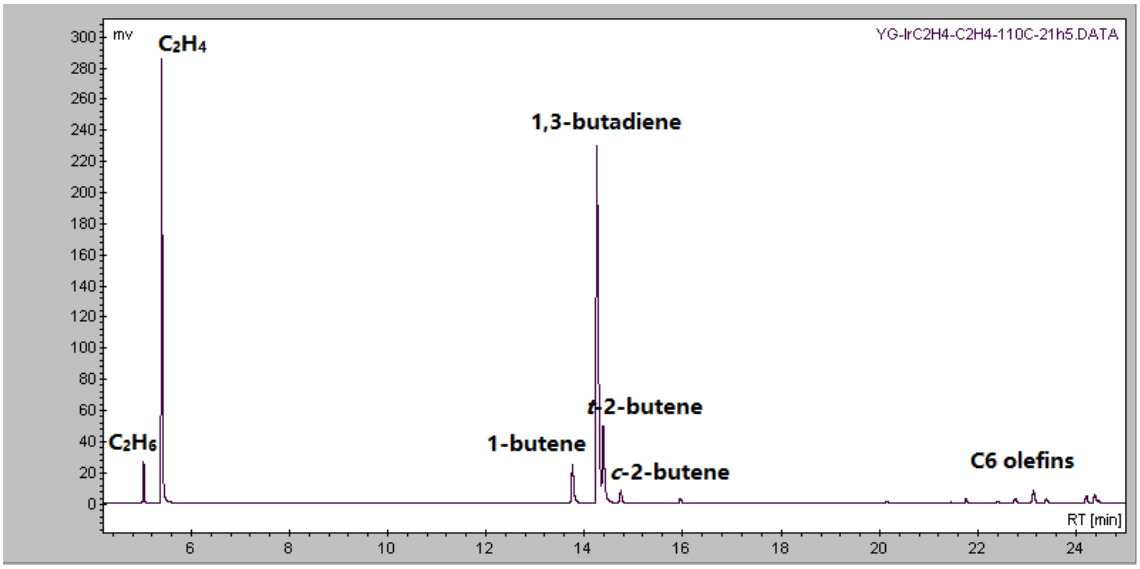

Figure 4.8. GC trace showing product separation during ethylene dehydrogenative coupling catalyzed by **1** (5.0 mM); 2 atm C_2H_4, toluene-d_8, 110 °C, 21 h.

X-ray Structural Data for Complex 6

X-ray Structure Determination. Single-crystal X-ray diffraction data were collected on a Bruker Smart APEX CCD diffractometer with graphite monochromatized Mo Kα radiation (λ = 0.71073Å) at 120 K. The crystals were immersed in oil and placed on a nylon loop in the cold stream. The data were corrected for Lorenz effects, polarization, and absorption, the latter by a multi-scan method using program SAINT.[36] The structures were solved by direct methods using program SHELXS.[37] Using program SHELXL[38], all non-hydrogen atoms were refined based upon Fobs^3 and all hydrogen atom coordinates were calculated with idealized geometries.

CCDC # 1581264

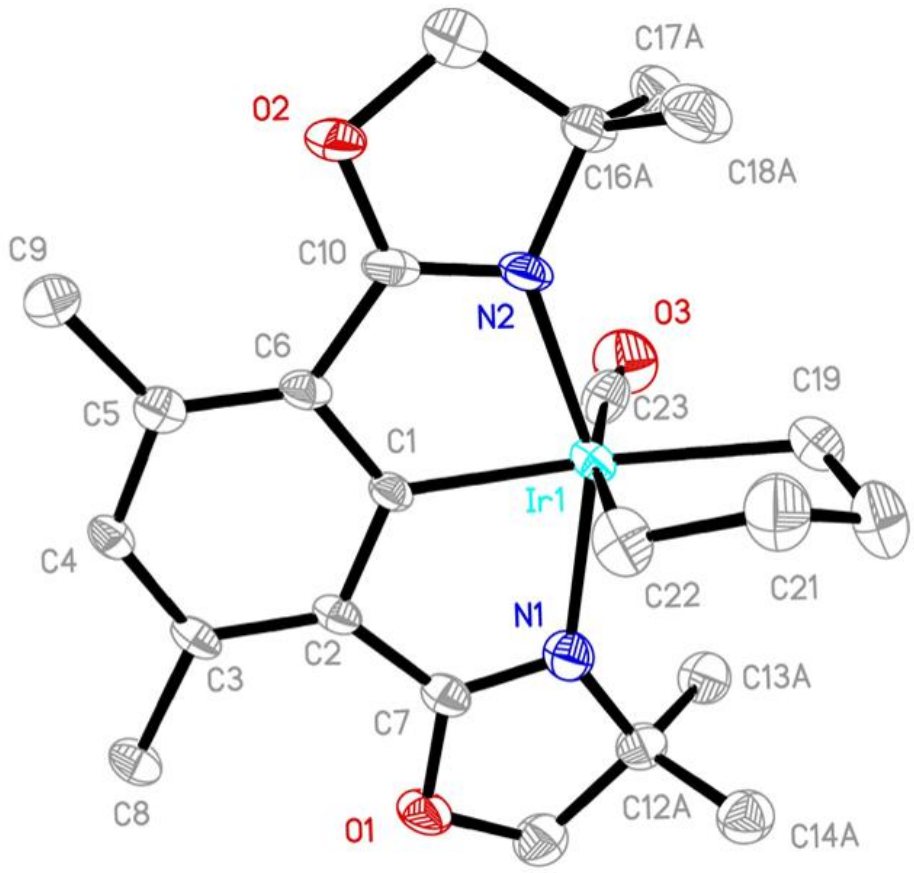

Figure 4.9. Solid-state molecular structure of complex **6** (ORTEP view, 50% probability ellipsoids). Hydrogen atoms omitted for clarity.

Table 4.4. Crystal data and structure refinement for **6**.

Identification code	irphebu1m_0m	
Empirical formula	C23 H31 Ir N2 O3	
Formula weight	575.70	
Temperature	120(2) K	
Wavelength	0.71073 Å	
Crystal system	Monoclinic	
Space group	$P2_1/n$	
Unit cell dimensions	a = 8.6341(12) Å	α= 90°.
	b = 22.668(3) Å	β= 108.945(2)°.
	c = 11.4074(16) Å	γ = 90°.
Volume	2111.7(5) $Å^3$	
Z	4	
Density (calculated)	1.811 Mg/m^3	
Absorption coefficient	6.350 mm^{-1}	
F(000)	1136	
Crystal size	0.500 x 0.170 x 0.010 mm^3	
Theta range for data collection	1.797 to 25.681°.	
Index ranges	-10<=h<=10, -27<=k<=27, -13<=l<=13	
Reflections collected	18032	
Independent reflections	4004 [R(int) = 0.0384]	
Completeness to theta = 25.242°	100.0 %	
Absorption correction	Numerical	
Max. and min. transmission	0.2664 and 0.0843	
Refinement method	Full-matrix least-squares on F^2	
Data / restraints / parameters	4004 / 132 / 298	
Goodness-of-fit on F^2	1.187	
Final R indices [I>2sigma(I)]	R1 = 0.0456, wR2 = 0.1029	
R indices (all data)	R1 = 0.0500, wR2 = 0.1049	
Largest diff. peak and hole	4.859 and -2.363 e.$Å^{-3}$	

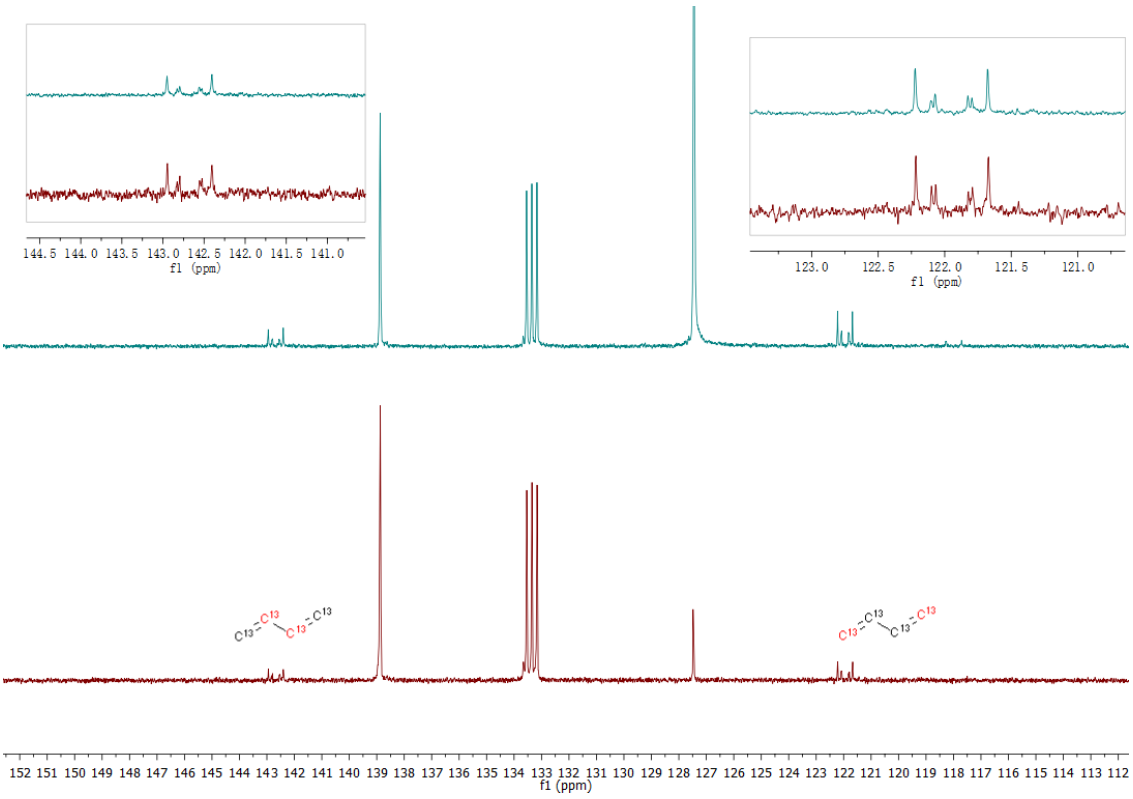

Figure 4.10. ^{13}C NMR spectra obtained after *p*-xylene-d_{10} solution of **1**-$^{13}C_4$ (3.0 mM) and **2**-$^{13}C_6$ (7.0 mM) was heated at 100 °C under unlabeled C_2H_4 (2 atm) for 30 min (spectrum in red) or under $^{13}C_2H_4$ (2 atm) for 2 h (spectrum in green). (125 MHz, *p*-xylene-d_{10}, 25 °C).

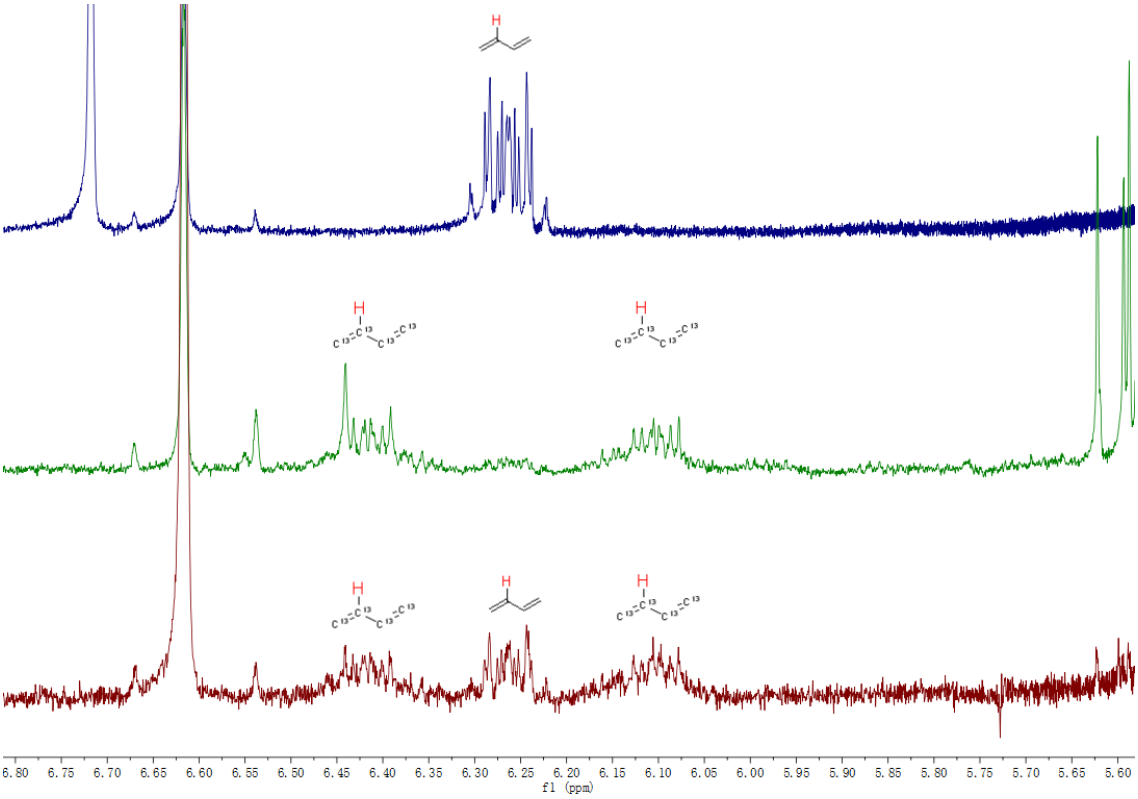

Figure 4.11. ^{1}H NMR spectra under different reaction conditions. Reaction condition (spectrum in blue): [**1**] = 5.0 mM, 4 atm of C_2H_4, *p*-xylene-d_{10}, 100 °C, 125 min. Reaction condition (spectrum in green): [**1**-$^{13}C_4$] = 10 mM, 2 atm of $^{13}C_2H_4$, *p*-xylene-d_{10}, 100 °C, 120 min. Reaction condition (spectrum in red): [**1**-$^{13}C_4$] = 3.0 mM, [**2**-$^{13}C_6$] = 7.0 mM, 2 atm of C_2H_4, *p*-xylene-d_{10}, 100 °C, 30 min.

Reference

(1) Makshina, E. V.; Dusselier, M.; Janssens, W.; Degreve, J.; Jacobs, P. A.; Sels, B. F. *Chem. Soc. Rev.* **2014**, *43*, 7917.

(2) White, W. C. *Chemico-Biological Interactions* **2007**, *166*, 10.

(3) Abdelrahman, O. A.; Park, D. S.; Vinter, K. P.; Spanjers, C. S.; Ren, L.; Cho, H. J.; Vlachos, D. G.; Fan, W.; Tsapatsis, M.; Dauenhauer, P. J. *ACS Sustainable Chemistry & Engineering* **2017**, *5*, 3732.

(4) Farzad, S.; Mandegari, M. A.; Gorgens, J. F. *Bioresour. Technol.* **2017**, *239*, 37.

(5) Stalpaert, M.; Cirujano, F. G.; De Vos, D. E. *ACS Catal.* **2017**, *7*, 5802.

(6) Gao, Y.; Guan, C.; Zhou, M.; Kumar, A.; Emge, T. J.; Wright, A. M.; Goldberg, K. I.; Krogh-Jespersen, K.; Goldman, A. S. *J. Am. Chem. Soc.* **2017**, *139*, 6338.

(7) Bercaw-Butadiene.

(8) Rolland, G.; Axens, Fr. . 2014, p 16pp.

(9) Kung, H. H.; Kung, M. C. *Adv. Catal.* **1985**, *33*, 159.

(10) Hong, E.; Park, J.-H.; Shin, C.-H. *Catal. Surv. Asia* **2016**, *20*, 23.

(11) McLain, S. J.; Wood, C. D.; Schrock, R. R. *J. Am. Chem. Soc.* **1979**, *101*, 4558.

(12) Grubbs, R. H.; Miyashita, A.; Liu, M.; Burk, P. *J. Am. Chem. Soc.* **1978**, *100*, 2418.

(13) Fellmann, J. D.; Rupprecht, G. A.; Schrock, R. R. *J. Am. Chem. Soc.* **1979**, *101*, 5099.

(14) Wang, S.-Y. S.; VanderLende, D. D.; Abboud, K. A.; Boncella, J. M. *Organometallics* **1998**, *17*, 2628.

(15) Schrock, R. R.; Coperet, C. *Organometallics* **2017**, *36*, 1884.

(16) Blom, B.; Clayton, H.; Kilkenny, M.; Moss, J. R. In *Advances in Organometallic Chemistry*; West, R., Hill, A. F., Eds.; Academic Press: 2006; Vol. 54, p 149.

(17) Acton, N.; Roth, R. J.; Katz, T. J.; Frank, J. K.; Maier, C. A.; Paul, I. C. *J. Am. Chem. Soc.* **1972**, *94*, 5446.

(18) Binger, P.; Doyle, M. J. *J. Organomet. Chem.* **1978**, *162*, 195.

(19) Briggs, J. R. *J. Chem. Soc., Chem. Comm.* **1989**, 674.

(20) Agapie, T.; Schofer, S. J.; Labinger, J. A.; Bercaw, J. E. *J. Am. Chem. Soc.* **2004**, *126*, 1304.

(21) Agapie, T.; Labinger, J. A.; Bercaw, J. E. *J. Am. Chem. Soc.* **2007**, *129*, 14281.

(22) Britovsek, G. J. P.; McGuinness, D. S.; Tomov, A. K. *Catal. Sci. Technol.* **2016**, *6*, 8234.

(23) Tobisch, S.; Ziegler, T. *Organometallics* **2005**, *24*, 256.

(24) McDermott, J. X.; White, J. F.; Whitesides, G. M. *J. Am. Chem. Soc.* **1973**, *95*, 4451.

(25) McDermott, J. X.; White, J. F.; Whitesides, G. M. *J. Am. Chem. Soc.* **1976**, *98*, 6521.

(26) Miller, T. M.; Whitesides, G. M. *Organometallics* **1986**, *5*, 1473.

(27) Cai, F. X.; Lepetit, C.; Kermarec, M.; Olivier, D. *J. Mol. Catal.* **1987**, *43*, 93.

(28) Jacobson, D. B.; Freiser, B. S. *J. Am. Chem. Soc.* **1983**, *105*, 7492.

(29) Jacobson, D. B.; Freiser, B. S. *Organometallics* **1984**, *3*, 513.

(30) Nagashima, H.; Michino, Y.; Ara, K.-i.; Fukahori, T.; Itoh, K. *J. Organomet. Chem.* **1991**, *406*, 189.

(31) Dudle, B.; Blacque, O.; Berke, H. *Organometallics* **2012**, *31*, 1832.

(32) Bowring, M. A.; Bergman, R. G.; Tilley, T. D. *Organometallics* **2011**, *30*, 1295.

(33) Padilla-Martinez, I. I.; Poveda, M. L.; Carmona, E.; Monge, M. A.; Ruiz-Valero, C. *Organometallics* **2002**, *21*, 93.

(34) Schaefer, B. A.; Margulieux, G. W.; Tiedemann, M. A.; Small, B. L.; Chirik, P. J. *Organometallics* **2015**, *34*, 5615.

(35) Brookhart, M.; Green, M. L. H.; Parkin, G. *Proc. Natl. Acad. Sci.* **2007**, *104*, 6908.

(36) Bruker-AXS. SADABS, Bruker area detector scaling and absorption correction, v2.05, Bruker-AXS Inc., Madison, Wisconsin, 2003; SAINTplus, Bruker area detector data reduction program, v6.45, Bruker-AXS Inc., Madison, Wisconsin, 2003.

(37) Sheldrick, G. *Acta Crystallographica Section A* **2008**, *64*, 112.

(38) Sheldrick, G. M. *Acta Crystallographica. Section C, Structural Chemistry* **2015**, *71*, 3.